EVALUATING THE GEOLOGY AND GROUND-WATER HYDROLOGY OF DEEP-BASIN LIGNITE IN TEXAS

INTERIM REPORT

by

W. R. Kaiser
Principal Investigator

M. L. Ambrose, W. B. Ayers, Jr., P. E. Blanchard, G. F. Collins,
G. E. Fogg, D. Gower, C. L. Ho, M. L. W. Jackson,
C. M. Jones, A. H. Lewis, C. Mahan,
G. L. Macpherson, D. A. Prouty,
S. J. Tewalt, and S. Tweedy

Prepared for Texas Energy and Natural Resources Advisory Council
under IAC (82-83)-0822

February 1983

Bureau of Economic Geology
W. L. Fisher, Director

The University of Texas at Austin
P. O. Box X
Austin, Texas 78712

CONTENTS

Page

Evaluating the geology and ground-water hydrology of deep-basin lignite in Texas: a summary, by W. R. Kaiser 1

Deep-basin lignite, Sabine Uplift area, by W. R. Kaiser, M. L. W. Jackson, and G. F. Collins 12

Sedimentology of the Carrizo Sand and Reklaw Formation (Claiborne Group) in east-central Texas, by C. M. Jones 25

Regional hydrogeologic considerations for deep-basin lignite development in Texas, by G. E. Fogg and W. R. Kaiser 31

Ground-water hydraulics of the Wilcox-Carrizo aquifer system, Sabine Uplift area, by G. E. Fogg and D. A. Prouty 36

Hydrology of the east-central Texas Wilcox Group, by G. L. Macpherson 53

Hydrochemical mapping in the Wilcox-Carrizo aquifer, Sabine Uplift area, by W. R. Kaiser and M. L. Ambrose 59

Hydrochemistry of the Carrizo Sand and Wilcox Group in east-central Texas, by G. L. Macpherson 80

Resistivity mapping of the east-central Texas Wilcox Group, by W. B. Ayers, Jr., and A. H. Lewis 92

Empirical relations between Wilcox ground-water quality and electric-log resistivity, Sabine Uplift area, by G. E. Fogg and P. E. Blanchard 99

Analytical methods for lignite characterization, by C. L. Ho, C. Mahan, S. Tweedy, and D. Gower 107

Lignite sample collection and preparation, by S. J. Tewalt 122

References 125

Figures

1. Distribution of deep-basin lignite in Texas 2

2. Eocene stratigraphy in east-central Texas and the Sabine Uplift area 3

3. Wilcox stratigraphy in the Sabine Uplift area and the occurrence of lignite 15

4. East-west cross section showing lignite occurrence in the Wilcox Group . . . 16

5. Map of lignite occurrence in the Wilcox Group 17

6. Maximum-sand map of the Wilcox Group 19

7. Identification of lignite on a TENRAC/BEG log and oil and gas log from nearby 23

8. Net-sand map of the stratigraphically highest sandstone in the Newby Sandstone Member in Bastrop, Lee, and Fayette Counties. 27

9. Isopach map of the Carrizo Formation and Newby Sandstone Member in Bastrop, Lee, and Fayette Counties showing the location of paleovalleys at the base of the Carrizo. 30

10. Potentiometric-surface map, Wilcox-Carrizo aquifer system 38

11. Ground-water flow lines inferred from the Wilcox-Carrizo potentiometric surface map. 39

12. Potentiometric-surface map, Carrizo aquifer 40

13. Graph of fluid pressure versus depth for the Wilcox-Carrizo system 41

14. Graph of mean slope of P-D regression lines for 50-ft intervals of land surface elevation 42

15. Map showing vertical component of the hydraulic gradient determined by least-squares linear regression for data in each 7.5-minute quadrangle 46

16. Generalized version of figure 6 indicating only the signs of $\partial h/\partial z$ 47

17. Histograms showing frequencies of log (hydraulic conductivity) (ft/d) and log (transmissivity) (ft^2/d) 50

18. Cumulative exceedance probability for log (hydraulic conductivity) (ft/d) and log (transmissivity) (ft^2/d) showing probability that a given value of K or T would be exceeded in a random sampling 51

19. Potentiometric-surface map of the Wilcox Group 55

20. Ground-water flowlines in the Wilcox Group 56

21. Piper diagrams of Carrizo and Wilcox waters 60

22. Schematic diagram illustrating ground-water evolution 63

23. Map of Carrizo $\log [Na^+]^{.33}/[Ca^{2+}]^{.16}$ ratios. 66

24. Map of Carrizo $\log [Ca^{2+}]^{.3}[Na^+]^{.7}$ products 67

25. Electric logs illustrating the Carrizo-Wilcox boundary. 68

26. Scatter plot of Wilcox log $[Na^+]^{.33}/[Ca^{2+}]^{.16}$ ratios versus depth 70

27. Map of Wilcox log $[Na^+]^{.33}/[Ca^{2+}]^{.16}$ ratios 71

28. Map of Wilcox log $[Ca^{2+}]^{.3}[Na^+]^{.7}$ products 72

29. Scatter plot of Wilcox log $[H_4SiO_4^o]$ values versus depth 75

30. Scatter plot of Wilcox log $[H_4SiO_4^o]$ values versus log $[Na^+]^{.33}/[Ca^{2+}]^{.16}$ 76

31. Scatter plot of Wilcox log $[H_4SiO_4^o]$ values versus Ca-montmorillonite saturation indices 77

32. Map of Wilcox log $[H_4SiO_4^o]$ values 78

33. Map of Wilcox Ca-montmorillonite saturation indices 79

34A. Map of Carrizo log $[Na^+]^{.33}/[Ca^{2+}]^{.16}$ ratios as derived from the montmorillonite-cation-exchange reaction 82

34B. Map of Wilcox log $[Na^+]^{.33}/[Ca^{2+}]^{.16}$ ratios as derived from the montmorillonite-cation-exchange reaction 83

35A. Map of Carrizo log $[Ca^{2+}]^{.3}[Na^+]^{.7}$ products as derived from the reaction describing feldspar argillation 85

35B. Map of Wilcox log $[Ca^{2+}]^{.3}[Na^+]^{.7}$ products as derived from the reaction describing feldspar argillation 86

36A. Map of Carrizo log $[H_4SiO_4^o]$ values 88

36B. Map of Wilcox log $[H_4SiO_4^o]$ values 89

37. Percentage of major sands in the Wilcox Group 94

38. Map of resistivity product of major sands in the Wilcox Group 96

39. Base of fresh water below sea level 97

40. Graph of TDS versus electric log resistivity (R_o; 64-inch long normal or induction), Wilcox-Carrizo aquifer system, Sabine Uplift area 100

41A. Plot of sodium (Na^+) concentrations versus R_o 101

41B. Plot of bicarbonate (HCO_3^-) concentrations versus R_o 102

41C. Plot of chloride (Cl^-) concentrations versus R_o 103

42. Graph of TDS versus specific conductance of the water samples 105

Tables

1. Number of lignites and thickness of maximum sands: predicted versus actual . . 21
2. Pressure versus depth statistics, Sabine Uplift region 43
3. Analytical methods for lignite characterization 109
4. Thermogravimetric analysis (TGA) procedure 113
5. Core sample collection and preparation 123
6. Preparing low-temperature ash (LTA) 124

EVALUATING THE GEOLOGY AND GROUND-WATER HYDROLOGY OF DEEP-BASIN LIGNITE IN TEXAS: A SUMMARY

W. R. Kaiser

INTRODUCTION

Lignite resources in Texas are currently estimated at 58 billion short tons (755 quadrillion Btu's or Quads [Q] of energy) (Kaiser and others, 1980), constituting just over one-fourth or 26 percent of the State's energy endowment of 2,915 Q. Resources of near-surface lignite, those at depths between 20 and 200 ft (6.1 and 61 m), are about 23 billion tons (300 Q), of which some 8.6 to 11.1 billion tons are exploitable by current surface-mining methods. Near-surface reserves are adequate to meet the demand for lignite in this century. Meeting the demand in the next century and beyond will require the recovery of deep-basin lignite, or that occurring between depths of 200 and 2,000 (61 and 610 m) below the surface. Resources of deep-basin lignite at these depths and in seams greater than 5 ft (1.5 m) thick are about 35 billion tons (455 Q) or 16 percent of the State's energy endowment. These resources occur mainly in East Texas north of the Colorado River (about 70 percent) in two geologic units, primarily in the lower Eocene Wilcox Group (55 percent) and secondarily in the upper Eocene Jackson Group (15 percent) (figs. 1 and 2).

Deep-basin lignite is not economically recoverable at this time; however, large tonnages are potentially recoverable by deep-surface mining or by in situ gasification. Small tonnages are now technically exploitable by in situ gasification, whereas deep mining on a routine basis remains to be demonstrated. Few details are known about the deep-basin lignite in Texas. In fact, lack of data is an important factor contributing to industry's reluctance at this time to make major commitments to in situ gasification or deep mining in Texas. Economics of deep recovery is a major concern. Is deep lignite a

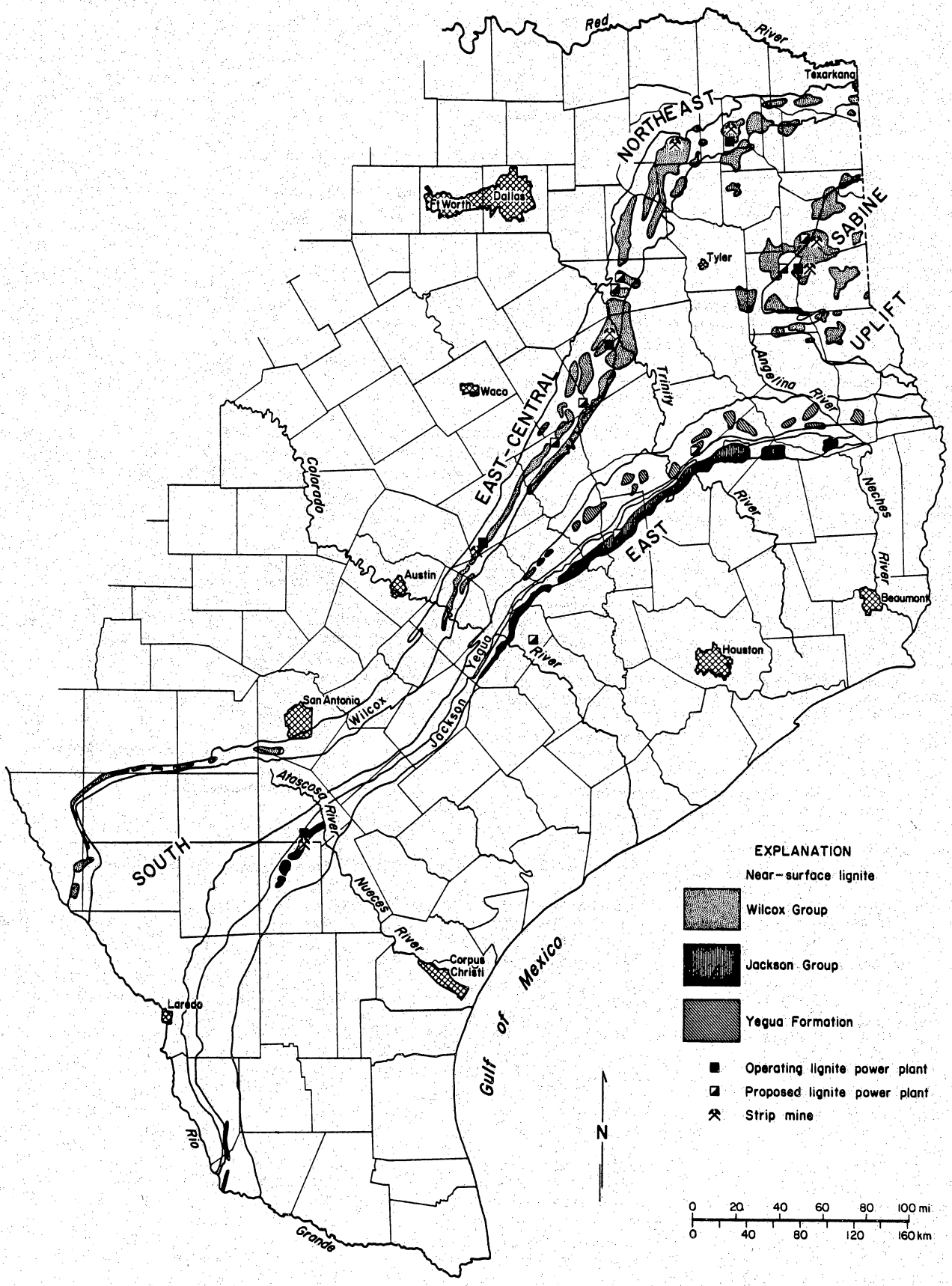

Figure 1. Distribution of deep-basin lignite in Texas (Kaiser and others, 1980).

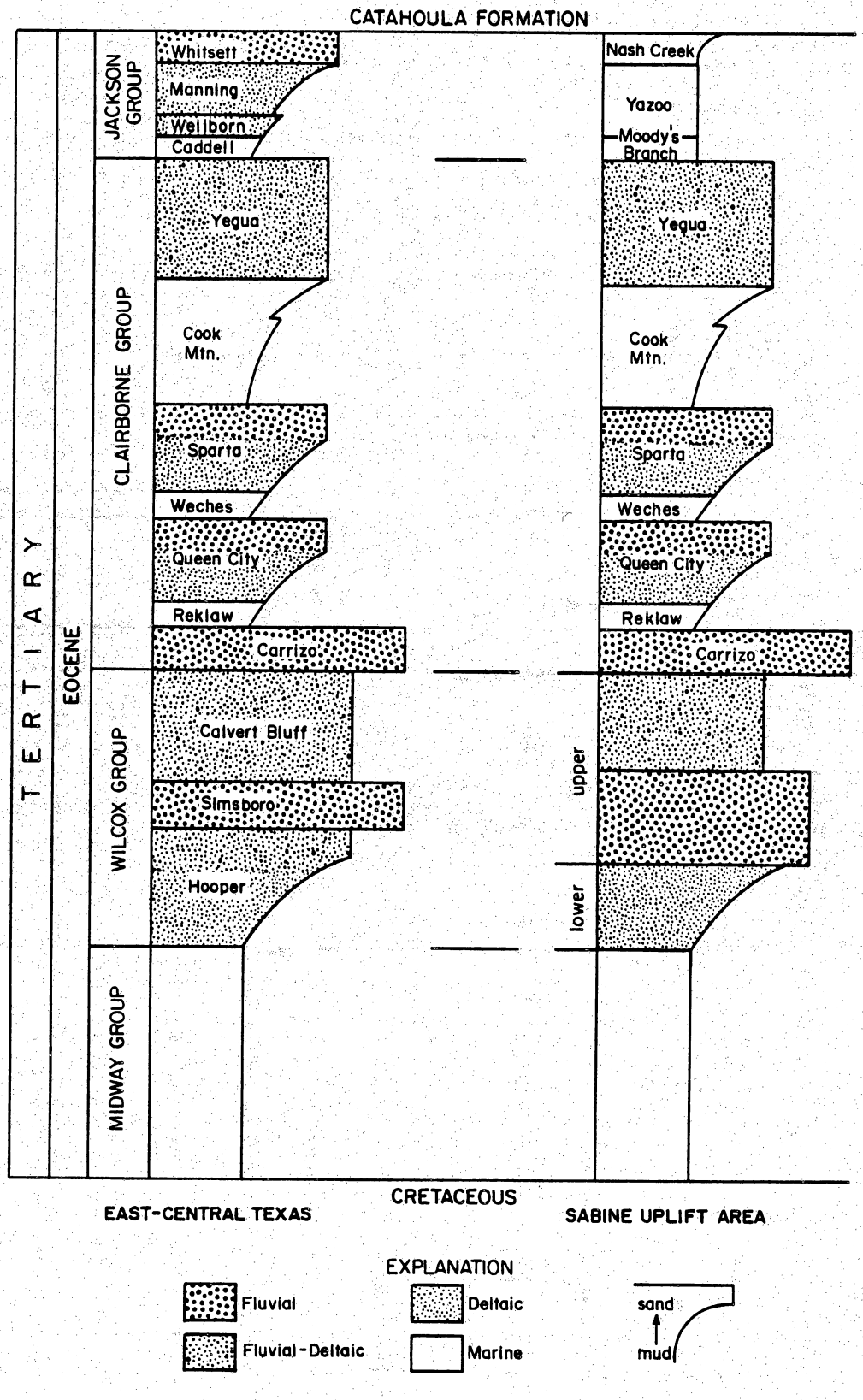

Figure 2. Eocene stratigraphy in east-central Texas and the Sabine Uplift area.

reserve? A multiyear program, funded by the Texas Energy and Natural Resources Advisory Council (TENRAC), was begun in September 1981 to collect, at the regional level, geologic, hydrologic, and chemical data about deep-basin lignite to ultimately stimulate private exploration and exploitation by providing reference data for future exploration, feasibility studies, and large-scale field tests of in situ gasification. This report presents the results of the first year of our research.

RESEARCH GOALS

Earlier research funded by TENRAC delineated four regions with high potential for recovery of deep lignite (Kaiser and others, 1980): the Sabine Uplift area and east-central Texas (Wilcox Group) and East and South Texas (Jackson Group) (fig. 1). Current research centers on the two Wilcox regions: (1) the Sabine Uplift area, a 12-county area in far East Texas centered on the semi-circular Wilcox outcrop in Harrison, Panola, and Shelby Counties, including counties downdip and ringing the outcrop and (2) east-central Texas, a 15-county area between the Neches and Colorado Rivers extending along the outcrop and into adjoining counties. An integrated program of subsurface geologic, hydraulic gradient, hydrochemical, and resistivity mapping and ground-water modeling is underway, along with a field program of drilling, logging, coring, and hydrologic testing to evaluate deep-basin resources and to unravel regional hydrology. The ultimate goal is to integrate geology and ground-water hydrology in the Wilcox of East Texas to identify areas of high potential for recovery of deep lignite.

Resource estimates of deep-basin lignite made to date rely on an operational definition to identify lignite on oil and gas logs; however, the definition is particularly difficult to apply at shallow depths (<1,000 ft or <305 m) in the presence of fresh formation waters. New criteria were needed to improve lignite identification on electric and induction logs. Thousands of oil and gas logs are available in the public sector; more

effective log analysis will expand our data base tremendously. TENRAC/BEG drilling and logging, coordinated by the BEG, has shown that oil and gas logs can be calibrated with confidence for lignite identification.

Little data exist on the chemical and mineralogical properties of deep-basin lignite; therefore, deep-basin lignite is being extensively characterized in the laboratory for comparison with near-surface lignite. If the two lignites are similar, then near-surface lignite can be used for combustion, gasification, and liquefaction experiments requiring large samples. Data on deep-basin lignite are now being collected.

Deep lignite occurs in the presence of highly transmissive or water-productive host sediments. Exploitation may not be possible in certain hydrogeologic settings. The Wilcox Group is a major aquifer in Texas containing thick sands with hydraulic conductivities or permeabilities of up to 66 ft/d (20 m/d). In situ gasification will be impossible at some sites due to excessive water influx adversely affecting process behavior. Deep-seated seams cannot be surface mined without dewatering and depressurization, a formidable task that will involve the pumping of many billions of gallons of water over the lifetime of a mine. The success or failure of deep-recovery projects is governed mainly by such hydrogeologic factors as seam thickness and continuity; transmissivity, strength, and thickness of roof and floor; seam permeability; aquifer geometry and orientation; and ground-water flow direction. These factors are being evaluated. In the Sabine Uplift area, lignite resources, aquifer geometry, and flow direction have been mapped.

SUBSURFACE GEOLOGY

In the Sabine Uplift area, geologic mapping, using about 1,100 oil and gas logs, guided an associated field program of drilling, logging, and coring designed to test an evolving depositional model, facilitate lignite identification on oil and gas logs, and recover lignite for characterization. Lignite was operationally defined on oil and gas logs

and its occurrence was mapped. Maximum-sand mapping established a fluvial-deltaic origin for the lignite. Drilling locations were selected, using the lignite-occurrence and maximum-sand maps; 15 holes were drilled to depths between 700 and 1,820 ft (213 and 555 m) by Andrews & Foster Drilling Company, Inc. of Athens, Texas, at a cost of $92,055 or $4.79 per ft ($15.71/m). The 94-day field program began June 28, 1982 and was completed October 28, 1982. All holes were extensively logged (natural gamma, density, neutron, 16-inch normal, focused resistivity, SP, and caliper) by Century Geophysical Corporation of Tulsa, Oklahoma, for a total cost of $39,931, or $1.86 per drilled ft ($6.10/m). Down-hole data were digitally recorded for later computer manipulations of scale, curve format, and cross plotting for correlation with oil and gas logs and lithology (cuttings and core). Good relations were established with landowners, ensuring land access for future hydrologic drilling and testing in the Sabine Uplift area.

Drilling has confirmed the stratigraphy of lignite occurrence in the lower and upper Wilcox in the Sabine Uplift area established by regional subsurface mapping. Lignite can be identified on electric and induction logs, although distinguishing thin lignites (<4-ft or <1.2-m thick) from thin, highly resistive, carbonate-cemented sandstones (hard streaks) remains a problem. Oil and gas logs can be calibrated for lignite identification in the presence of only a few density logs, thereby greatly expanding our data base. In effect, 15 wells were drilled to calibrate 1,100 oil and gas logs for more efficient use in resource assessment.

The thickest (5 to 10 ft or 1.5 to 3.0 m), most laterally extensive lignite seams (10 to 15 mi or 16 to 24 km) occur in Shelby and Panola Counties in the lower 200 to 500 ft (61 to 153 m) of progradational Wilcox strata. Maximum-sand mapping was successfully tested, predicting range of sand thickness and continuity of lignite seams. Maximum- or major-sand mapping has proven to be a powerful tool in basin analysis that can be done rapidly before or even during drilling to guide exploration.

Four holes were offset and cored, recovering 106 ft (32.3 m) of lignite, overburden, and underburden at a cost of $128.82 per ft ($422.53/m) of core. One-third of the core is being archived at 4°C (39°F) in sealed PVC pipe. Recovered lignite is undergoing chemical analysis using new instruments jointly purchased by TENRAC and The University of Texas at Austin in 1981. Analyses include proximate, ultimate, Btu, forms of sulfur, major oxides, and major, minor, and trace elements on a whole-coal basis. In a cooperative program with Texas Tech University, mineral matter (low-temperature ash) is being examined by analytical electron microscopy and with Texas A&M University trace metal speciation is underway. During the first year of this project, the Bureau of Economic Geology's Mineral Studies Laboratory (MSL) developed analytical methodologies for lignite characterization. These instrumental methods are highly sensitive, precise, and reliable for lignite analysis; they are far more efficient than the classical ASTM methods. The MSL is handicapped by the lack of certified lignite reference materials and by limited information on the few bituminous coals available. To alleviate these difficulties and to gain more confidence in its analytical results, the MSL is participating in round-robin test programs with government and industry laboratories around the country.

In east-central Texas, data collection, focusing on lignite occurrence and maximum or major sands, is largely complete. Mapping is underway in the Calvert Bluff Formation, host of major lignite reserves, and in two major fresh-water aquifers, the Simsboro Formation and the Carrizo Sand (fig. 2). In the shallow subsurface, the Carrizo is predominantly a multilateral channel-fill complex, forming a series of dip-oriented paleovalleys cut into the underlying Wilcox strata. Lignite-occurrence and lithofacies mapping will guide a forthcoming field program in the region.

GROUND-WATER HYDROLOGY

Regional data on hydraulic head, fluid pressure, hydraulic conductivity and transmissivity, and water chemistry are being compiled and plotted for the Wilcox-Carrizo aquifer

system as potentiometric-surface maps, a vertical hydraulic gradient map, pressure versus depth diagrams, frequency diagrams, and hydrochemical maps. The framework necessary for interpreting site-specific hydrologic data in the assessment of mine sites or in situ gasifiers is evolving.

Hydraulic head and water chemistry data indicate that regional ground-water circulation in the Wilcox-Carrizo aquifer system closely follows topography in the outcrop. Elsewhere, correlation with topography is poorer owing to greater depths of the aquifer and hence to greater confinement by overlying strata. Major recharge areas such as central Rusk County coincide with topographic highs or stream divides and sand hills in the outcrop, whereas major discharge areas coincide with major streams such as the Brazos/Little Brazos/Little River floodplain. Potential for downward flow is present nearly everywhere, except beneath floodplains of major rivers and several of their tributaries. Discharge areas make up a small percent of the total area and potentially include strong, upward ground-water flow components. Surface-mine dewatering or depressurization might be more difficult in discharge than in recharge areas. For example, the Martin Lake surface mine, which produces 11 million tons of lignite per year in Panola County, is in a well-defined discharge area.

Areas of recharge and discharge were mapped by integrating data on aquifer hydraulics (head and pressure versus depth), ground-water chemistry, and sand-body geometry. Potentiometric-surface (head) mapping has been completed; it is used to delineate regional flow in the horizontal plane and will help eliminate uncertainty about flow direction in the Wilcox (downdip, toward major rivers, or updip), as was evident in the recent controversy over surface mining in Bastrop County. Local conditions can be much more complex than is indicated by the head maps. Induced discharge, caused by relatively intense municipal pumpage of ground water (as in the cities of Jacksonville and Henderson), is reflected in local depressions in the potentiometric surface.

Analyses of fluid pressure versus depth together with mapping of the vertical hydraulic gradient ($\partial h/\partial z$) were used to delineate potential for and direction of the vertical component of flow. Only a small fraction of the water entering at the Wilcox outcrop actually reaches the deep Wilcox. Values of the vertical hydraulic gradient were calculated for 7.5-minute quadrangles in the Sabine Uplift area by linear regression and were mapped with two degrees of certainty. The resulting map can be used to evaluate mine or in situ gasifier sites with respect to potential for vertical flow and interconnection of sand bodies. Regionally consistent, non-zero values of $\partial h/\partial z$ indicate poor vertical interconnection, and anomalous zero values can indicate good interconnection vertically. Moreover, without information on horizontal- and vertical-flow direction, monitoring of deep-recovery projects cannot be effectively designed nor, for example, can hydraulic barriers be designed and placed.

Major uncertainties are lateral interconnectedness of sand bodies, hydraulic conductivity of the less permeable interchannel splay and overbank sands associated with many of the lignites, vertical and horizontal hydraulic conductivity of the lignites, and vertical hydraulic gradients at depths below about 500 ft (153 m). These issues will be addressed in a limited field program of hydrologic drilling and testing in the Sabine Uplift area.

Regional trends in water chemistry are mappable (contourable) and vary in a predictable fashion, as shown by hydrochemical mapping. Because the mapping of concentrations has proved difficult, ground-water evolution was linked to water-rock interaction through solution-mineral equilibria. Activity indices derived from reactions believed to influence evolution of Wilcox-Carrizo waters were mapped. All maps reflect the same regional geochemical patterns; they show a positive correlation with areas of recharge and discharge identified in head mapping and outcrop geology. Recharge is defined by small $\log[Na^+]^{.33}/[Ca^{2+}]^{.16}$ ratios and $\log[Ca^{2+}]^{.3}[Na^+]^{.7}$ products and large $\log[H_4SiO_4^o]$ values and montmorillonite saturation indices. Hydrochemical mapping complements head mapping and helps to define recharge and discharge where head

data are sparse or ambiguous, such as local recharge within regional discharge areas (e.g., high alluvial terraces) or losing lakes (e.g., Lake Cherokee). Hydrochemical mapping is also sensitive to induced discharge. The framework has been provided for interpreting water-chemistry data at individual mines by establishing pre-mining conditions in the Wilcox. For example, typically basic, high HCO_3^- waters of the Wilcox will tend to neutralize acid mine waters. Moreover, in interchannel splay and overbank sands the $\log [Na^+]^{.33}/[Ca^{2+}]^{.16}$ ratio or $\log [Ca^{2+}]^{.3}[Na^+]^{.7}$ product should be higher, reflecting longer residence time. These activity indices may be effective tools for assessing the degree of interconnection with major channel sands, where ground-water circulation is active and the activity indices are smaller. Water sampling will be done to test this hypothesis.

The role of sand-body geometry in controlling ground-water flow is poorly understood. Hydraulic conductivity (K), transmissivity (T), and advective dispersion of solutes are responsive to sand-body geometry. Channel-fill sands (maximum or major sands) focus ground-water flow and control average K of a stratigraphic interval. Channel sands are more permeable than surrounding Wilcox sediments by a factor of at least 10 to 100. Sand-body interconnectedness is a key factor affecting flow; Wilcox sands are seldom interconnected vertically. Evaluation of lateral interconnectedness remains an elusive goal, but it is critical to linking geology and hydrology. Equivalent vertical K is 1,000 to 10,000 times lower than equivalent horizontal K.

Because maximum or major sands reveal the framework elements of a depositional system as well as control ground-water flow, lithofacies and resistivity mapping has focused on these sands. In east-central Texas, Anderson and Houston Counties were selected as a test area and 10 was made. Resistivity reflects K in the shallow subsurface; therefore, thickness (b in meters) times resistivity (ohm-m^2/m) should reflect relative variations in transmissivity ($T = Kb$). Hence, a map of the resistivity-thickness product (units of ohm-m^2) was made to identify areas of high relative transmissivity and recharge.

The resistivity-product map shows that recharge occurs at the outcrop and around salt domes, whereas ground-water flow is inferred to be downdip and, in Anderson County, toward the Neches and Trinity Rivers.

Empirical relations have been established for the Wilcox-Carrizo aquifer between formation resistivity and water chemistry to approximate water quality (total dissolved solids) from oil and gas logs. Regional salinity mapping indicates that deep-basin lignite in the lower Wilcox of the Sabine Uplift area occurs in intervals containing brackish or saline ground water whereas upper Wilcox lignite occurs in the fresh-water interval. The base of fresh water is low near the outcrop and along the axes of major channel sand belts; it is high basinward or in muddy interchannel areas. The Railroad Commission of Texas, Surface Mining and Reclamation Division, is using the curve relating resistivity to TDS to establish standards for enforcing plugging and abandonment regulations for protecting drinking water.

DEEP-BASIN LIGNITE, SABINE UPLIFT AREA

W. R. Kaiser, Mary L. W. Jackson, and Gary F. Collins

ABSTRACT

Subsurface geologic mapping, using approximately 1,100 oil and gas logs, is under way and was used to guide an associated field program of drilling, logging, and coring. Lignite is operationally defined on oil and gas logs. Maximum-sand mapping was used to establish a fluvial-deltaic origin for the lignite. Drilling locations were selected using the lignite-occurrence and maximum-sand maps; 15 holes were drilled and four of these were offset and cored. Drilling has confirmed the stratigraphy of lignite occurrence in the lower and upper Wilcox established in regional, subsurface mapping. The thickest (5 to 10 ft or 1.5 to 3.0 m), most laterally extensive lignite seams occur in Shelby and Panola Counties in the lower Wilcox. Maximum-sand mapping successfully predicts range of sand thickness and continuity of lignite seams.

INTRODUCTION

The Sabine Uplift area, a 12-county area in far East Texas, is centered on the semicircular Wilcox outcrop in Harrison, Panola, and Shelby Counties and includes counties downdip and ringing the outcrop (fig. 1). Subsurface geologic mapping, using approximately 1,100 oil and gas logs, is being used to map lignite and associated sediments in the deep basin between depths of 200 and 2,000 ft (61 and 610 m). These data were used to guide the associated field program of drilling, coring, and logging designed to test the evolving depositional model, facilitate lignite identification on oil and gas logs, and recover lignite for characterization.

Lignite is operationally defined on oil and gas logs, in the absence of a porosity log, as those beds with a sharp resistivity spike (high resistivity) and baseline or shale SP (Kaiser, 1974). The latter is a function of the low water content (low chemical activity), high resistivity, bed thickness, and shalyness. Lignites cannot be easily distinguished from thin, fresh-water sands or high resistivity, carbonate-cemented sandstones (hard streaks),

especially as formation water becomes fresher and the resulting SP less well defined. Thus, picking lignites in the fresh-water column depends heavily on worker experience and intuition. Lignites are best picked on electric logs. Opposite a lignite seam, the long-lateral curve (18-ft 8-inch spacing) has a resistivity kick of extreme peakedness. This curve will identify resistive beds as thin as 1 ft (30 cm). The long-normal curve (64-inch spacing) displays a reversal toward the baseline in resistive beds thinner than 64 inches, or those about 5 ft (1.5 m) thick, and serves as the basis for separating thick and thin lignites. The induction log is not well suited for identification of lignite beds less than 4 ft (1.2 m) thick; thicker beds can be picked reasonably well using resistivity and curve peakedness.

Earlier regional geologic mapping in the subsurface omitted the Wilcox outcrop centered on Panola County and failed to work all available logs. To establish the geologic setting and to map sand-body geometry throughout the Sabine Uplift area, a maximum-sand map was made. The single thickest or maximum sand was picked and mapped irrespective of its stratigraphic position. This map can be prepared quickly, without time-consuming mapping of net sand and can be done in areas where the stratigraphic section is incomplete (i.e., at the outcrop). Experience shows that the maximum-sand map closely reflects geometries established by sand-percent and net-sand mapping. Delineated are the depositional system's framework elements; associated splay and overbank sands are excluded in the mapping. Moreover, because maximum or major sands control average hydraulic conductivity of a stratigraphic interval, the map becomes a tool for hydrologic evaluation.

LIGNITE OCCURRENCE

The lower Eocene Wilcox Group in the Sabine Uplift area is composed of 400 to 3,600 ft (122 to 1,098 m) of sand, mud, and lignite; it is thinnest at the outcrop, thickening

basinward where it attains thicknesses of 1,000 to 3,600 ft (305 to 1,098 m). Previously mapped as undivided, Wilcox strata are here informally divided on the basis of log character into two units: a progradational lower unit and an aggradational upper unit (fig. 2). The progradational unit is defined by inverted-Christmas-tree log patterns and the aggradational unit by blocky, Christmas-tree, and sawtooth log patterns (Fisher and others, 1969; Kaiser, 1978). Operationally defined lignite occurs in the 200 to 500 ft (61 to 152 m) thick progradational unit and predominantly in the upper 200 to 300 ft (61 to 91 m) of the aggradational unit (figs. 3 and 4).

The thickest (5 to 10 ft or 1.5 to 3.0 m), most laterally extensive lignite seams occur in Shelby and Panola Counties in the progradational unit (fig. 5). In these counties, lignites occur stratigraphically at two places, immediately above the Midway and at the top of the unit. Thick seams at exploitable depths also occur in north-central Cherokee, northwest Rusk, east-central Smith, and north-central Nacogdoches Counties in the upper Wilcox aggradational unit. These seams are generally less continuous and thinner than lower Wilcox seams; most are 5 to 6 ft (1.5 to 1.8 m) thick, although 10-ft (3-m) seams are thought to occur in northeast Cherokee County not far below the Carrizo Sand.

GEOLOGIC SETTING

In the Sabine Uplift area and northeast of the Trinity River, the Wilcox Group displays sand-body geometries and vertical sequences characteristic of fluvial depositional systems (Kaiser and others, 1978). Two prominent north-south oriented channel sand belts, a western and an eastern belt, merge and lose their separate identities in Cherokee County. The study area is traversed on the west by the eastern channel complex. Regionally, lignite is most abundant in the sand-poor interchannel areas between major channel sand belts and the tributaries feeding these belts; it accumulated in hardwood swamps established between bounding alluvial ridges. The best lignite, in terms of seam

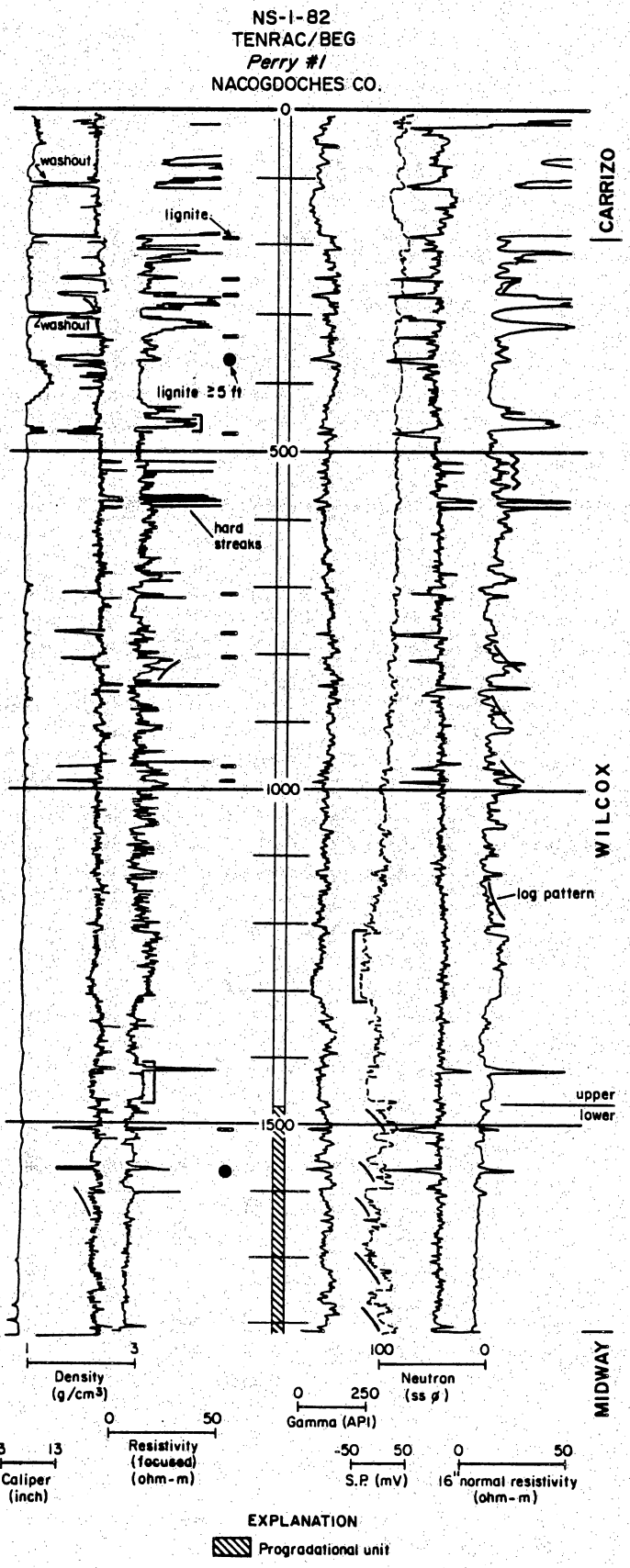

Figure 3. Wilcox stratigraphy in the Sabine Uplift area and the occurrence of lignite. NS-1-82 is in Trawick gas field; see figure 5 for location.

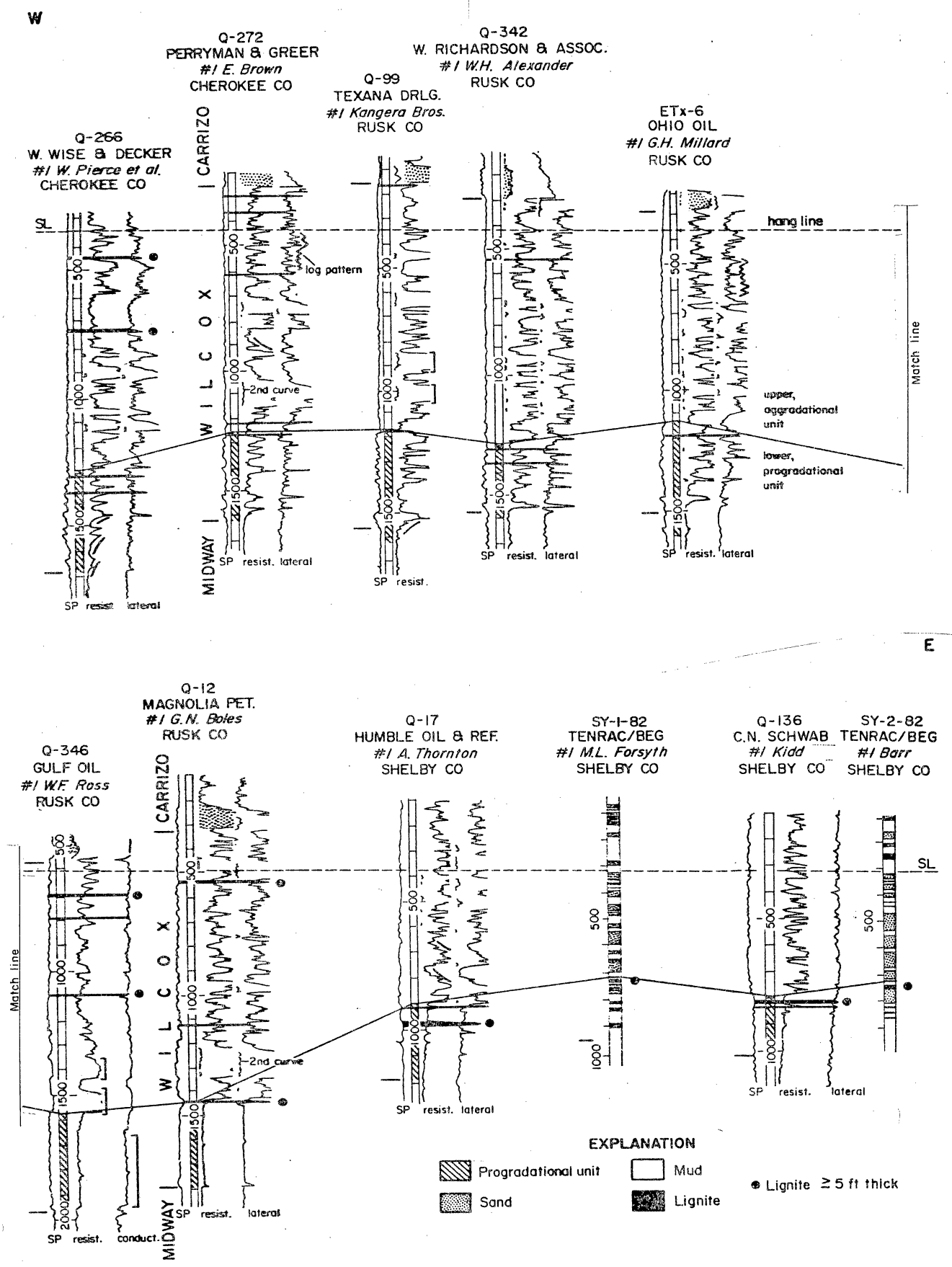

Figure 4. East-west cross section showing lignite occurrence in the Wilcox Group. See figure 6 for location of section.

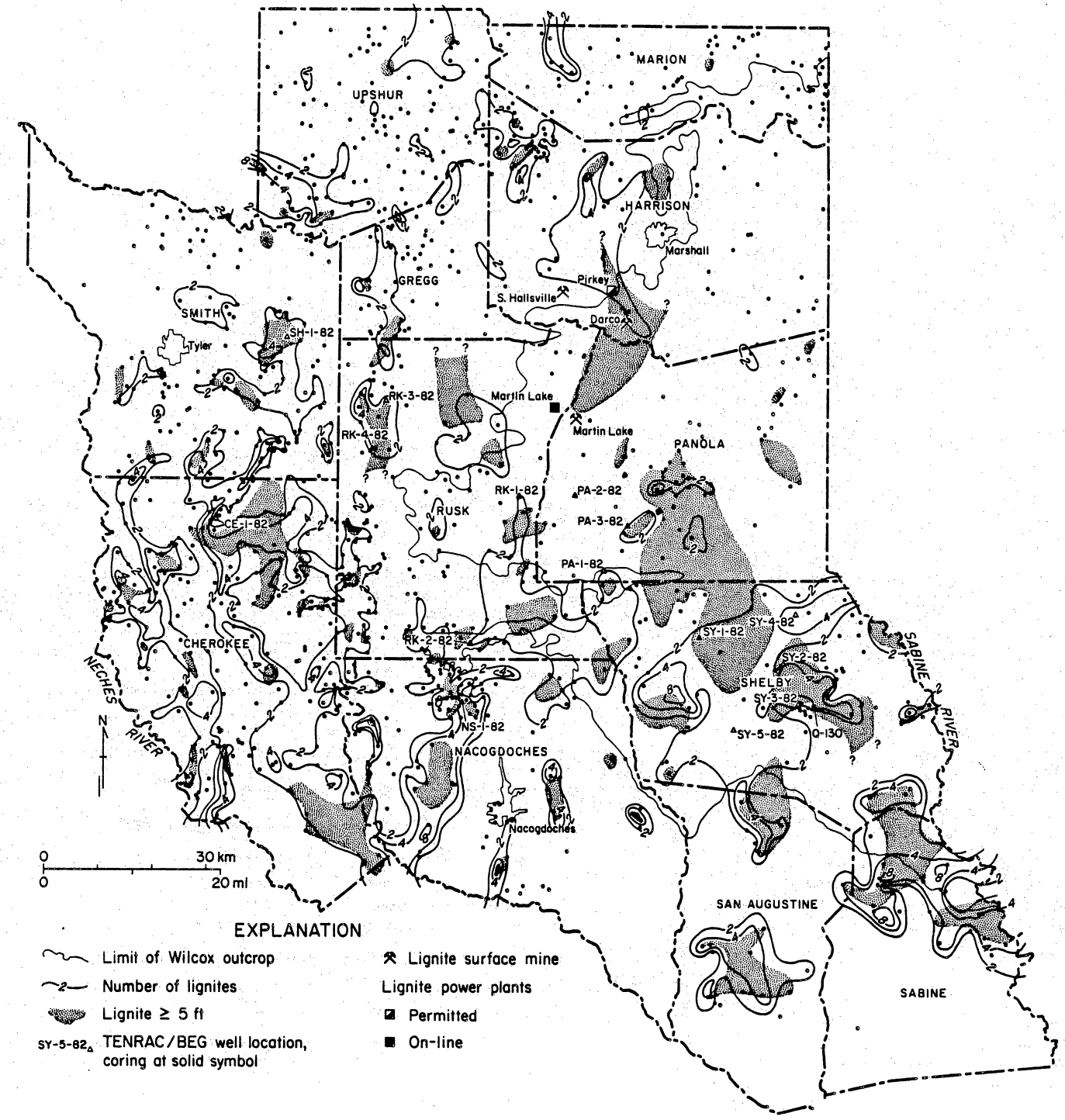

Figure 5. Map of lignite occurrence in the Wilcox Group.

thickness, continuity, and grade, is found in the southern half of the Sabine Uplift area at the transition zone between the ancient alluvial and delta plains. Superior quality is attributed to accumulation in larger, structurally more stable interchannel basins subject to less overbank flooding and crevassing than are smaller basins up the paleoslope (Kaiser and others, 1980).

Three prominent channel sand belts, defined by maximum sands in excess of 80 ft (24.4 m), are present in the Wilcox of the study area (fig. 6). One occupies the western half of Cherokee County and trends slightly west of north. Another runs northeast-southwest across Panola, Rusk, and Nacogdoches Counties, merging with the former in southern Cherokee County. A third skirts the eastern edge of Panola County, extending south across eastern Shelby County into San Augustine and Sabine Counties. Tributary channel geometries typify the western and central sand belts, whereas distributary geometries characterize the eastern belt. Preserved in the Wilcox are elements of fluvial and deltaic systems. Thick, lower Wilcox lignite in Panola and Shelby Counties occupies a position between the central fluvial channel system and the eastern distributary channel system. Eastward, the central system gradually passes into distributive, characteristically deltaic sand-body geometries. Lower Wilcox lignites are assigned a deltaic origin, initially spreading across a platform of muddy, distal delta sediments and later across sandy, more proximal sediments as deltation proceeded. Lignites occur directly above inverted-Christmas-tree log patterns, thought to represent delta-front sequences that mark the initial advance of the Wilcox deltas. Upper Wilcox lignites are assigned a fluvial origin and occupy interchannel positions; note in particular the occurrences in Cherokee County (fig. 5). Upper Wilcox lignites also commonly top inverted-Christmas-tree patterns; however, these are believed to be crevasse splays (mini-deltas) and overbank deposits associated with nearby channel complexes, representing sediment advance into an interchannel basin. The largest occurrence of thick upper Wilcox lignite occurs in north-

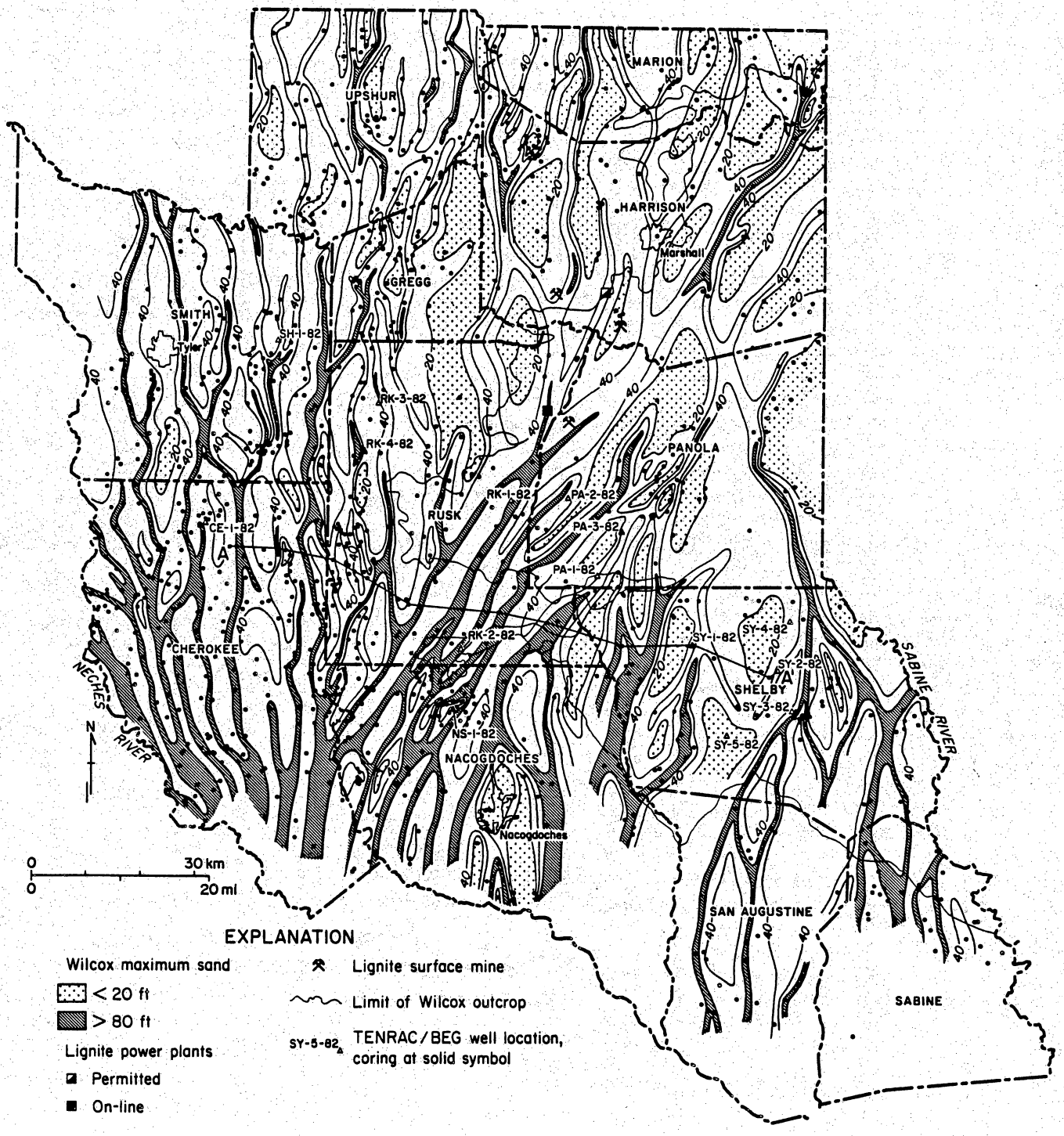

Figure 6. Maximum-sand map of the Wilcox Group.

central Cherokee County. Notable examples at the near-surface are the Martin Lake, South Hallsville, and Darco deposits (fig. 5).

FIELD PROGRAM

Drilling locations were selected, using the lignite-occurrence and maximum-sand maps (figs. 5 and 6), to test thick lignite in the deep basin. Locations were selected, in accordance with the depositional model, by placement in low-sand (interchannel) areas determined from the maximum-sand map. First priority was assigned to testing the presence and westward extent of lower Wilcox lignites in Panola and Shelby Counties. Secondary priority was given to testing upper Wilcox lignite in western Rusk and northern Cherokee Counties. Consideration was also given to testing locations that would be suitable for subsequent hydrologic drilling and testing.

Fifteen holes were drilled to depths between 700 and 1,820 ft (213 and 555 m) and four of these were offset and cored, recovering 106 ft (32.3 m) of lignite, overburden, and underburden (fig. 5). Drilling has confirmed the stratigraphy of lignite occurrence in the lower and upper Wilcox established in regional, subsurface mapping. The number of lignites picked on oil and gas logs has proven to be fewer than the number found in TENRAC/BEG drilling (table 1), reflecting a conservative bias and difficulty in identifying thin seams. The additional seams identified on TENRAC/BEG logs were usually thin. The operational definition of lignite works well for thicker, greater than 5-ft (1.5 m) seams. Maximum-sand mapping was successfully tested in the TENRAC/BEG drilling; maximum-sand thicknesses were within the estimated range in 10 of 15 instances (table 1).

Wells SY-1, -2, and -3 confirm the presence of thick lignites in the lowermost Wilcox in Shelby and Panola Counties. These seams were originally mapped by Kaiser (1974) as hard streaks because of their occurrence just above the marine Midway Group in muddy sequences of presumed marine origin. Density and resistivity logging has shown

Table 1. Number of lignites and thickness of maximum sands: predicted versus actual.

Well	Lignite				Maximum Sand	
	Predicted		Actual		Predicted	
	Total	>5 ft	Total	>5 ft	Range (ft)	Actual (ft)
PA-1-82	2	0	2	0	41-80	27
PA-2-82	1	0	1	0	21-40	42
PA-3-82	2	1	2	0	21-40	78
SY-1-82	2	0	3	2	21-40	40
SY-2-82	2	1	4	1	41-80	52
SY-3-82	3	0	3	1	41-80	49
SY-4-82	2	0	3	0	21-40	22
SY-5-82	2	?	5	2	<20-40	15
RK-1-82	1	1	2	0	81-160	116
RK-2-82	1	1	1	0	81-160	200
RK-3-82	2	1	4	2	21-40	39
RK-4-82	2	1	3	1	21-40	63
SH-1-82	3	1	5	1	21-40	21
CE-1-82	3	1	5	0	41-80	62
NS-1-82	5	2	6	2	41-80	51

many of these thick resistive beds to be lignites (fig. 7). Illustrated is the importance of TENRAC/BEG drilling in the identification of lignite using oil and gas logs. In effect, the former calibrates the latter.

Wells PA-1, -2, and -3 were drilled to trace the Panola County lignites westward. No thick lignites were penetrated (table 1). RK-1 and -2 were likewise a part of that effort as well as a specific test of the maximum-sand mapping. It was postulated that the Shelby and Panola County lignites would be lost westward as the central channel sand belt was approached in Rusk County (figs. 4 and 6). This proved to be the case; no thick lignites were found, and maximum sands were in excess of 100 ft (30.5 m) thick (table 1).

Wells RK-3 and -4 were drilled to test upper Wilcox lignite and the possible westward extent into the deep-basin of near-surface lignite north of Henderson. Thick lignite was found, but it is probably limited westward by a channel system along the Rusk-Smith County line (fig. 6); it may have greater extent southward along the western limit of Rusk County. Well CE-1 was drilled to establish a western boundary on upper Wilcox lignites present in northeast Cherokee County. Thick lignites are apparently east and south of CE-1. Well SH-1 was drilled to test thick lignite in a large, regional interchannel basin; one 6-ft (1.8-m) seam of unknown lateral extent was found at 1,034 ft (315 m). Well NS-1 (fig. 3) was drilled to calibrate lignite identification on numerous oil and gas logs in the Trawick gas field and as a potential site for hydrologic testing. The potential for thick lignite in Nacogdoches County is highest eastward of NS-1 in interchannel basins flanking the central channel complex.

Well SY-5 was drilled last to test the regional depositional model. As the drilling program progressed, we became more confident in picking lignites on oil and gas logs and of the predictive capability of the maximum-sand mapping. Four areas of mapped, thick lignite converged on the SY-5 site, an area of no control lying in a large interchannel area

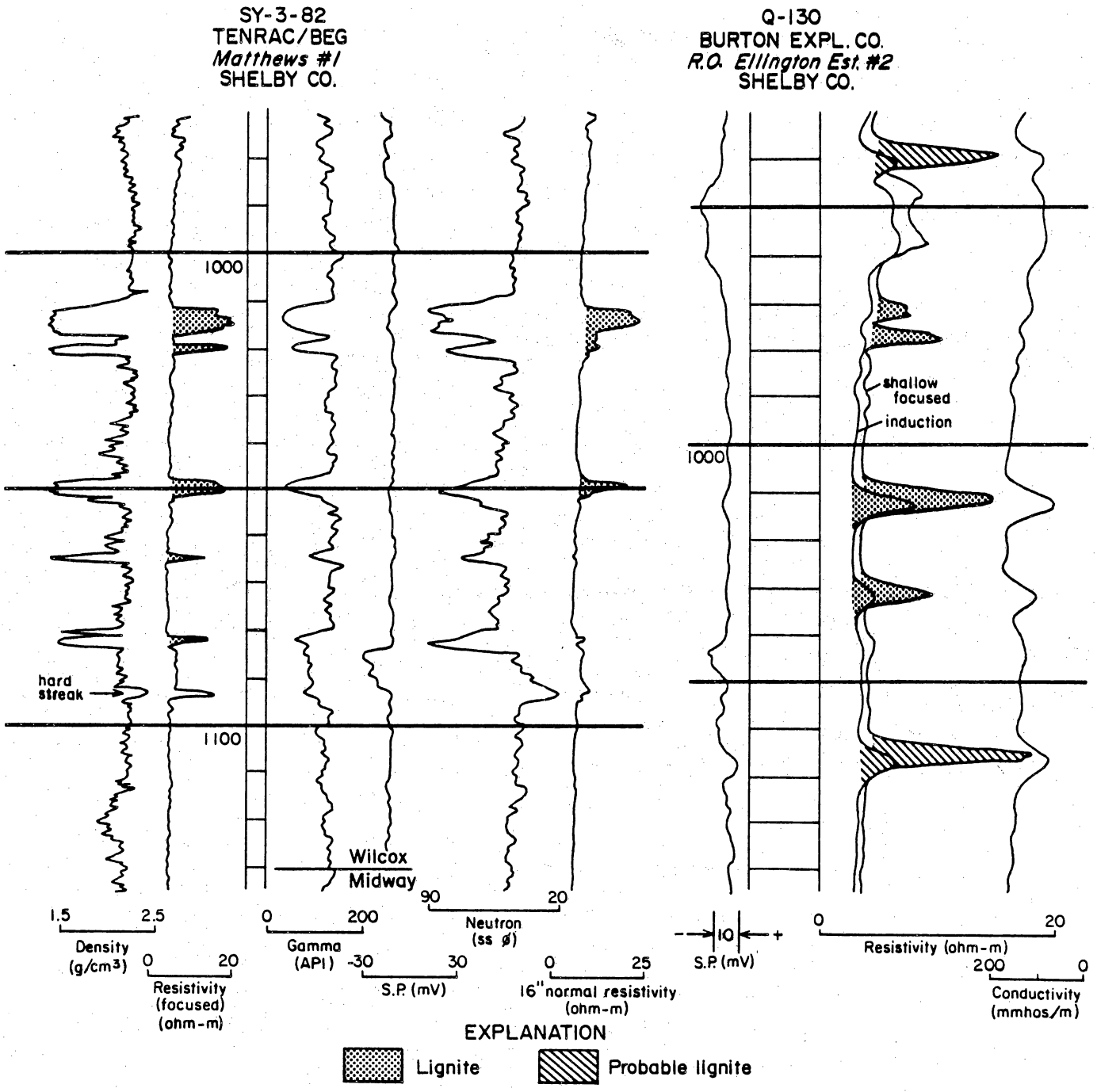

Figure 7. Identification of lignite on a TENRAC/BEG log and oil and gas log from nearby. See figure 5 for location of logs.

(figs. 5 and 6). SY-5 was successful, penetrating a 10-ft (3-m) seam at 1,520 ft (463 m) as well as other seams and a sequence of muddy sediments (table 1).

FUTURE WORK

Future work will focus on lithofacies mapping of the two lignite-bearing stratigraphic intervals. Currently, data are being collected from the lower progradational unit. The upper aggradational unit must be subdivided to stratigraphically separate the lignite-bearing interval. This is proving to be a difficult task. Net-sand, maximum-sand, sand-percent, and lignite-occurrence maps will be prepared to improve prediction of lignite occurrence and seam continuity. Resistivity mapping will be completed to augment hydrogeologic evaluation. Distinguishing thin lignites from thin hard streaks remains a problem. Hard streaks are generally more resistive than lignites; the difference between them will be statistically tested. Strip logs will be prepared from cuttings collected from TENRAC/BEG wells and correlated with the geophysical logs to facilitate lithologic interpretation of the geophysical logs. This work has now begun.

SEDIMENTOLOGY OF THE CARRIZO SAND AND REKLAW FORMATION (CLAIBORNE GROUP) IN EAST-CENTRAL TEXAS

Colin M. Jones

ABSTRACT

The sedimentology of the Carrizo Sand and Reklaw Formation, a major aquifer immediately overlying the lignite bearing Wilcox, is being investigated. The base of the Carrizo is irregular, forming a series of dip-oriented paleovalleys cut into the Wilcox. In the shallow subsurface the Carrizo is predominantly a multilateral channel complex forming a good aquifer flushed with fresh water. Further downdip it is more thinly bedded. The overlying sandstones in the lower Reklaw form a series of relatively thin, strike-oriented sand bodies.

INTRODUCTION

The hydrogeological study of major aquifers associated with Wilcox lignites requires a proper understanding of the sedimentology of the formations, particularly with respect to sand-body geometry and interconnectedness. Whereas a number of regional studies of the Wilcox Group exist (Fisher and McGowen, 1967; Kaiser, 1978), there has been no similar investigation of the Carrizo Sand and Newby Sandstone Member of the Reklaw Formation. These sands directly overlie the lignite-bearing Calvert Bluff Formation, have high porosity and permeability, and are important aquifers (fig. 2).

The present sedimentological study, which began in May 1982, covers the east-central Texas area (fig. 1) and aims to provide information on the following:

(1) Regional variations in thickness and distribution of the Carrizo and Newby;

(2) The nature and origin of the Carrizo-Wilcox contact, particularly with respect to the interconnectedness of Carrizo and Wilcox sands and the relationship of the Carrizo to major upper Calvert Bluff lignites;

(3) Sand-body geometry and interconnectedness both within the Carrizo and between the Carrizo and overlying Newby;

(4) Sand percentage variation in the Carrizo;

(5) Resistivity variation in the Carrizo;

(6) Thickness and resistivity of the Marquez Shale aquitard overlying the Newby.

DATA BASE

The major source of our information is geophysical logs, mostly from oil and gas wells. Most are spontaneous-potential and normal and induction resistivity logs; in addition there are a few gamma ray, density, neutron, and sonic logs. The data base is essentially the same as that used in the Wilcox subsurface mapping (see Ayers and Lewis, this report), although the lower Claiborne is cased off in many of the wells. The study has so far been restricted to Bastrop, Lee, and Fayette Counties.

In addition, cuttings from selected wells and all relevant core material held in the Bureau of Economic Geology core collection will be examined. The best field exposures will also be studied. This information should improve the sedimentological interpretation of the geophysical logs.

REKLAW FORMATION: NEWBY SANDSTONE MEMBER

The Newby Sandstone Member forms the lower part of the Reklaw Formation (fig. 2). It can usually be recognized in the subsurface and is informally subdivided into two units. The lower part of the Newby contains a series of 10- to 60-ft (3- to 18-m) thick, highly resistive, and laterally extensive sand bodies. These may rest directly on the Carrizo, but being separated from the Carrizo by a thin shale break often coarsen upward. The upper part of the Newby consists of 5- to 45-ft (1.5- to 14-m) thick sands and silts with interbedded muds, often forming a series of fining-upward units. These are extremely persistent laterally. A net-sand map of the stratigraphically highest unit shows a number of sand thicks oriented obliquely with respect to the outcrop (fig. 8) and the

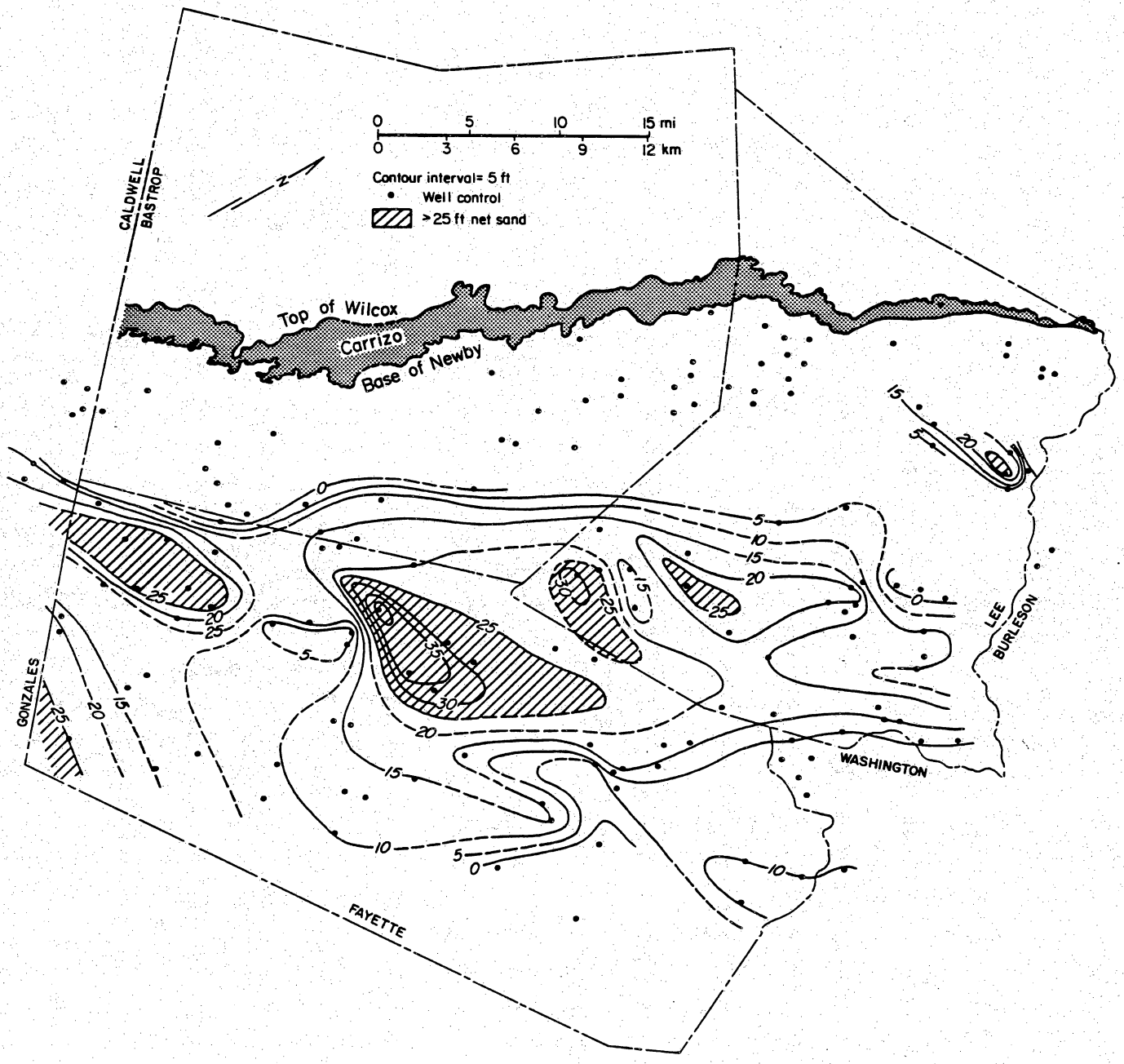

Figure 8. Net sand map of the stratigraphically highest sandstone in the Newby Sandstone Member in Bastrop, Lee, and Fayette Counties.

inferred depositional strike. The Newby thickens downdip, reaching 250 ft (76 m) in southern Fayette County. Updip it thins to as little as 30 ft (9 m) or less near Bastrop County.

CARRIZO SAND

The Carrizo Sand can be subdivided into two facies using geophysical logs. The predominant facies is a massive, highly resistive sand in beds up to 100 ft (30 m) thick, displaying blocky log patterns and separated by thin shales. In many wells, particularly in the shallow subsurface, the sand percent exceeds 80 percent. The subordinate facies consists of thinly bedded fine sands, silts, and shales, which show both coarsening-upward and fining-upward trends. Much of the Carrizo appears to consist of a multistory and multilateral channel complex. The poor lateral continuity of the finer interchannel sediments suggests a high degree of interconnectedness between the sands.

In the shallow subsurface it is usually possible to pick the base of the Carrizo fairly accurately because the massive sand facies predominates, whereas the underlying Wilcox usually exhibits a lower sand percentage. Even where the Carrizo rests directly on Wilcox sand, it can often be distinguished by its higher resistivity and different (usually depressed) SP. In the deeper subsurface, below the base of fresh water, the Carrizo and Wilcox sands have a similar log response and differentiation is more difficult. Problems also occur where the lowermost Carrizo is developed in shaly facies that may be difficult to distinguish from the Wilcox.

The configuration of the base of the Carrizo has been determined by mapping the thickness of the Carrizo Sand and Newby Sandstone using the contact between the highest Newby sand and overlying Marquez Shale Member of the Reklaw as the upper marker horizon. Although at least two, and possibly more, separate sands exist at different stratigraphic levels at the top of the Newby, this has only a limited effect on the

mapping. There is also some slight distortion because of the effects of differential compaction in wells with different sand/shale ratios.

The configuration of the contour patterns may be largely determined, however, by the irregular shape of the pre-Carrizo surface. These suggest that the Carrizo may rest unconformably on the Wilcox (fig. 9), and the lower part of the Carrizo Sand fills a series of broad generally dip-oriented valleys. These have a dendritic pattern, joining downdip into larger valleys which can be traced deep into the subsurface for as far as the base of the Carrizo can be recognized.

The large thickness increase in southwestern Bastrop and western Fayette Counties is probably not a paleovalley. There the underlying Wilcox consists predominantly of thick, fine-grained sediments, and it is possible that compaction of these during Carrizo deposition caused greater local subsidence leading to the increase in Carrizo thickness.

FUTURE WORK

The objective of this and related projects is a better understanding of the geologic controls on the hydrology of the Wilcox-Carrizo aquifer system, particularly with respect to the location of discharge and recharge areas. The relationship of resistivity to thickness and facies variations in the Carrizo Sand is now being investigated.

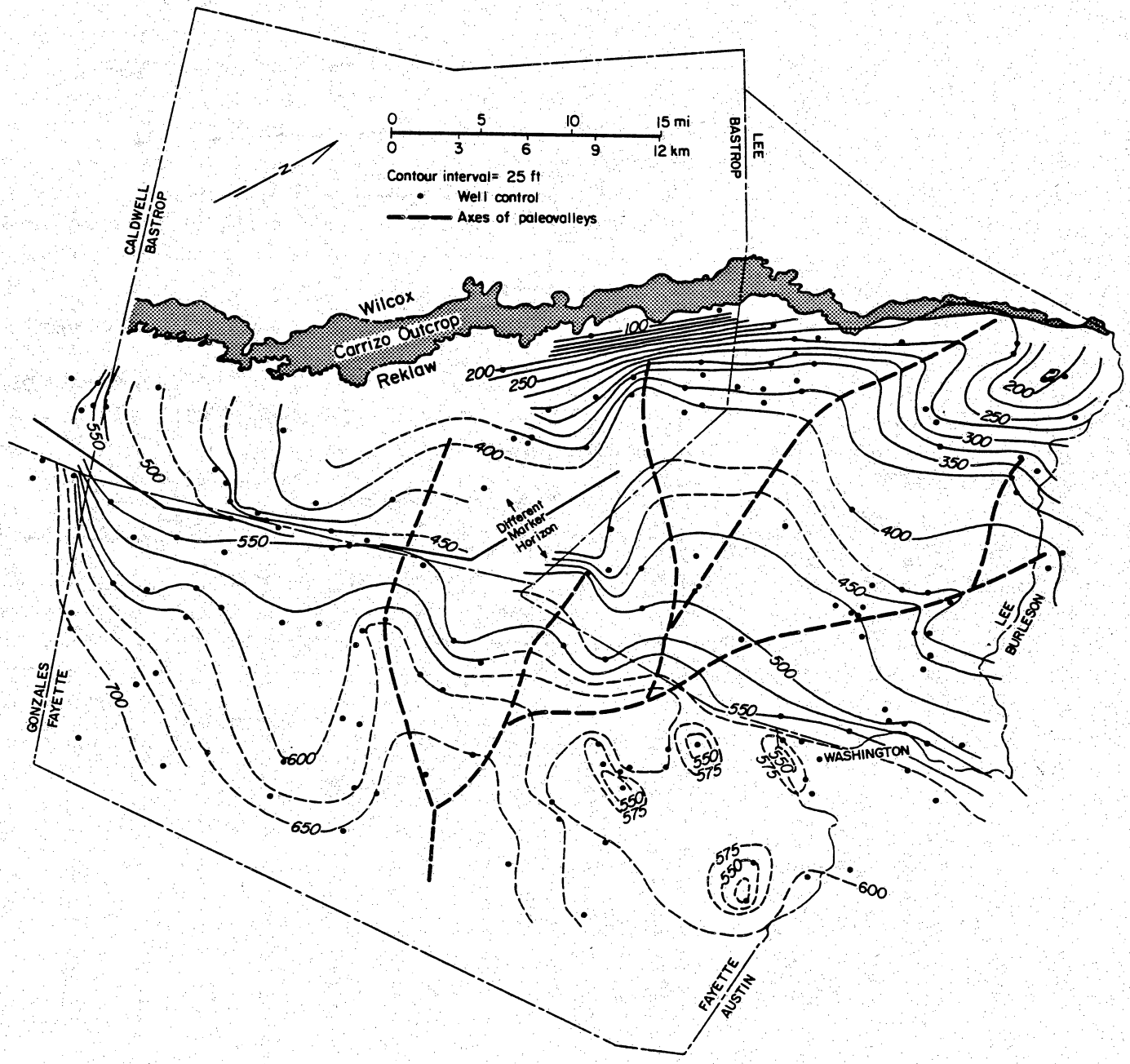

Figure 9. Isopach map of the Carrizo Formation and Newby Sandstone Member in Bastrop, Lee, and Fayette Counties showing the location of paleovalleys at the base of the Carrizo.

REGIONAL HYDROGEOLOGIC CONSIDERATIONS FOR DEEP-BASIN LIGNITE DEVELOPMENT IN TEXAS

Graham E. Fogg and W. R. Kaiser

ABSTRACT

Study of regional hydrogeology provides the framework necessary for addressing site-specific problems. Previous studies of the Wilcox aquifer system in Texas highlight the need for understanding the role of Wilcox sand bodies in controlling ground-water flow and for mapping recharge and discharge areas and trends in ground-water chemistry. Ground-water velocities and potential water-related water problems are intimately tied to distribution and interconnectedness of the sand bodies. Surface mine dewatering or depressurization problems might be more serious in discharge areas than in recharge areas.

INTRODUCTION

As do most hydrogeologic problems, deep-basin lignite development will require site-specific investigations. A premise of this study is that the site-specific investigation is most successful when conceived and executed with knowledge of regional hydrogeologic conditions. The regional study provides a framework enabling better understanding of the physical/chemical system. As concluded by the Committee on Ground-Water Resources in Relation to Coal Mining and others (1981, p. 190): "Presently available information and ongoing research are inadequate to provide a [regional] framework for analyzing the site-specific information that will be generated during hydrogeologic assessment of existing and future mine sites."

Much regional work has already been completed for the Wilcox Group of the East Texas Basin (Kreitler and others, 1980, 1981; Fogg and Kreitler, 1981, 1982; Fogg and others, in press) and of east-central Texas (Henry and Basciano, 1979; Henry and others, 1979). The present study builds on previous work and focuses on the Sabine Uplift area (located on the eastern margin of the East Texas Basin) and the Wilcox outcrop belt of

east-central Texas. Following is a brief summary of our present knowledge of regional Wilcox hydrogeology related to potential deep-basin lignite development.

The Wilcox Group is a multiple aquifer system containing primarily dip-oriented fluvial channel-fill sand bodies distributed complexly in a matrix of lower permeability, interchannel sands, muds, and lignites (Kaiser and others, 1978, 1980). In east-central Texas (fig. 1), the Wilcox contains relatively homogeneous, laterally extensive sands of the Simsboro Formation. Directly overlying the Wilcox in subcrop is the Carrizo Sand, which is similar in lithology to the Simsboro and probably interconnects with upper sands of the Wilcox (Calvert Bluff Formation or its equivalent) in many areas (fig. 2). The Carrizo Sand and channel-fill sands of the Wilcox Group and its Simsboro Formation are the major water-transmissive elements that might pose the most serious water-inflow problems to surface or subsurface mines.

WILCOX SAND BODIES AND GROUND-WATER FLOW

Ground-water flow through the multiple sand bodies of the Wilcox Group was recently analyzed quantitatively using a three-dimensional, numerical model of an area located in the southwest corner of the East Texas Basin (Fogg and others, in press). The area covers about 500 mi^2 (1,300 km^2) and is centered on deep-basin lignite resource block 8 of Kaiser and others (1980) (fig. 1). Following is a list of pertinent conclusions.

(1) Channel-fill sand bodies form the major aquifers, and according to lab and field testing of hydraulic conductivity, they are more permeable than surrounding Wilcox strata by a factor of at least 10 to 100.

(2) Average ground-water flow rates are generally on the order of 10^{-2} to 10^{-3} ft/d (3×10^{-3} m/d) in sections where channel-fill sands are numerous and interconnected, but 10^{-3} to 10^{-5} ft/d (3×10^{-4} to 3×10^{-6} m/d) in sections where channel-fill sands are either missing or too sparse to be interconnected (such as, in interchannel areas). Sand

body interconnectedness is a key factor affecting ground-water flow. Lignite resources are preferentially located in muddy, interchannel facies, where the probability of encountering channel-fill sands, and hence mine-related water problems, is smallest. However, channel-fill sands do exist in the interchannel sections, and the model demonstrates that if these sands are laterally interconnected, they will support ground-water fluxes comparable to those in sections where channel-fill sands appear more numerous and interconnected.

(3) The model together with measured hydraulic head versus depth (or pressure versus depth) trends demonstrate that, in the East Texas Basin, Wilcox sands are seldom interconnected vertically. In fact, average vertical hydraulic conductivity of aquitards that separate the channel-fill sands is lower than hydraulic conductivity of the sands by a factor of at least 10^3 to 10^4. This low conductivity is favorable to mining because it retards the vertical leakage (recharge) to sands that will drain laterally into a pit mine or to lignite strata that would be tapped by an in situ gasifier. Instances where sands are interconnected vertically can be detected by observing vertical hydraulic gradients ($\partial h/\partial z$) measured between wells. A $\partial h/\partial z$ value of 0.0 ± 0.01 surrounded on all sides by larger negative or positive values indicates good vertical interconnection (assuming hydraulic heads have not been changed artificially by ground-water pumping). Regionally persistent, non-zero values of $\partial h/\partial z$ indicate poor vertical interconnection.

(4) Ground-water flow rates may decrease by a factor of as much as 100 from top to bottom of the Wilcox, owing to a corresponding decrease in horizontal hydraulic gradients.

(5) Key uncertainties in the model and in our overall understanding of deep-basin Wilcox hydrology are lateral interconnectedness of sand bodies, hydraulic conductivity of the less permeable interchannel sands, and hydraulic heads at depths below about 1,000 ft

(305 m). A drilling program that will collect these and other types of hydrogeologic data is currently being planned.

RECHARGE AND DISCHARGE AREAS

Hydraulic head data and water chemistry indicate that regional ground-water circulation in the Wilcox-Carrizo system is controlled primarily by topography and geologic structure. Major recharge areas coincide with topographic highs in outcrops, and major discharge areas coincide with major streams (such as the Sabine, Trinity, Brazos, and Colorado Rivers). Outcropping sand bodies commonly form "sand hills" that are presumably important recharge areas (Henry and Basciano, 1979). Downdip of outcrops, where the Wilcox-Carrizo is overlain by the Reklaw aquitard, there is potential for recharge and discharge via downward and upward leakage across the aquitard. In the East Texas Basin, fluid pressure versus depth trends and hydraulic head differentials measured between aquifers at depths generally less than 1,000 ft (305 m) indicate potential for downward fluid movement practically everywhere except beneath floodplains of certain streams.

Surface mine dewatering or depressurization problems might be more serious in discharge areas than in recharge areas. Discharge areas are characterized by a shallow or artesian potentiometric surfaces, increasing hydraulic head with depth, and converging ground-water flow. Recharge areas are characterized by a relatively deep water table, decreasing hydraulic head with depth, and diverging ground-water flow. Similarly, the fate of ground-water contaminants should be quite different in recharge areas and discharge areas, owing to differing hydraulic conditions and ground-water chemistry. Mine effluent that is introduced to a recharge zone should move downward, thereby lengthening the travel time and distance to the biosphere and allowing greater dispersion and geochemical attenuation (adsorption, ion exchange, and precipitation) of dissolved

contaminants. Of course, the major recharge areas that sustain large parts of the aquifer should not be mined extensively, in order to avert large-scale impacts on the ground-water system.

Recharge and discharge areas can be mapped through a collective analysis of data on geology, aquifer hydraulics (head and pressure), and ground-water chemistry. Many of the maps and plots basic to such an analysis are included elsewhere in this report. The chemical composition of ground water is commonly observed to evolve systematically along the flow path and thus can be used as a tracer for ground-water flow. In general, as Wilcox and Carrizo ground waters flow from recharge areas to discharge areas, they are altered chemically from acidic, oxidized calcium-magnesium-bicarbonate waters to basic, reduced sodium-bicarbonate waters. Kaiser and Ambrose (this report) and Macpherson (this report) discuss the reactions that control this change.

Water chemistry is particularly useful for detecting anomalous hydraulic conditions, such as local recharge areas located within regional discharge areas. Furthermore, delineation of water chemistry trends is necessary for predicting the degree to which mine effluent will be attenuated by the aquifer. For example, the typically basic, high-bicarbonate waters of the Wilcox will tend to neutralize acid mine-drainage and to reduce the mobility of most trace metals (Committee on Ground-Water Resources in Relation to Coal Mining and others, 1981; Stumm and Morgan, 1981). Finally, knowledge of the ground-water chemistry and quality is necessary for assessing impacts of mining on fresh-water resources. General water quality can often be inferred from electric logs (Fogg and Blanchard, this report). Regional salinity mapping in the Wilcox of the East Texas Basin indicates that much of the deep-basin lignite in the lower Wilcox coincides with intervals containing moderately brackish ground-water, beneath the fresh-water section (Fogg and Kreitler, in press).

GROUND-WATER HYDRAULICS OF THE WILCOX-CARRIZO AQUIFER SYSTEM, SABINE UPLIFT AREA

Graham E. Fogg and David A. Prouty

ABSTRACT

Data on hydraulic head, fluid pressure, hydraulic conductivity, and transmissivity for the Wilcox-Carrizo aquifer system were accumulated and plotted on potentiometric surface maps, a vertical hydraulic gradient map, pressure versus depth diagrams, and frequency diagrams. Ground-water flow closely follows topography in the Wilcox-Carrizo outcrop area. Elsewhere, correlation with topography is weaker, owing to greater depths of the aquifer and hence greater confinement by overlying mud strata. Major ground-water discharge areas appear to be the Sabine River, Big and Little Cypress Bayous, Attoyac Bayou, and several of their tributaries. The vertical flow component is predominantly downward. Low values of the vertical hydraulic gradient may in some cases indicate vertically interconnected sand bodies.

INTRODUCTION

Ground-water hydraulics is the study of ground-water circulation as a distribution of potential energy (hydraulic head) in the system. Available data on hydraulic head from measurements in monitoring wells were analyzed and mapped, resulting in delineation of recharge and discharge areas and ground-water flow patterns. Horizontal flow components for the Wilcox-Carrizo aquifer system and the Carrizo aquifer are shown in potentiometric surface maps; and vertical flow components for the Wilcox-Carrizo are shown using fluid pressure versus depth relationships and maps showing vertical component of the hydraulic gradient. This three-dimensional approach is necessary because the Wilcox is thick (up to 3,600 ft [1,098 m]) and contains multiple sand bodies that may not always be interconnected (Fogg and others, in press). Also included in this section are frequency distributions of hydraulic conductivity and transmissivity values obtained from pumping tests.

METHODS

The sources of hydraulic head data are the Water-Oriented Data Bank of the Texas Natural Resources Information System (TNRIS), Central Records of the Texas Department of Water Resources (TDWR), and several TDWR reports on ground-water resources of individual counties in the study area (Dillard, 1963; Broom and Myers, 1966; Anders, 1967; Broom, 1969 and 1971; and Guyton and Associates, 1970 and 1972). The data are from measurements made during the 1950's-60's and 70's, although 80 percent were made during the 1960's and early 1970's. This time period was chosen because it provides the greatest number of data points. Water level changes resulting from pumpage during the period of measurements were generally slight, except near certain cities where pumping rates are relatively high.

The potentiometric surface contours in figures 10 and 12 were drawn to closely conform to the data, but in some cases an anomalous data point was ignored or given less weight in the contouring process. Probable causes of anomalies include: (1) head measurements made at different times in areas of intense pumpage, (2) adjacent wells tapping different horizons of the Wilcox-Carrizo that have different hydraulic heads, and (3) measurement error. The resulting potentiometric surface maps are reliable for regional interpretation, but local conditions can be much more complex than is indicated by the maps.

The pressure-depth (P-D) method of analysis was applied to the East Texas Basin (excluding most of the present study area) by Fogg and Kreitler (1982) (see also Fogg, 1980 and 1981) and was found effective for delineating regional trends in the vertical component of flow. Slope of the P-D trend indicates direction of the vertical flow component: downward when $\underline{m} < 1$ and upward when $\underline{m} > 1$ (figs. 13 and 14; table 2). Vertical component of the hydraulic gradient ($\partial h / \partial z$) equals $\underline{m}$ minus 1.00. As mentioned in Fogg and Kaiser (this report), regionally consistent, non-zero values of $\partial h / \partial z$ strongly

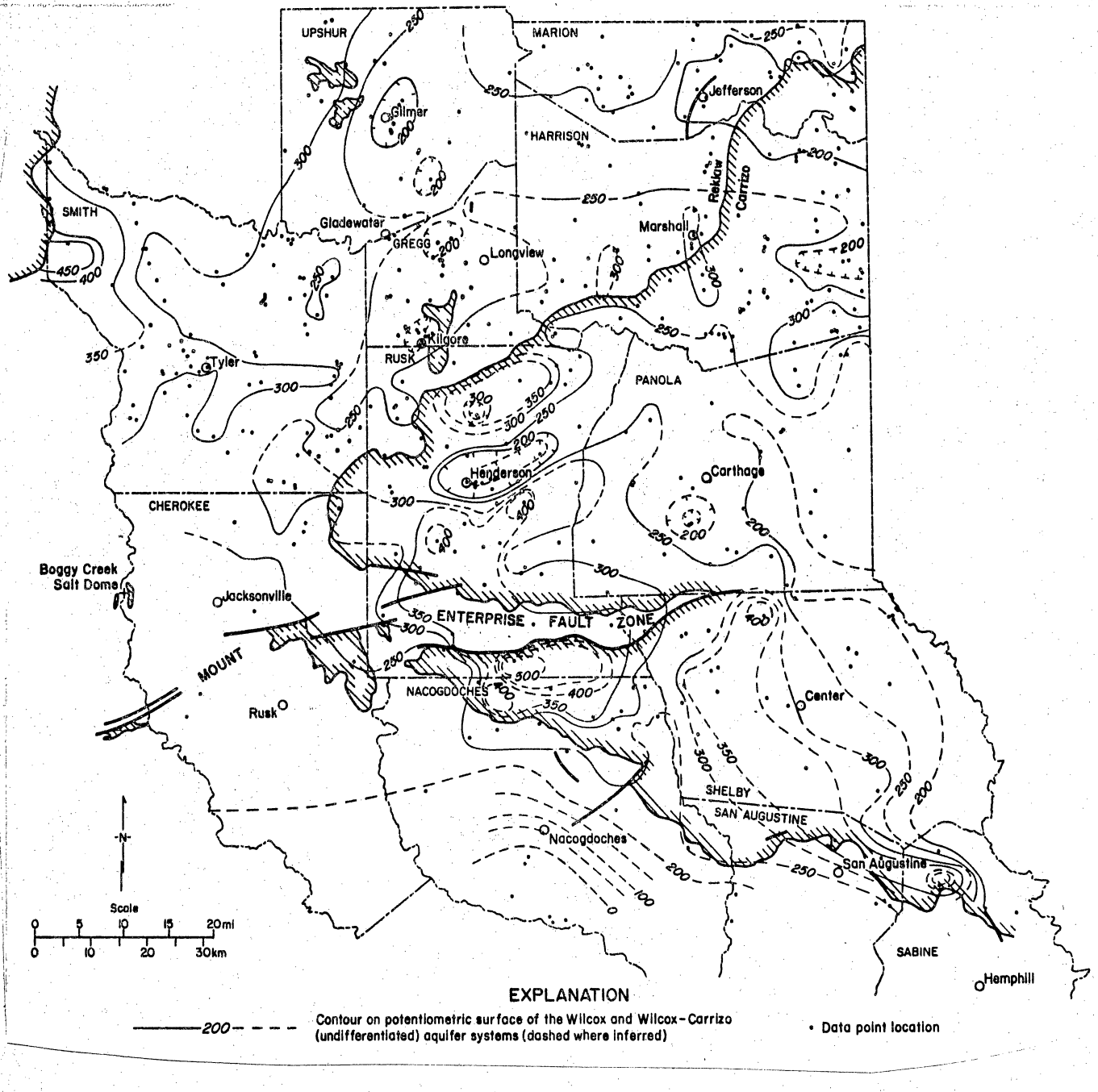

Figure 10. Potentiometric-surface map, Wilcox-Carrizo aquifer system. Data are from wells tapping Wilcox and Wilcox (undivided) strata. Measurements are circa 1960's and early 1970's. The map is considered reliable for regional interpretation, but local hydraulic gradients can be much more complex.

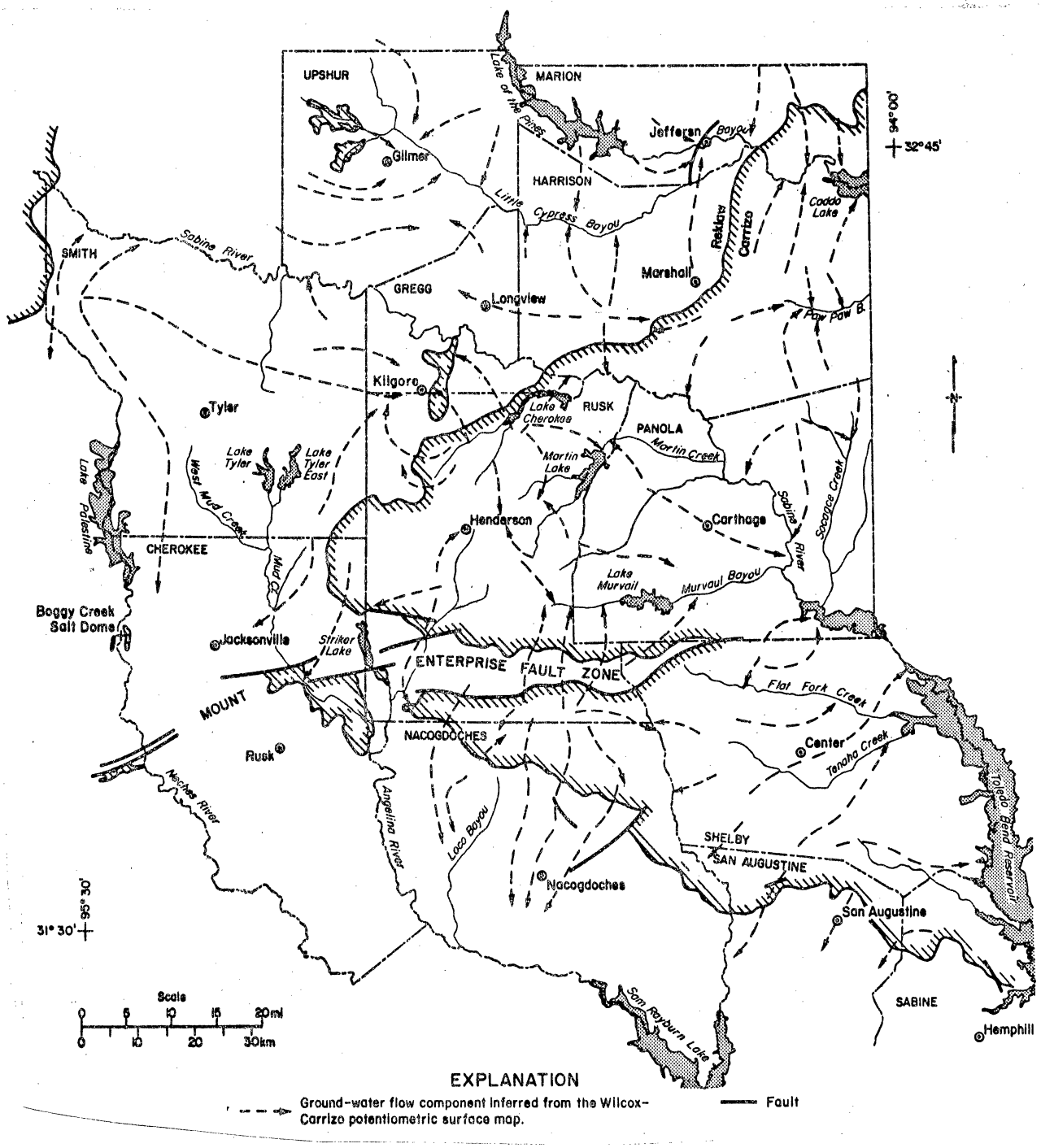

Figure 11. Ground-water flow lines inferred from the Wilcox-Carrizo potentiometric surface map. Major discharge areas are the Sabine River, Big and Little Cypress Bayous, Attoyac Bayou, and several of their tributaries. Major recharge areas are in the Wilcox-Carrizo outcrop areas in Rusk, Nacogdoches, and Shelby Counties.

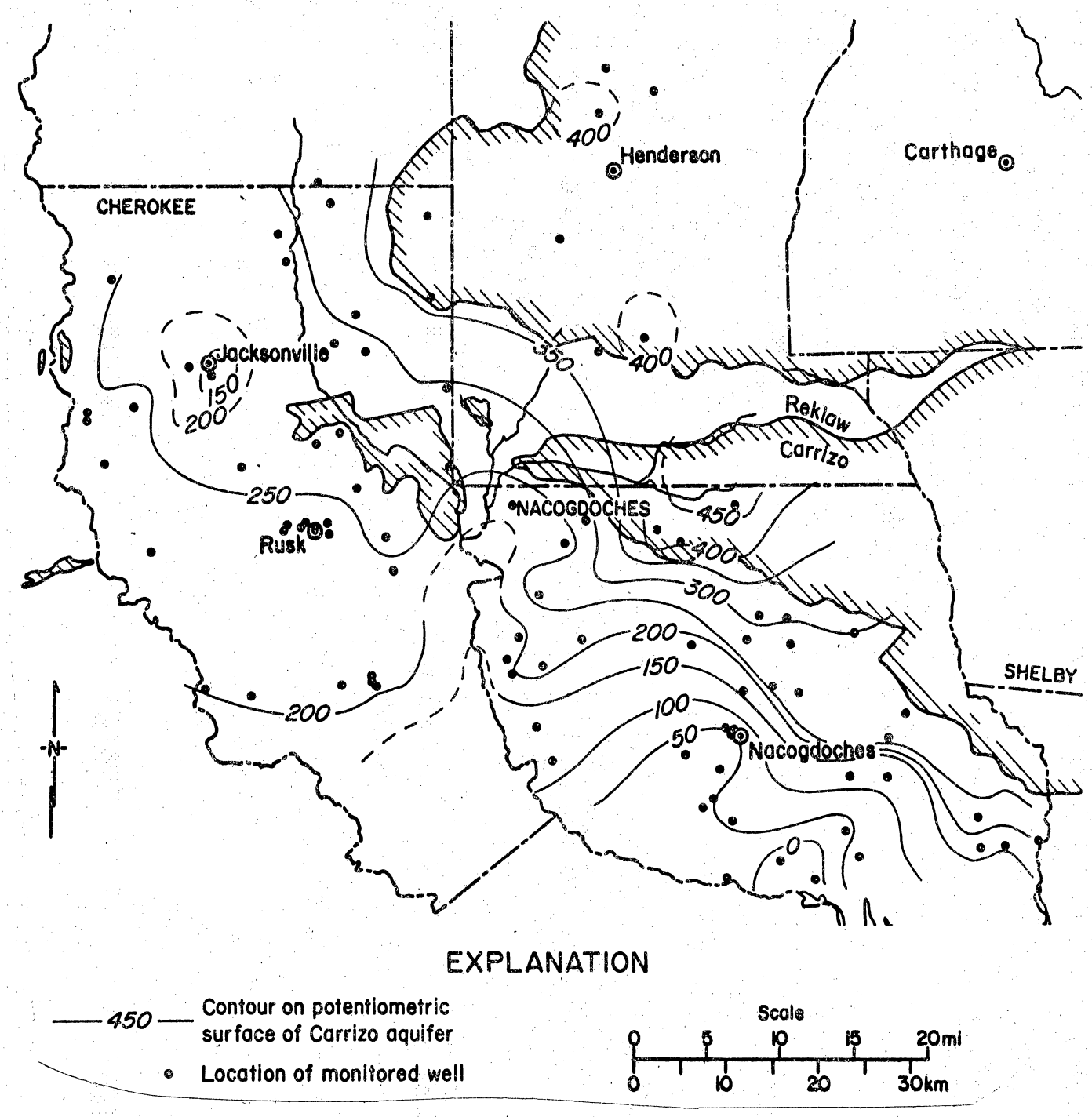

Figure 12. Potentiometric-surface map, Carrizo aquifer.

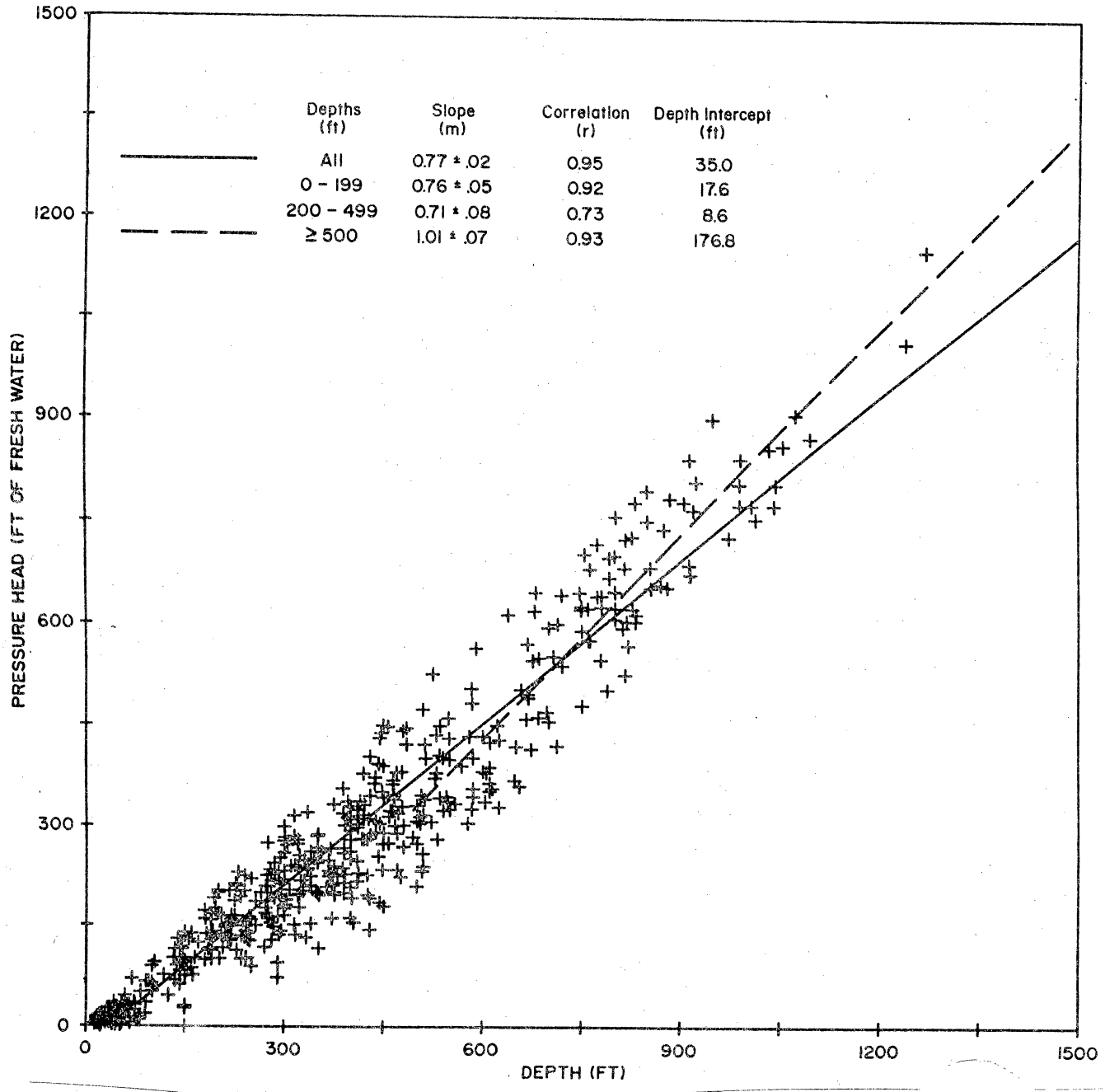

Figure 13. Graph of fluid pressure versus depth (P-D) for Wilcox-Carrizo system. Data are from wells tapping Wilcox-Carrizo (undivided). Measurements are circa 1960's and early 1970's. Pressure data indicating water levels deeper than 300 ft (91.4 m) were not included in order to minimize errors caused by drawdowns from heavy pumpage; virgin water levels are presumed to have been less than 300 ft (91.4 m) deep. Slope ($\underline{m}$) of the P-D regression line indicates direction of the vertical flow component: flow is upward when $\underline{m} > 1$ and downward when $\underline{m} < 1$. The depth intercept represents the depth at which the regression line intersects zero pressure. The vertical component of flow is generally downward in the Sabine Uplift region, except below 500 ft (152 m), where there is apparently little potential for vertical flow.

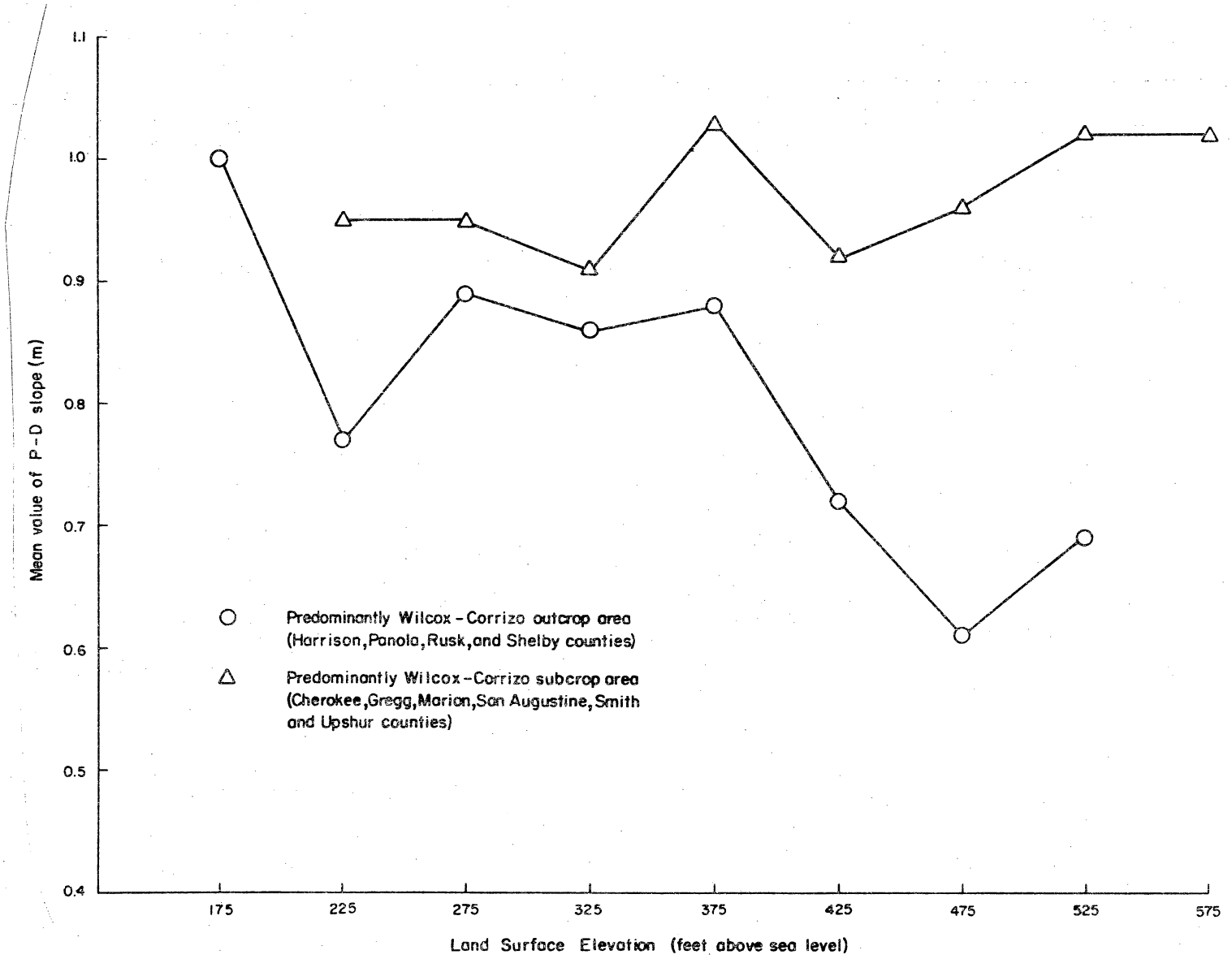

Figure 14. Graph of mean slope (m) of P-D regression lines (table 1) for 50-ft (15.2 m) intervals of land surface elevation. The outcrop data show a general trend of decreasing m with increasing elevations, reflecting greater recharge (and hence greater downward movement) at higher elevations. In comparison, the subcrop m values are everywhere closer to a value of 1.00 and generally increase with elevation. This increase is partly caused by high m values in Smith County above 500 ft (152.4 m) (table 1).

Table 2. Pressure versus depth (P-D) statistics, Sabine Uplift region.

Land Surface (ft)	150 - 200 m (D-range)	r	n	200 - 250 m (D-range)	r	n	250 - 300 m (D-range)	r	n	300 - 350 m (D-range)	r	n	350 - 400 m (D-range)	r	n
Cherokee	n.d.			n.d.			n.d.			n.s.			n.d.		
Gregg	n.d.			n.d.			0.99 ± .04 (50-975)	0.99	7	0.96 ± .22 (300-825)	0.96	8	**1.05 ± .08 (225-975)**	0.98	19
Harrison	0.99 ± .19 (75-375)	0.99	3	0.91 ± .22 (10-225)	0.93	11	0.98 ± .10 (10-600)	0.97	23	0.88 ± .05 (10-900)	0.96	34	0.93 ± .08 (10-825)	0.97	24
Marion	n.d.			0.95 ± .04 (10-900)	0.99	11	0.91 ± .03 (10-825)	0.99	24	0.94 ± .13 (10-750)	0.99	7	n.d.		
Nacogdoches	n.d.			n.s.			n.s.			0.61 ± .13 (50-675)	0.94	11	0.48 ± .26 (10-600)	0.91	5
Panola	n.d.			0.54 ± .53 (10-75)	0.77	5	0.92 ± .10 (10-450)	0.99	9	0.84 ± .23 (50-450)	0.86	17	n.d.		
Rusk	n.d.			n.d.			n.s.			0.86 ± .56 (75-450)	0.96	3	0.82 ± .16 (50-375)	0.97	8
Sabine	n.d.			n.s.			n.d.			n.d.			n.d.		
San Augustine	n.d.			n.d.			n.d.			n.d.			n.s.		
Shelby	**1.01 ± .05 (10-225)**	0.99	3	0.85 ± .22 (10-225)	0.93	6	0.78 ± .10 (50-375)	0.99	3	0.85 ± .11 (10-225)	0.99	5	0.88 ± .01 (50-825)	0.99	4
Smith	n.d.			n.d.			n.d.			0.93 ± .05 (150-825)	0.99	5	**1.06 ± .07 (225-900)**	0.99	10
Upshur	n.d.			n.d.			n.d.			0.82 ± 1.30 (375-600)	0.83	3	0.99 ± .20 (300-750)	0.94	12
MEAN m	1.00			0.81			0.92			0.85			0.89		

m - slope
D-range - depth (ft) range of data
r - correlation coefficient
n - number of data points
n.d. - no data
n.s. - not significant
Boldface - indicates m>1.00

Table 2. (cont.)

Land Surface (ft)	400 - 450 m (D-range)	r	n	450 - 500 m (D-range)	r	n	500 - 550 m (D-range)	r	n	550 - 600 m (D-range)	r	n
Cherokee	0.91 ± .09 (225-600)	0.99	6	n.d			n.s			n.d.		
Gregg	0.98 ± .07 (300-900)	0.99	5	n.d.			n.d.			n.d.		
Harrison	n.s.			n.d.			n.d.			n.d.		
Marion	n.d.			n.d.			n.d.			n.d.		
Nacogdoches	0.83 ± .46 (225-675)	0.87	6	0.46 ± .56 (225-600)	0.78	4	n.d.			n.d.		
Panola	n.s.			n.d.			n.d.			n.d.		
Rusk	0.83 ± .11 (10-1125)	0.93	16	0.61 ± .16 (225-825)	0.79	14	0.69 ± .17 (375-825)	0.94	10	n.d.		
Sabine	n.d.			n.d.			n.d.			n.d.		
San Augustine	**1.12 ± .08 (50-225)**	0.99	3	n.d.			n.d.			n.d.		
Shelby	0.61 ± .07 (50-375)	0.99	5	n.d.			n.d.			n.d.		
Smith	0.91 ± .05 (150-1275)	0.99	25	0.96 ± .07 (300-900)	0.99	15	**1.02 ± .06 (450-1050)**	0.99	17	**1.02 ± .04 (450-1050)**	0.99	9
Upshur	0.69 ± .41 (300-675)	0.79	8	n.d.			n.d.			n.d.		
MEAN m	0.86			0.68			0.86			1.02		

indicate that Wilcox-Carrizo sands are not interconnected vertically; and anomalous, zero values of $\partial h/\partial z$ indicate good interconnection vertically.

The value of $\partial h/\partial z$ shown in 7.5-minute quadrangle in figures 15 and 16 represents the slope of a least-squares regression line fit through a plot of hydraulic head versus well depth (measured from mean sea level) for wells contained in the quadrangle. Regressions and statistics were run with the SPSS computer statistical package (Nie and others, 1975). The additional information on standard error of $\partial h/\partial z$ and number of data points in each quadrangle can be used to set confidence limits for $\partial h/\partial z$. For example, assuming the data are normally distributed, there is approximately a 68-percent chance that true $\partial h/\partial z$ values are within an interval defined by plus or minus the standard error. Different confidence limits (for example, 95-percent) might be calculated by applying a student's t distribution using the number of data points as the number of degrees of freedom (Nie and others, 1975, or Hoel, 1971). In the generalized map of $\partial h/\partial z$ (fig. 16) only directions of $\partial h/\partial z$ are indicated (positive-up and negative-down) in order to illustrate probable locations of recharge and discharge areas. Quadrangles in which the standard error is less than or equal to the absolute value of $\partial h/\partial z$ are indicated by the lighter patterns. Thus, the lighter patterns indicate either lack of a consistent $\partial h/\partial z$ trend or a consistent $\partial h/\partial z$ trend that is close to zero.

RESULTS

The head and pressure data show trends in ground-water circulation similar to those found by Fogg and Kreitler (1982). Moreover, many of these same trends are evident in the hydrochemical maps by Kaiser and Ambrose (this report). Ground-water flow follows closely the surface topography in the Wilcox-Carrizo outcrop area. Elsewhere, the correlation with topography is weaker, owing to greater depths of the aquifer and hence to greater confinement by muds of the Wilcox Group and the Reklaw and Queen City

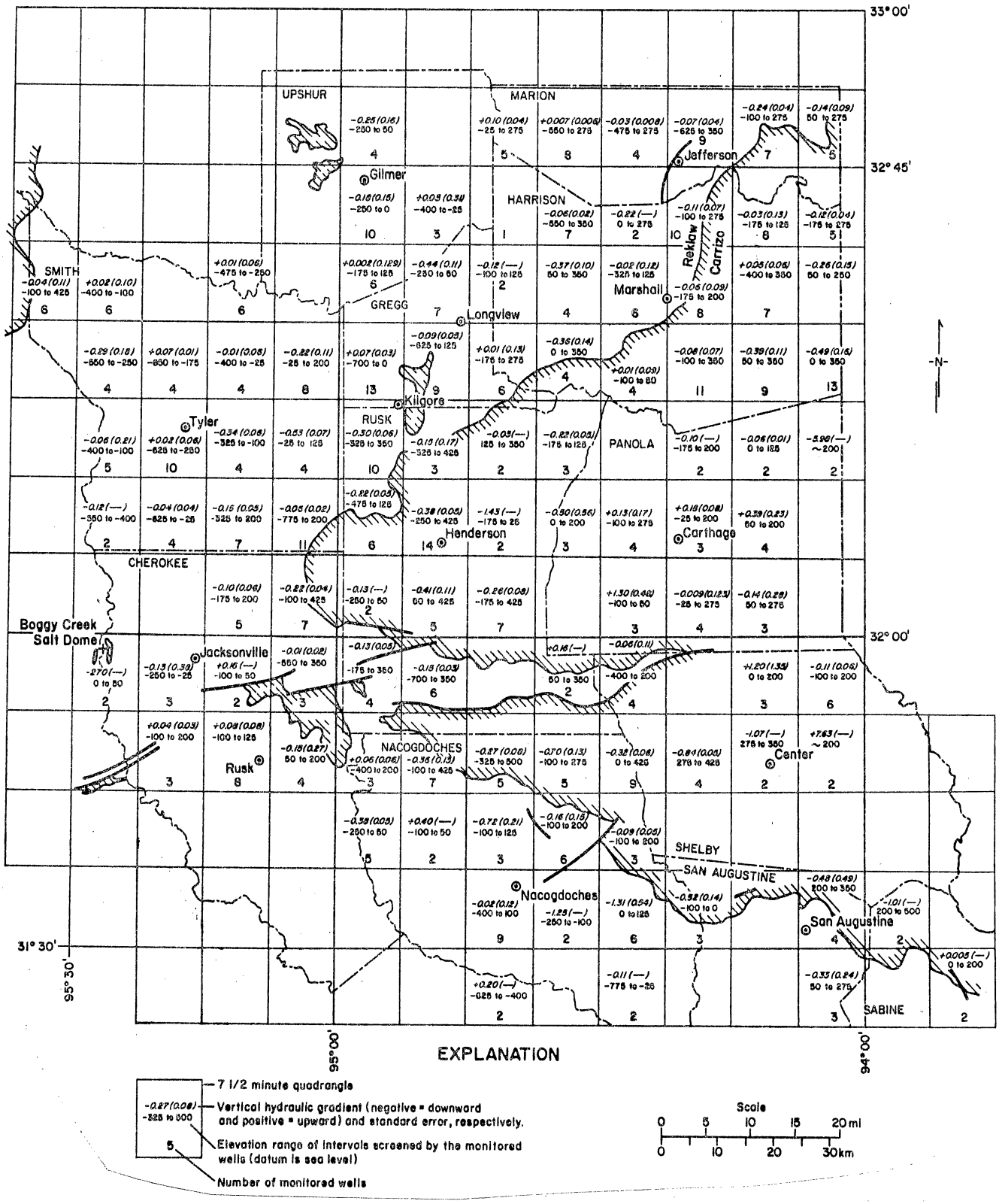

Figure 15. Map showing vertical component of the hydraulic gradient ($\partial h / \partial z$) determined by least-squares linear regression for data in each 7.5-minute quadrangle. Positive and negative values indicate potential for upward and downward movement, respectively. Presence of a measurable $\partial h / \partial z$ value indicates potential for vertical flow and poor vertical interconnection of sand bodies. The standard error values shown can be used to calculate confidence limits for the vertical hydraulic gradient.

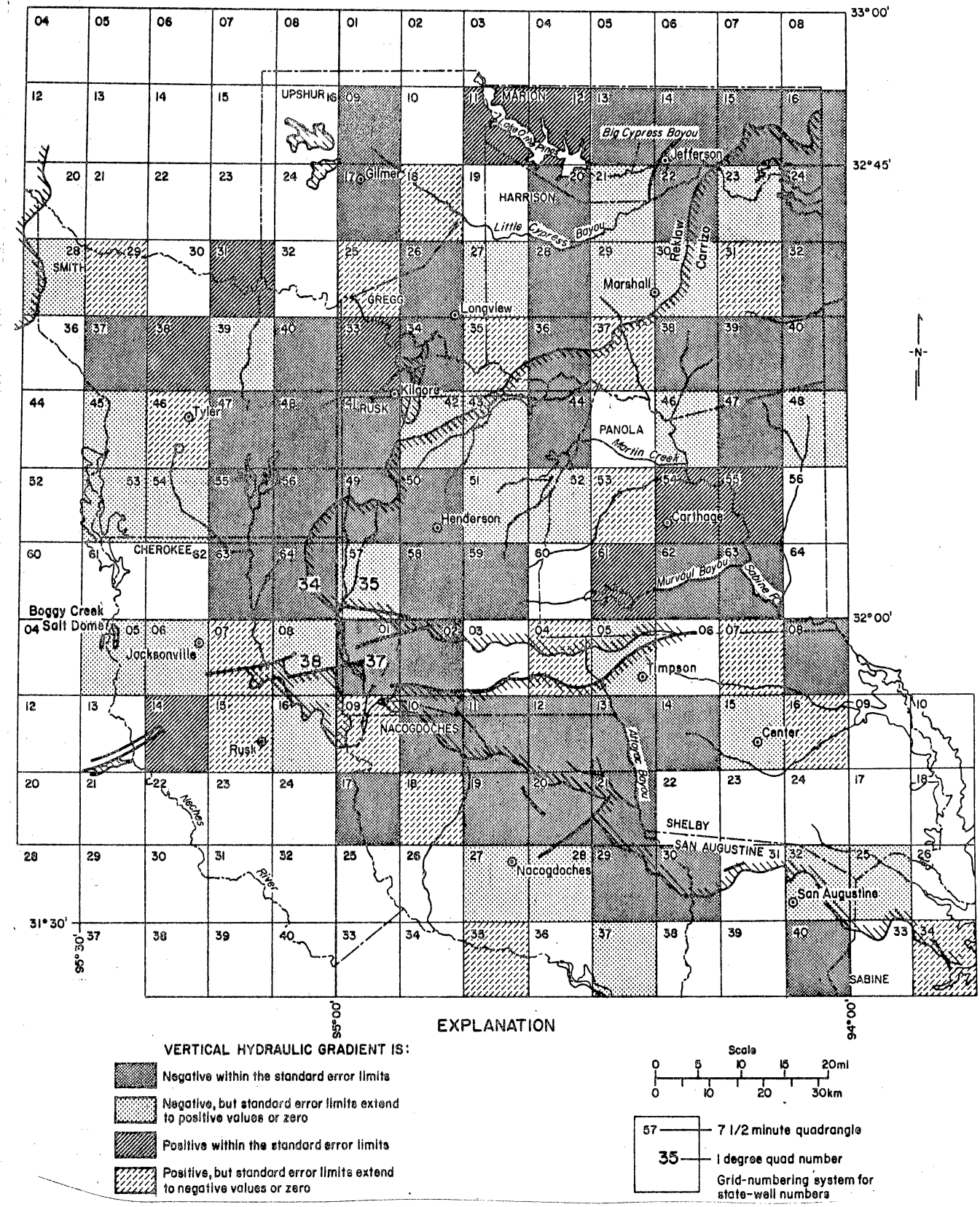

Figure 16. Generalized version of figure 6 indicating only the signs of $\partial h/\partial z$: positive indicates upward flow and negative, downward flow. Darker patterns represent relatively reliable trends for which the standard error is less than the absolute value of $\partial h/\partial z$; lighter patterns indicate less reliable trends for which the standard error is greater than or equal to the absolute value of $\partial h/\partial z$.

Formations. Major discharge areas appear to be the Sabine River, Big and Little Cypress Bayous, and Attoyac Bayou. Several smaller streams are also important discharge areas (Martin Creek and Murvaul Bayou in Rusk and Panola Counties, fig. 11). Localized closed depressions in the potentiometric surface maps (figs. 10 and 12) are caused by relatively intense ground-water pumpage in Cherokee County (city of Jacksonville), Gregg County, Upshur County, and Rusk County (city of Henderson). Pumpage in Nacogdoches County has lowered heads to near sea level.

The P-D and $\partial h/\partial z$ data (table 2 and figs. 13, 14, 15, and 16) indicate that the vertical flow component is predominantly downward, especially at higher land surface elevations in the Wilcox-Carrizo outcrop area. Discharge areas make up a small percentage of the total area, and should therefore contain relatively intense ground-water flow velocities. Most of our data are for depths less than 1,000 ft (305 m), and thus deeper hydraulic conditions can only be inferred.

Note that in the pressure-depth plot of all the data (fig. 13) three different trends are evident at depth intervals 0 to 199 ft (0 to 61 m), 200 to 499 ft (61 to 152 m), and greater than 500 ft (152 m). These three trends are reminiscent of Tóth's (1963) theoretical delineation of shallow, intermediate, and deep flow systems. The data for the shallow system indicate predominantly downward flow ($\underline{m} = .76 \pm .05$) and good correlation. The data for intermediate system show a similar trend but with a much lower correlation, suggesting greater variability in flow direction and perhaps a transition between shallow and deep hydrodynamic conditions. The deep data indicate predominantly horizontal flow ($\underline{m} = 1.01 \pm .07$), probably reflecting greater confinement and isolation from overlying recharge areas. Furthermore, the depth intercept of the deep data exceeds that of the rest by as much as 168 ft (51.2 m), indicating much lower hydraulic heads.

Finally, the frequency distributions of hydraulic conductivity (K) and transmissivity (T) (figs. 17 and 18), can be used to estimate probabilities for different values of K and T. Figures 18a and 18b are cumulative probability plots showing the probability that a given value of K or T would be exceeded in a random sampling. Nearly all of these data are from the relatively permeable, channel-fill sand bodies of the Wilcox or Carrizo. No published data are available for the muddier, interchannel sands that are commonly associated with the lignite seams. Note that K forms approximately a log-normal distribution, as is commonly found with K data (Freeze, 1975).

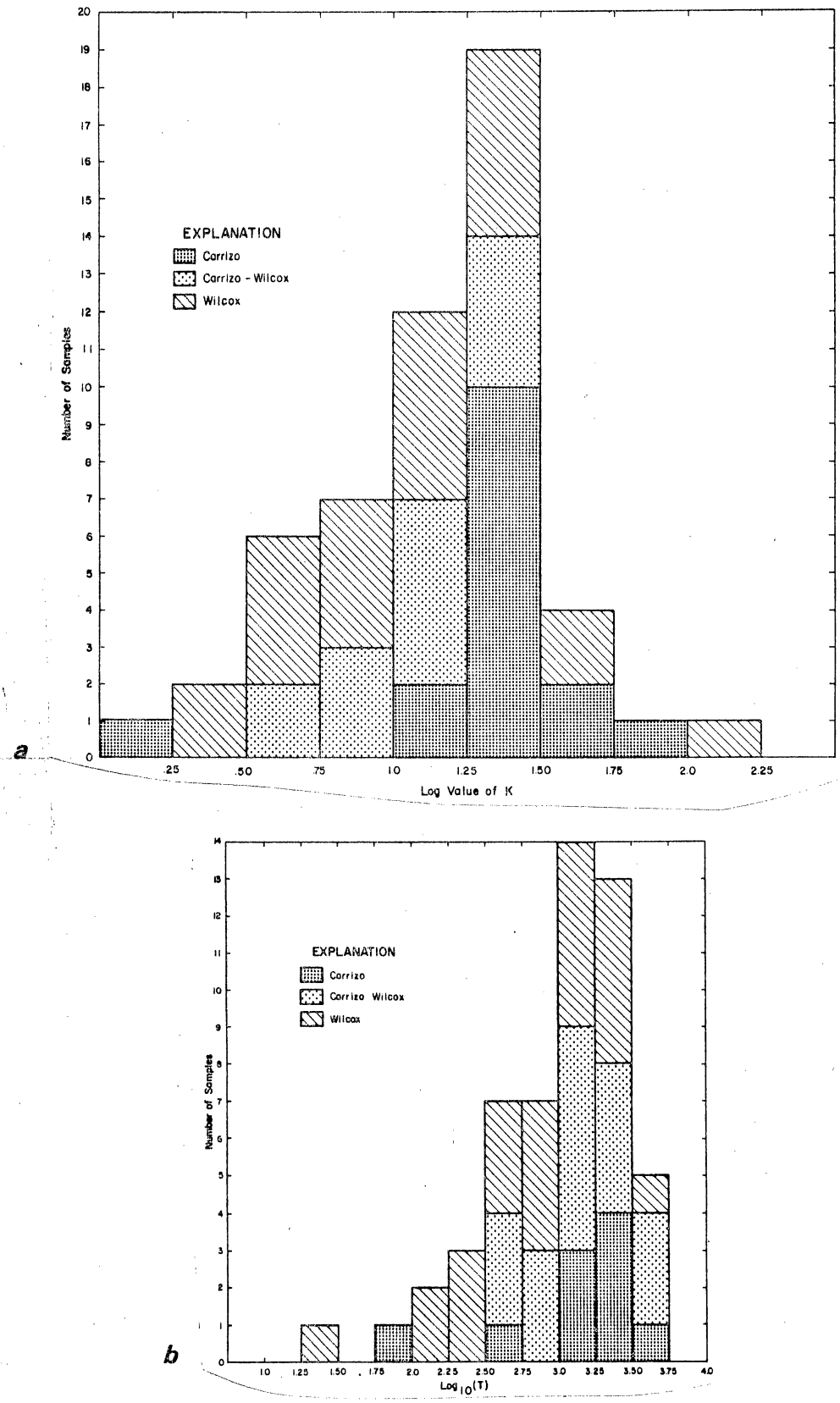

Figure 17. Histograms showing frequencies of (a) log [hydraulic conductivity] (ft/day) and (b) log [transmissivity] (ft^2/day). Data are from pumping test results published in W. F. Guyton and Associates (1972, 1970), Myers (1969), and Broom (1971). Hydraulic conductivity is distributed approximately log-normally.

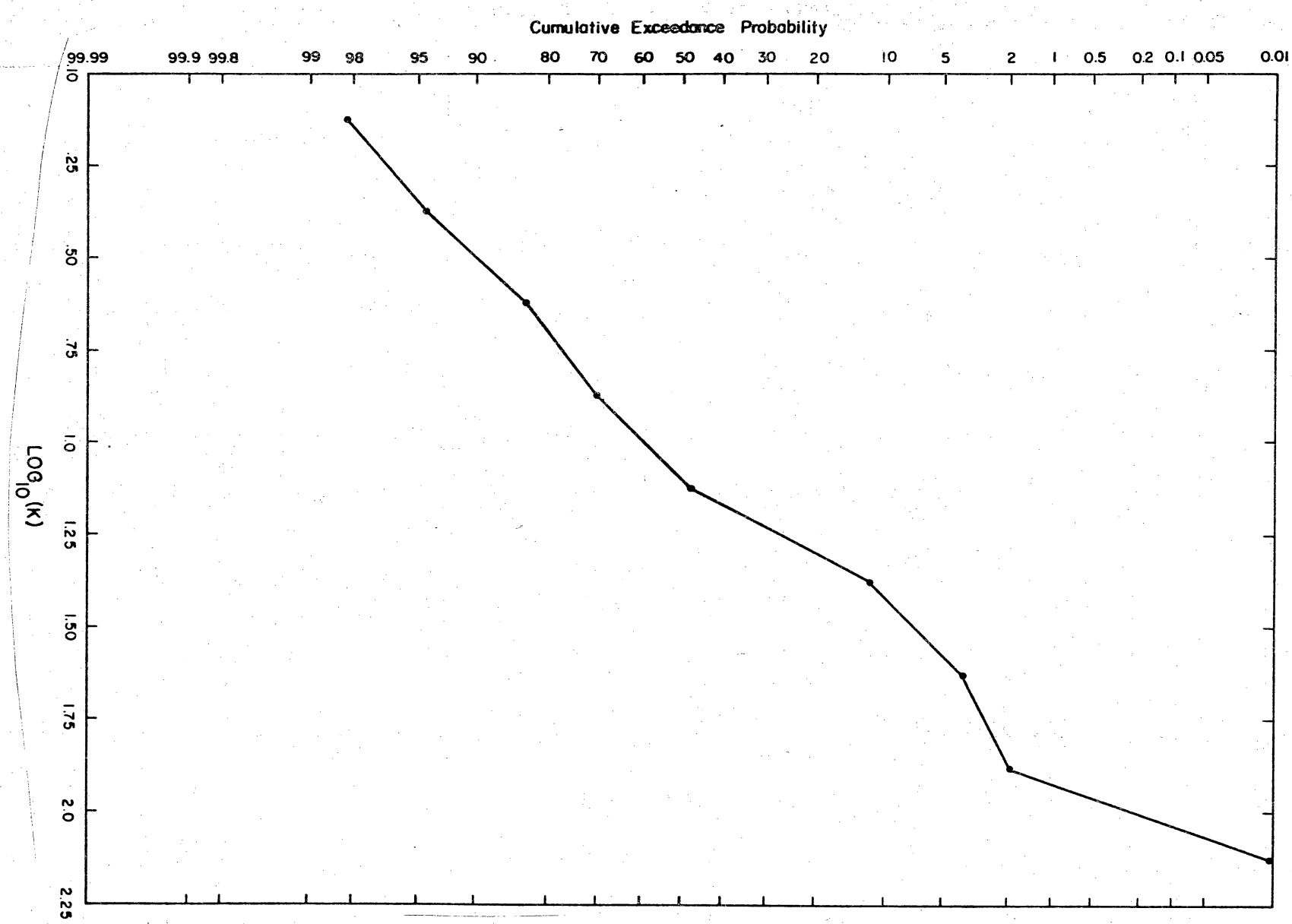

Figure 18A. Cumulative exceedance probability for log [hydraulic conductivity] (ft/day) showing probability that a given value of K or T would be exceeded in a random sampling. For example, there is a 27 percent chance that a log (K) value of 1.25 ($K = 10^{1.25} = 17.8$ ft/day) would be exceeded. Most of these data are from depths of less than 1,000 ft (305 m).

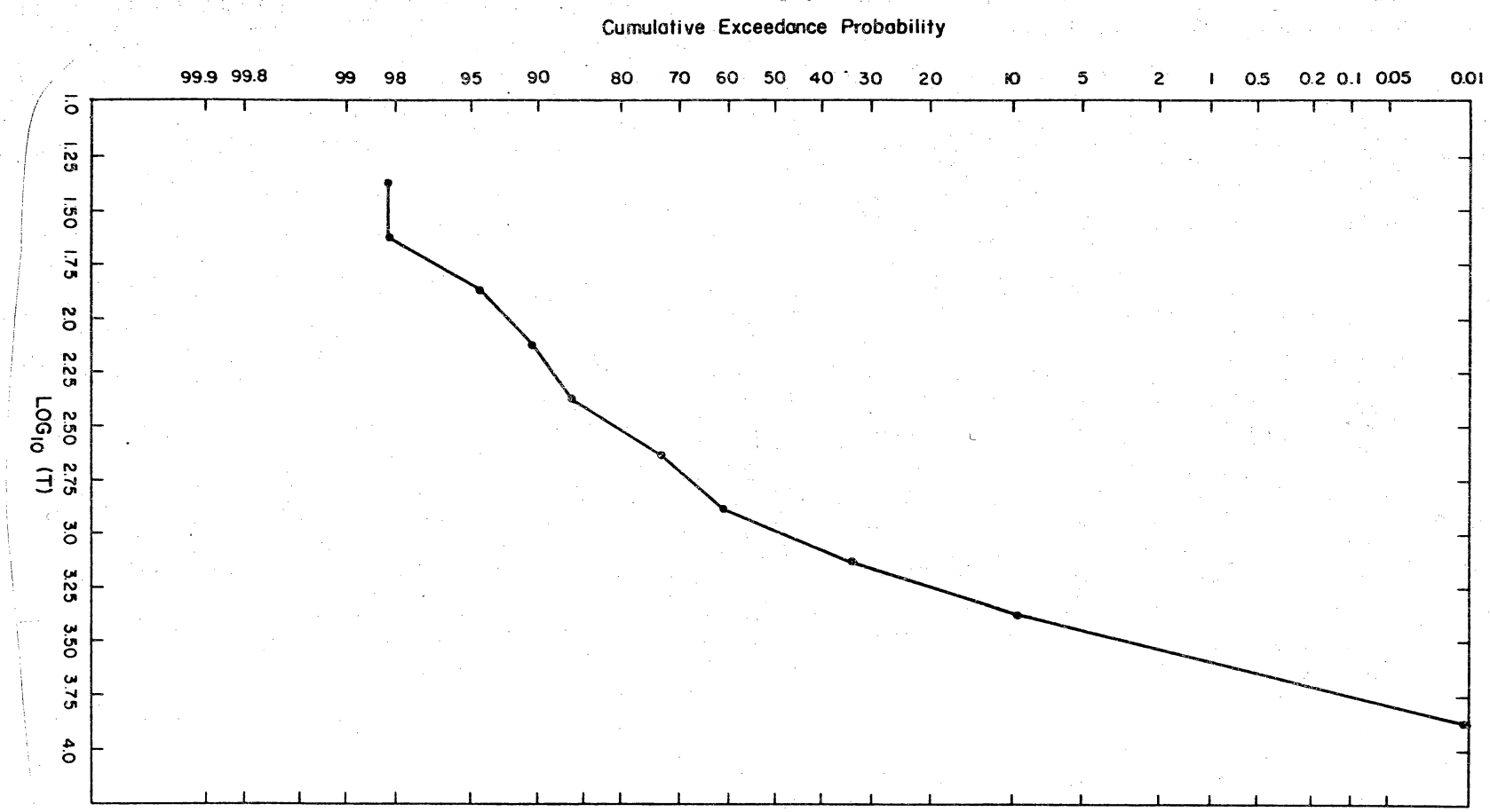

Figure 18B. Cumulative exceedance probability for log[transmissivity] (ft^2/day) showing probability that a given value of K or T would be exceeded in a random sampling. For example, there is a 27 percent chance that a log (K) value of 1.25 ($K = 10^{1.25} = 17.8$ ft/day) would be exceeded. Most of these data are from depths of less than 1,000 ft (305 m).

HYDROLOGY OF THE EAST-CENTRAL TEXAS WILCOX GROUP

by G. L. Macpherson

ABSTRACT

The Wilcox Group potentiometric surface in east-central Texas is largely topographically controlled. Potentiometric highs are found along surface-water drainage divides; potentiometric lows correspond to rivers and major streams. Hydraulic gradients are steeper near the divides than near the rivers and streams, and larger rivers are underlain by larger discharge areas. Southeastward, the Wilcox Group is covered by younger sediments. In this area, limited water-level data suggest that the hydraulic gradient is low and that discharge areas still appear to coincide with the locations of rivers and major streams.

In the overlying Carrizo Sand very few data are available but the potentiometric surface is also topographically controlled. Carrizo hydraulic heads are usually higher than Wilcox heads, indicating potential for movement of ground water from the Carrizo into the Wilcox.

INTRODUCTION

The east-central Texas area includes the region between the Colorado and Trinity Rivers along and just southeast of the outcrops of the Carrizo Sand and the Wilcox Group (Kaiser and others, 1980). For this study, Freestone and Leon Counties, located along the Trinity River, were excluded because of detailed work already completed in these counties (Kreitler and others, 1980, 1981; Fogg and others, in press).

The two maps constructed for this report are based entirely on water-level data available from two sources: the Water-Oriented Data Bank of the Texas Natural Resources Information System and the Texas Department of Water Resources files. One of the difficulties in constructing a regional potentiometric surface map is the wide variety of times at which water-level measurements have been taken. In the study area, water level measurements were typically made in county surveys; hence, measurements in the same county were generally made within 5 months of each other. Overall, however,

the measurements were made during 1964 to 1981. Because some water levels changed significantly from 1964 to 1981, the potentiometric surface (fig. 19) is contoured on a county-wide basis, and contours may be discontinuous at county borders. Flowlines, which represent the flow paths of ground water, integrate the county-wide potentiometric surfaces and identify the direction of ground-water flow in the Wilcox Group.

GROUND-WATER HYDRAULICS

The potentiometric surface map (fig. 19) illustrates the close relationship between potentiometric highs (recharge areas) and surface-water drainage divides and between potentiometric lows (presumed discharge areas) and rivers or major streams. The Brazos River, which forms the border between Milam and Robertson Counties, coincides with a large area in which the potentiometric surface is low. The Little Brazos River parallels the Brazos River in this area (fig. 20), and the San Gabriel/Little River joins the Brazos in the outcrop of the Wilcox Group. The existence of these rivers in the outcrop and the corresponding low in the potentiometric surface suggests that the size of the surface-water drainage system reflects the size of the ground-water discharge area. In contrast, the Navasota River in eastern Limestone and Robertson Counties and the Colorado River in central Bastrop County, which are smaller river systems in the region, are coincident with areas of potentiometric lows, but the areas are much smaller. The flowlines (fig. 20) also show that ground water in the Wilcox moves from the vicinity of surface-water drainage divides, which are topographically high, to rivers and streams. Even relatively small streams, such as Cedar Creek in Bastrop County and Plum Creek in Caldwell County, appear to be receiving effluent from the Wilcox aquifer, as evidenced by relative potentiometric lows and converging flowlines along the streams. The hydraulic gradient (change in hydraulic head per unit length) is steeper near the surface-water drainage divides than in the vicinity of the rivers. This is presumably because of the greater

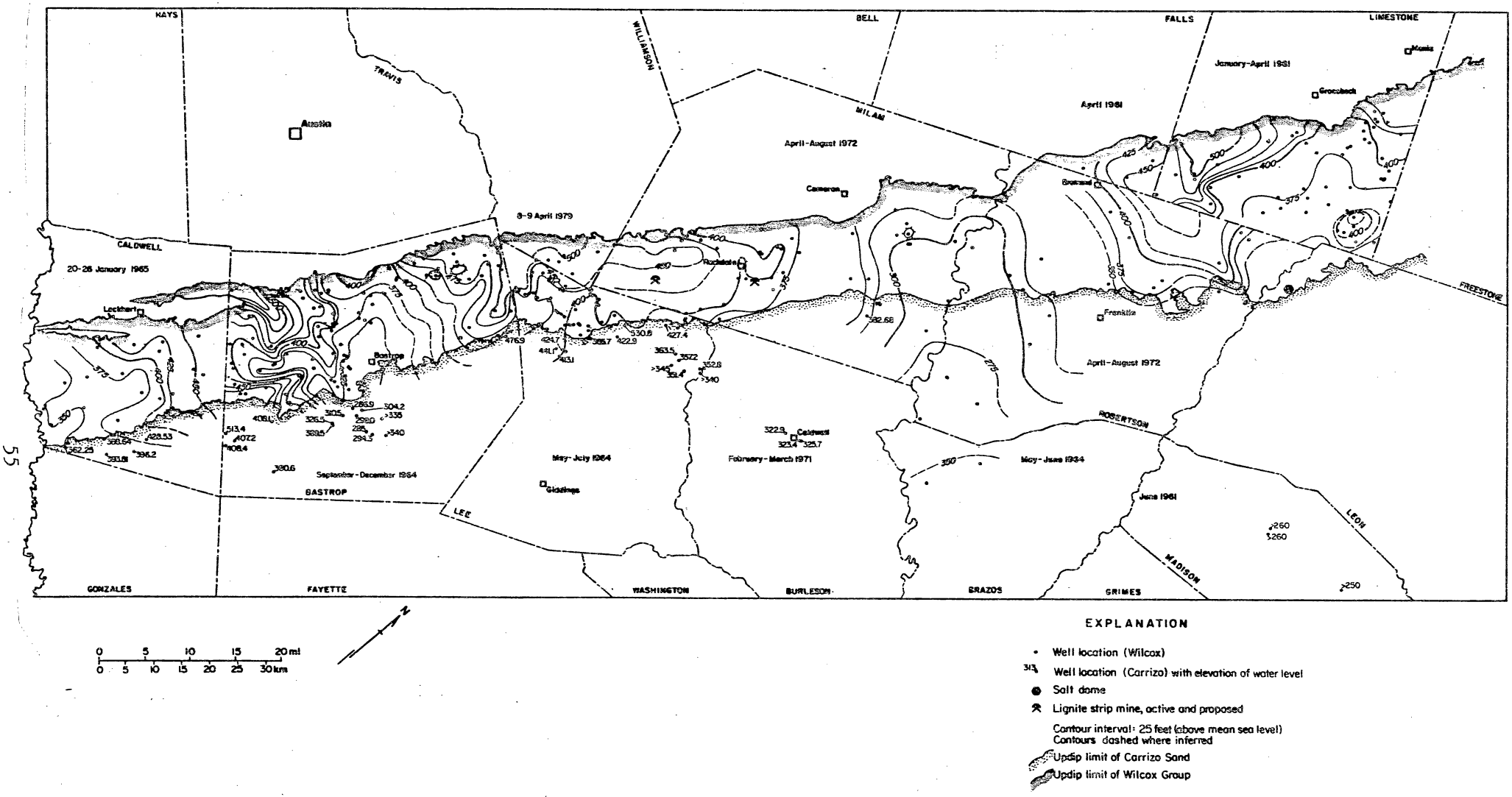

Figure 19. Potentiometric-surface map of the Wilcox Group. Within each county, a time period was selected to include the most data within a reasonably short time. For this reason, contours are not continuous over county lines. The map is considered reliable for regional interpretation, but local hydraulic gradients can be much more complex.

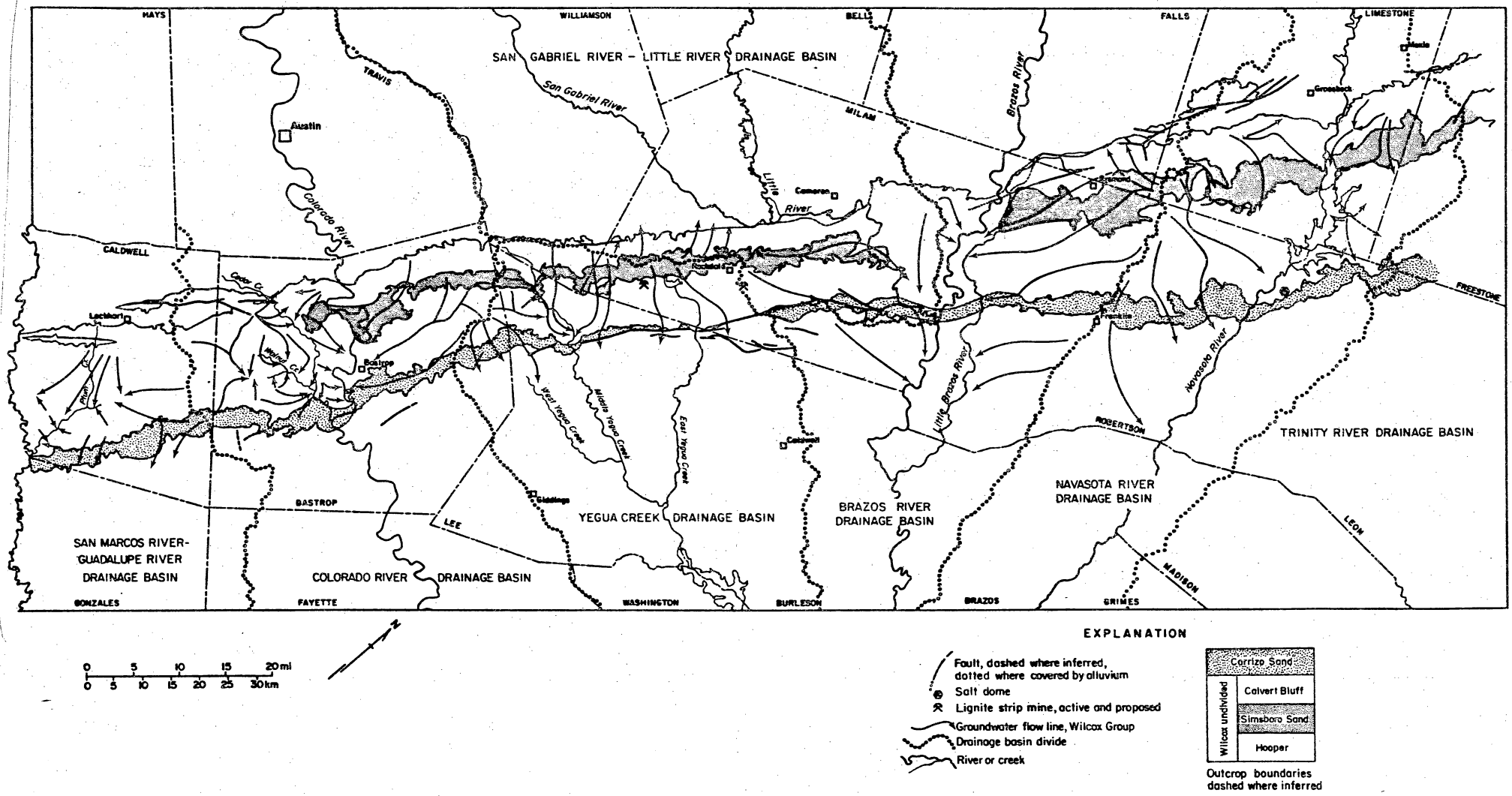

Figure 20. Ground-water flowlines in the Wilcox Group. Ground water appears to move away from surface-water drainage divides toward rivers or streams; only a very small proportion of ground water recharging the Wilcox moves downdip to become part of the deep Wilcox system.

topographic relief near the drainage divides and because much of the water that enters the aquifer in the major recharge areas is discharged to small streams (as part of a smaller flow system) before it reaches the discharge areas near rivers. Furthermore, only a very small proportion of water entering the Wilcox ground-water system actually travels down gradient into the deep Wilcox (downdip from the outcrop area), as evidenced by the relatively small number of flowlines (fig. 20) showing water movement to the southeast.

Two other processes may be important locally. The head map and flowline map (figs. 19 and 20) in the southeastern corner of Limestone County indicate a recharge mound near Lake Limestone. Although the 1981 water-level measurements are the only evidence, the recharge mound probably exists. The mound coincides with an area mapped as part of the "Sand Hills" environmental geologic unit (Henry and Basciano, 1979). These "Sand Hills" are part of the Calvert Bluff outcrop but appear to serve as a recharge area like the "Sand Hills" of the Simsboro or Carrizo. The second process that may be operating locally in the study area is updip flow. In southwestern and central Milam County, the drainage divide between the San Gabriel/Little River Basin and the Yegua Creek Basin falls within 5 km or less of the updip limit of the Wilcox Group. The limited water-level data in this area suggest that ground water flows away from the divide toward the San Gabriel River, and thus flows updip.

Very few data were available for water levels in the Carrizo Sand. In figure 19, the Carrizo potentiometric surface is not contoured, but the data suggest that ground water flows from drainage divides toward rivers or streams. Throughout most of the region, heads in the Carrizo appear to be higher than heads in the Wilcox. Between the Colorado River and the Colorado River/San Marcos River drainage divide in Bastrop County, this relationship may be reversed and heads in the Wilcox may be higher than heads in the Carrizo. A clear description of the relationship between these heads is not possible

without more head data from both the Wilcox and the Carrizo in the vicinity of the Carrizo outcrop and in the area downdip of the outcrop.

CONCLUSIONS

In the Wilcox Group, most ground water flows from major recharge areas along drainage divides and in "Sand Hills" toward streams and rivers. Only a relatively small amount flows downdip into the area basinward of the outcrop. In the Carrizo, ground water also appears to flow from drainage divides to streams or rivers, although this conclusion is less certain because of meager data. The relationship between heads in the Wilcox and the Carrizo is also difficult to define because of limited data, but throughout most of the region Carrizo heads are higher than Wilcox heads, indicating downward flow into the Wilcox. In southwestern Bastrop County this relationship may be reversed.

HYDROCHEMICAL MAPPING IN THE WILCOX-CARRIZO AQUIFER, SABINE UPLIFT AREA

W. R. Kaiser and M. L. Ambrose

ABSTRACT

Waters of Gulf Coast Tertiary aquifers interact with host sediments and evolve from Ca^{2+}-HCO_3^- to Na^+-HCO_3^- water. We linked ground-water evolution to water-rock interaction through solution-mineral equilibria. Activity indices derived from reactions believed to play a role in the evolution of Wilcox-Carrizo waters were mapped. All hydrochemical maps reflect the same regional geochemical patterns; they show a positive correlation with outcrop geology and areas of recharge and discharge identified in hydraulic head mapping. Recharge is defined by relatively small $\log[Na^+]^{.33}/[Ca^{2+}]^{.16}$ ratios and $\log[Ca^{2+}]^{.3}[Na^+]^{.7}$ products and large $\log[H_4SiO_4^0]$ values and montmorillonite saturation indices.

GROUND-WATER EVOLUTION

The geochemical evolution of ground water was originally described by Chebotarev (1955), who concluded that ground water tends to evolve from HCO_3^-- to SO_4^{2-} - or Cl^--rich water in the deep basin. The anion-evolution sequence (Freeze and Cherry, 1979) is as follows:

$$HCO_3^- \rightarrow HCO_3^- + SO_4^{2-} \rightarrow SO_4^{2-} + HCO_3^- \rightarrow SO_4^{2-} + Cl^- \rightarrow Cl^- + SO_4^{2-} \rightarrow Cl^-$$

No generalized cation-evolution sequence has been established. Major factors controlling ground-water evolution are bulk composition or mineralogy (water-rock interaction), flow velocity, distance along flow path, residence time, and mixing.

Waters of Gulf Coast Tertiary aquifers evolve from Ca^{2+}-HCO_3^- to Na^+-HCO_3^- water. This evolution has been documented for the Wilcox-Carrizo aquifer in the East Texas Basin (Kreitler and Fogg, 1979; Fogg and Kreitler, 1982) and here for the Sabine Uplift area (fig. 21). The dominance of Na^+ and HCO_3^- ions can be explained by the combined effects of calcite dissolution and cation exchange (Foster, 1950; Freeze and Cherry, 1979). Two reactions are of special importance:

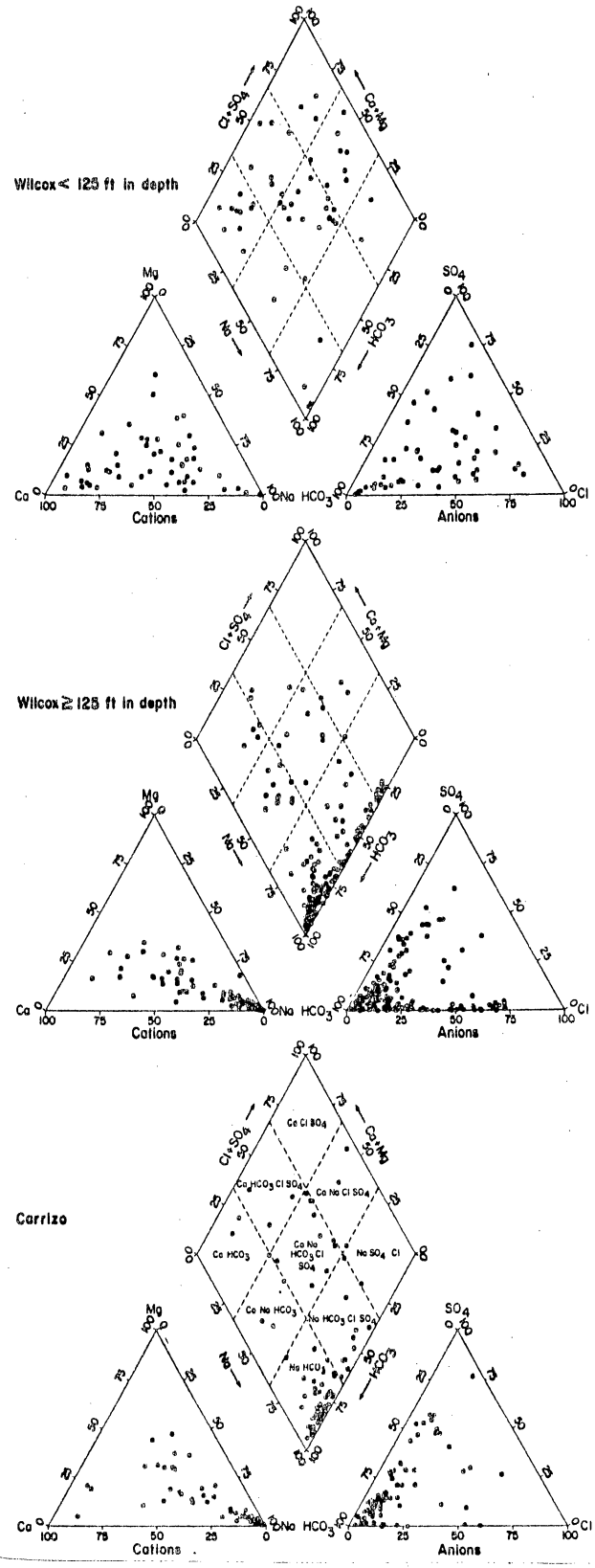

Figure 21. Piper diagrams of Carrizo and Wilcox waters show them to be Na^{+}-HCO_3^{-} dominated. Wilcox samples are divided by depth into two groups based on a data break at approximately 125 ft on scatter plots (fig. 26). Shallow waters are Ca^{2+}-HCO_3^{-} dominated, becoming Na^{+}-HCO_3^{-} dominated in the deeper, confined portion of the Wilcox.

$$CaCO_3 + H_2CO_3 = Ca^{2+} + 2HCO_3^-$$

$$\text{Na-mont} + Ca^{2+} = 2Na^+ + \text{Ca-mont}$$

Because of these simultaneous reactions Na^+ and HCO_3^- concentrations increase. Removal of Ca^{2+} by cation exchange causes the water to become or remain undersaturated with respect to calcite; thus calcite dissolution continues. CO_2, generated in the biologically active soil zone, combines with water to form H_2CO_3. At depth CO_2 may be generated by coalification or SO_4^{2-} reduction (Freeze and Cherry, 1979).

Other chemical trends seen in the Wilcox-Carrizo of East Texas (Fogg and Kreitler, 1982) are: loss of SiO_2 with depth; loss of SO_4^{2-} with depth; and decrease of Cl^- with depth. High SiO_2 concentration in the shallow aquifer is attributed to leaching of feldspar or dissolution of unstable SiO_2 species. The former may be important initially in H_2CO_3-rich waters. The loss of SiO_2 with depth is attributed to precipitation of authigenic silica minerals or clay minerals (Fogg and Kreitler, 1982). SO_4^{2-} loss can be explained by its reduction at depth to H_2S (HS^-) under low Eh conditions. There is no ready explanation for Cl^- behavior.

Fogg and Kreitler mapped the evolving chemical trends, using concentrations, and showed that Wilcox-Carrizo waters shift from oxidizing and acidic in the recharge zone to reducing and basic deep in the aquifer. Fogg and Kreitler chemically characterized recharge and discharge as follows:

Recharge --

pH < 7, high Ca^{2+}, low Na^+, low HCO_3^-, moderate SO_4^{2-}, high SiO_2, high Eh

Discharge --

pH 8 to 9, low Ca^{2+}, high Na^+, high HCO_3^-, no SO_4^{2-}, low SiO_2, low Eh

SOLUTION-MINERAL EQUILIBRIA

Our objective, using the concept of ground-water evolution and chemical trends established in the Wilcox-Carrizo aquifer, was to use water chemistry, in conjunction with head mapping, to identify regional areas of recharge and discharge (fig. 22). Because mapping of concentrations proved to be difficult, we decided to link water-rock interaction to ground-water evolution through solution-mineral equilibria. Our approach was to map activity indices derived from reactions believed to affect the evolution of Wilcox-Carrizo waters. In this way interpretation could be linked to specific reactions. Reactions considered in this report are:

1. $\text{Na-mont} + 0.16Ca^{2+} = \text{Ca-mont} + 0.33Na^{+}$
2. $\text{Plagioclase } (An_{30}) + 1.3H^{+} + 3.45H_2O =$
   $0.65\text{Kaolinite} + 0.3Ca^{2+} + 0.7Na^{+} + 1.4H_4SiO_4^{\circ}$
3. $SiO_2c + 2H_2O = H_4SiO_4^{\circ}$
4. $\text{Ca-mont} + 10.24H_2O =$
   $0.16Ca^{2+} + 1.56\ Al(OH)_4^{-} + 0.5Mg^{2+} + 4H_4SiO_4^{\circ} + 0.24H^{+}$

Reaction (1) is the key cation-exchange reaction, where the equilibrium constant for the reaction, $\log K_r = [Na^{+}]^{.33}/[Ca^{2+}]^{.16}$. This log activity ratio was mapped to evaluate the evolution of Na^{+}-HCO_3^{-} water. Reaction (2) generates SiO_2, Na^{+}, and Ca^{2+}, relevant to the leaching or kaolinization of feldspar; the log activity product $[Ca^{2+}]^{.3}[Na^{+}]^{.7}$ was mapped. In reaction (3) the stability of crystalline silica is considered and $\log[H_4SiO_4^{\circ}]$ was mapped. Reaction (4) is the hydrolysis of Ca-montmorillonite. In this case, using thermodynamic data from Galloway and Kaiser (1980), the saturation index (SI) = log ionic activity product (IAP)/$\log K_r$ was mapped. Reactions (3) and (4) test possible controls on SiO_2 concentration.

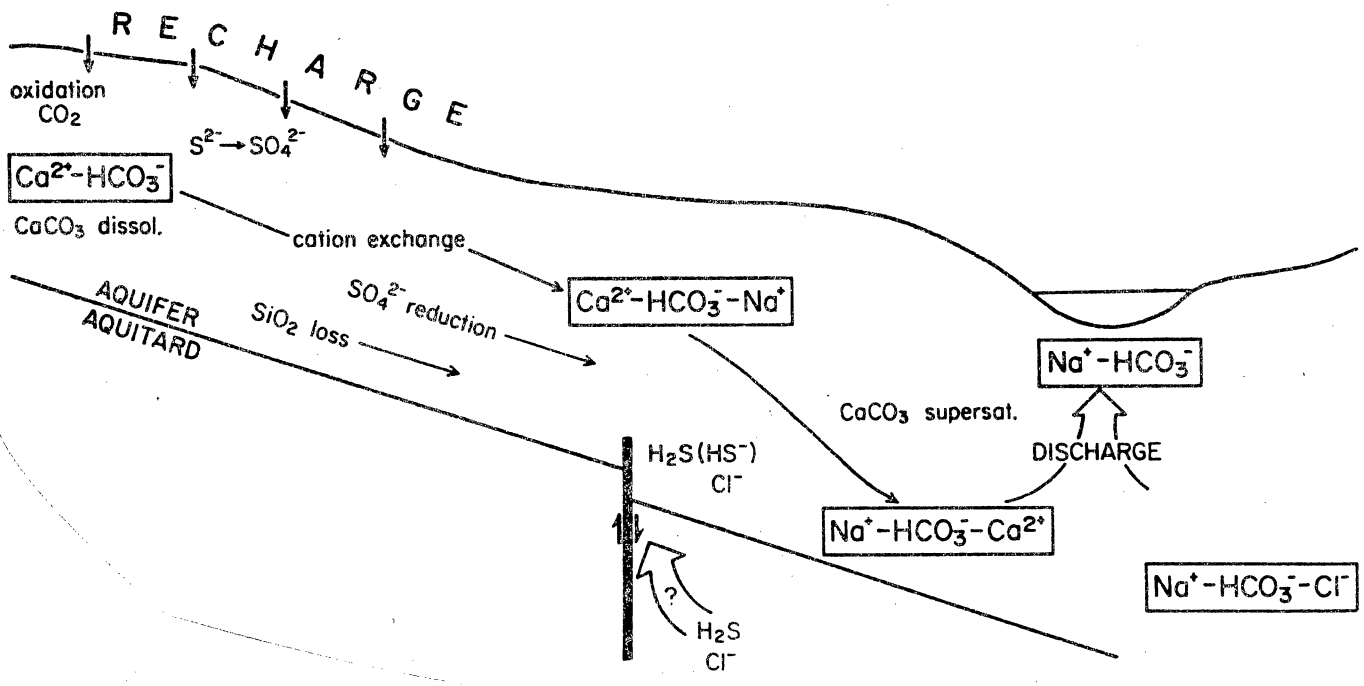

Figure 22. Schematic diagram illustrating ground-water evolution from Ca^{2+}-HCO_3^- to Na^+-HCO_3^- domination. Ca^{2+}-HCO_3^- waters typify recharge, whereas Na^+-HCO_3^- waters characterize discharge.

DATA BASE

The major source of data for this study was the Texas Water-Oriented Data Bank kept by the Texas Natural Resources Information System (TNRIS). Additional chemical analyses were acquired from a U.S. Department of Energy open file report (Oak Ridge Gaseous Diffusion Plant, 1979).

The accuracy of these chemical analyses was checked using an ionic balance formula, expressed as:

$$\text{percent of error} = \frac{\Sigma \text{ cations} - \Sigma \text{ anions}}{\Sigma \text{ cations} + \Sigma \text{ anions}} \times 100$$

(Edmunds, 1981). Analyses having a percent-error greater than ± 2.59 percent were deleted from the data base, resulting in a total of 310 unique chemical analyses. Two hundred twenty-two are from the Wilcox or Wilcox-Carrizo aquifer undivided, and 88 are from the Carrizo aquifer. These two groups will be referred to here as the Wilcox and Carrizo, respectively.

The chemically balanced analyses were processed using the computer program SOLMNEQ (Solution-Mineral Equilibrium Computations) (Kharaka and Barnes, 1973). This version calculates the activities of selected ions in natural waters and calculates saturation indices. The following assumptions were included for this study: default temperature, pH, and Eh were 25°C, 7, and -0.200, respectively; the concentration of aluminum was set at 10 ppb (Hem, 1970). Activity and saturation indices generated by SOLMNEQ were mapped independent of geology. Six of these hydrochemical maps are presented (figs. 23, 24, 27, 28, 32, and 33).

Scatter plots were computer generated using a statistical software package BMDP-77 (Biomedical Computer Programs) (Dixon, 1981). The plots were made using the bivariate plot program BMDP6D (Chasen, 1979), which performs least-squares linear regression on the variables.

HYDROCHEMICAL MAPS

Two hydrochemical maps of the lithologically homogeneous and geochemically simpler Carrizo aquifer (figs. 23 and 24) illustrate our interpretation of the maps. The $\log [Na^+]^{.33}/[Ca^{2+}]^{.16}$ ratio is mapped in figure 23. Log ratios less than -0.4 occur in areas in or near outcrop and faults. In these areas the activity or effective concentration of Ca^{2+} is large compared to Na^+. These are areas of postulated recharge and active water movement, as illustrated by the bands of changing chemistry that ring the Carrizo outcrop belt. Basinward, to the west, waters with a log ratio of greater than 0.0 occur where the effective concentration of Na^+ is high compared with Ca^{2+}. Implied is basinward flow from the outcrop, centered on the Sabine Uplift, as illustrated in figure 12. Another example of basinward flow lies in northwestern Smith County, where waters are postulated to be moving in from a large recharge mound located in the Carrizo outcrop to the west (Fogg, 1980).

The Carrizo map of $\log [Ca^{2+}]^{.3}[Na^+]^{.7}$ (fig. 24) has more negative values (less than -3.15) in the updip and outcrop areas. The activity product is more positive in the downdip areas westward toward the basinal axis, such as in central Cherokee County. More negative values over the Boggy Creek Dome reflect probable recharge over the dome (Fogg, 1980). Highly negative values (recharge) also occur along the Mount Enterprise Fault Zone where outcrop of the Carrizo is exposed.

On both Carrizo maps there are fingers of Na-rich waters trending towards outcrop, (in central Nacogdoches County). In this area, possible communication exists between the Carrizo and the Wilcox. Representative electric logs (fig. 25) illustrate a difference in percent sand across the Carrizo-Wilcox boundary. In Q23 the base of the Carrizo sits upon another thick, highly resistive sand unit of the Wilcox. Through these sands discharge of Wilcox waters into the Carrizo could result in a water chemistry characteristic of discharge areas. The mud break in Q112 separates the Carrizo from this possible

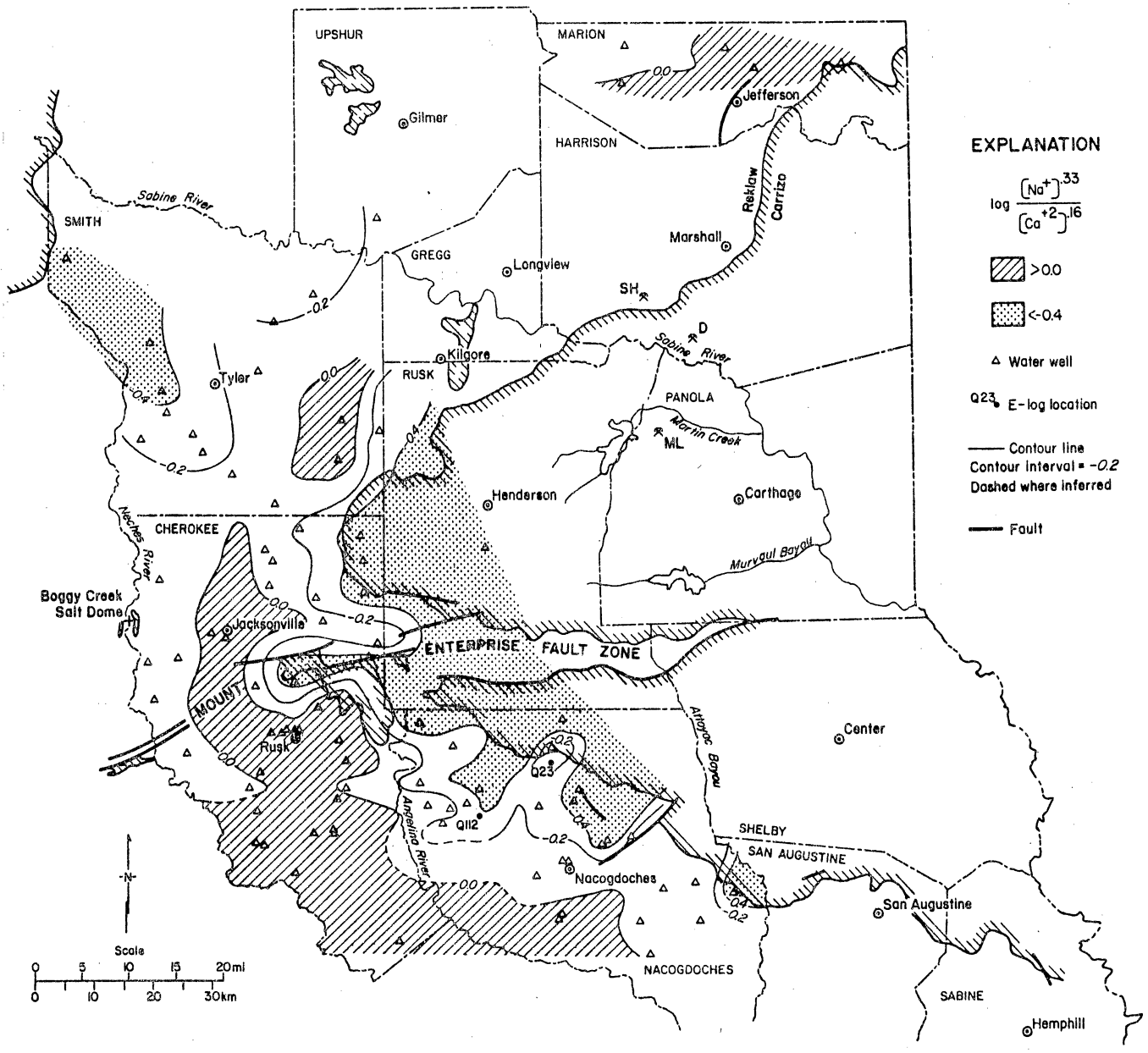

Figure 23. Map of Carrizo $\log [Na^+]^{.33}/[Ca^{2+}]^{.16}$ ratios. Log activity ratios <-0.4 indicate recharge. Flow is basinward, toward areas of log ratio values > 0.0. Martin Lake (ML), Darco (D), and South Hallsville (SH) lignite mines are shown for reference. Nearly all Carrizo completions are between depths of 200 and 760 ft (61 and 232 m).

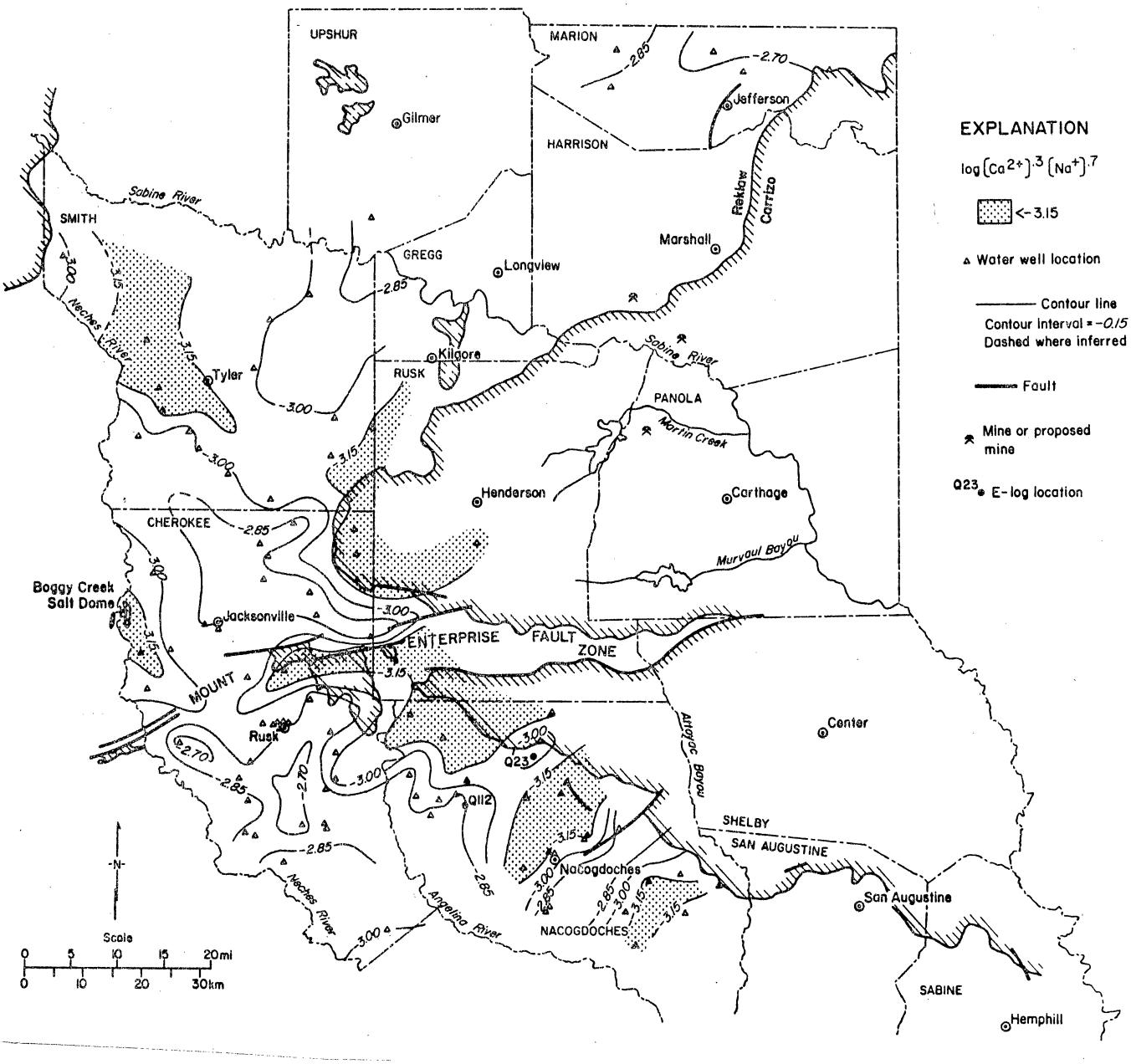

Figure 24. Map of Carrizo $\log[Ca^{2+}]^{.3}[Na^{+}]^{.7}$ products. Log activity products <-3.15 indicate recharge. More positive values occur basinward.

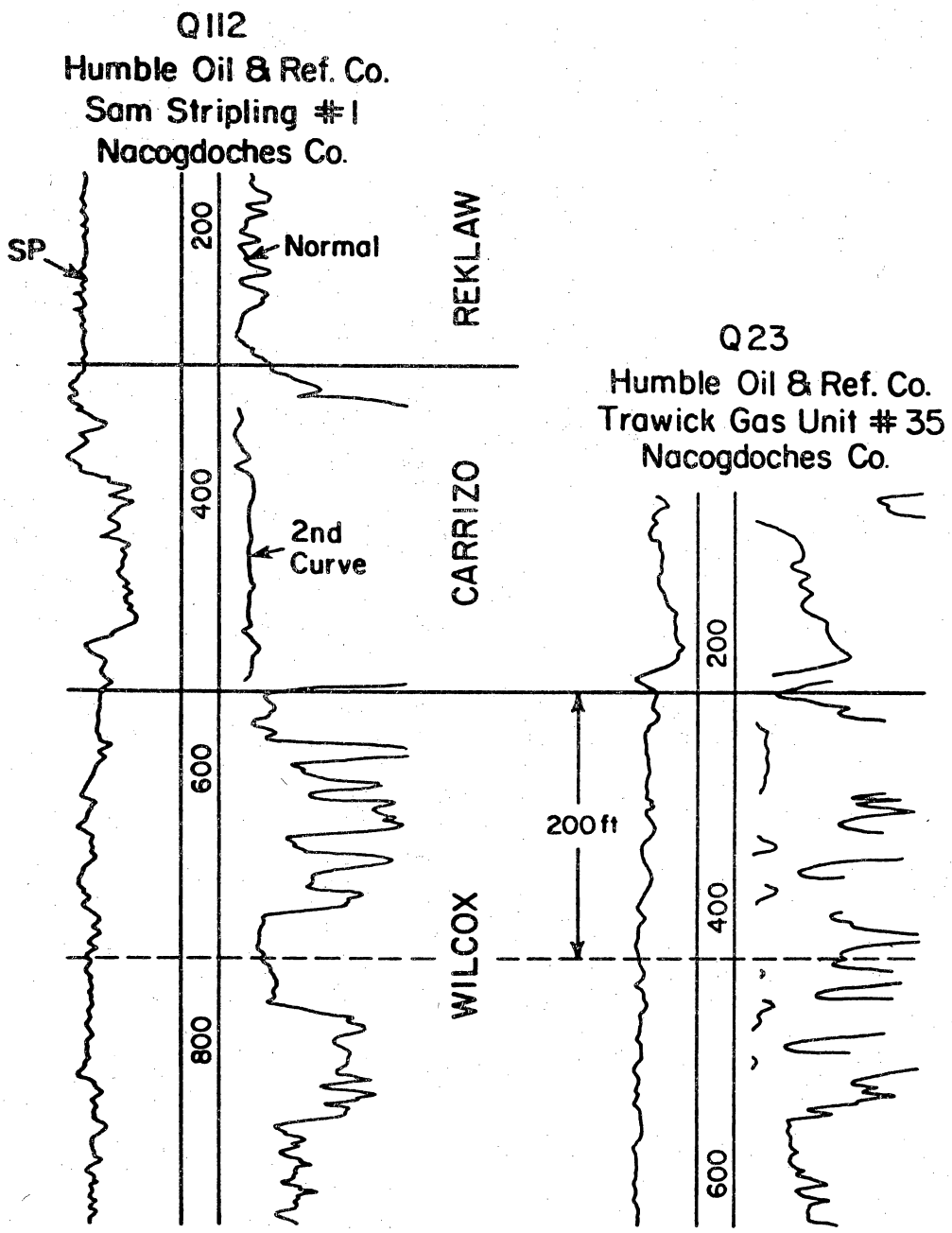

Figure 25. Electric logs illustrating the Carrizo-Wilcox boundary. The 200-ft interval directly below the Carrizo is sandier in Q23. See figures 23 and 24 for location of logs.

upward movement and may act locally as an aquitard. If this is the case, hydrochemical maps may be used to evaluate interconnectedness between aquifers.

Four hydrochemical maps of the Wilcox (figs. 27, 28, 32, 33) are presented. These maps are harder to interpret than the Carrizo maps because of large outcrop area, lithologic heterogeneity, greater thickness, municipal pumpage, and faulting of the Wilcox. $\text{Log}[Na^+]^{.33}/[Ca^{2+}]^{.16}$ increases with depth (fig. 26) and is mapped on figure 27; displayed are trends similar to those observed in the Carrizo. Small log activity ratios (<-0.4), indicative of inferred areas of recharge, underlie the Carrizo outcrop, such as in central Rusk County. More positive values occur basinward and in areas of apparent discharge toward streams (as shown in fig. 10), such as Martin Creek and Murvaul Bayou in Panola County. Partitioning of sand bodies, due to faulting, creates areas of smaller (more negative) log values (recharge), as are found in east-central Cherokee County. These areas are flanked by more positive values (discharge) as in Cherokee County and eastern Nacogdoches County near the Shelby County line. Heavy pumping of the aquifer has caused large areas of downdraw in Gregg County and around the town of Henderson, Rusk County. These areas are characterized by more positive log ratios due to induced discharge (Fogg, this report).

The $\log[Ca^{2+}]^{.3}[Na^+]^{.7}$ product map (fig. 28) shows many of the same trends recognized on the previous map. More negative values (<-3.00) underlie the Carrizo outcrop in areas of recharge, for example, potentiometric highs or recharge mounds in central Rusk County (fig. 10). Flow is presumed to be downward into the Wilcox (fig. 16). Apparent recharge is also occurring from the west, as shown in figures 24 and 10. More positive values are inferred to reflect discharge at Martin Creek and Murvaul Bayou in Panola County. Around the town of Tyler in Smith County and eastern Gregg County, positive log values indicate induced discharge due to pumping.

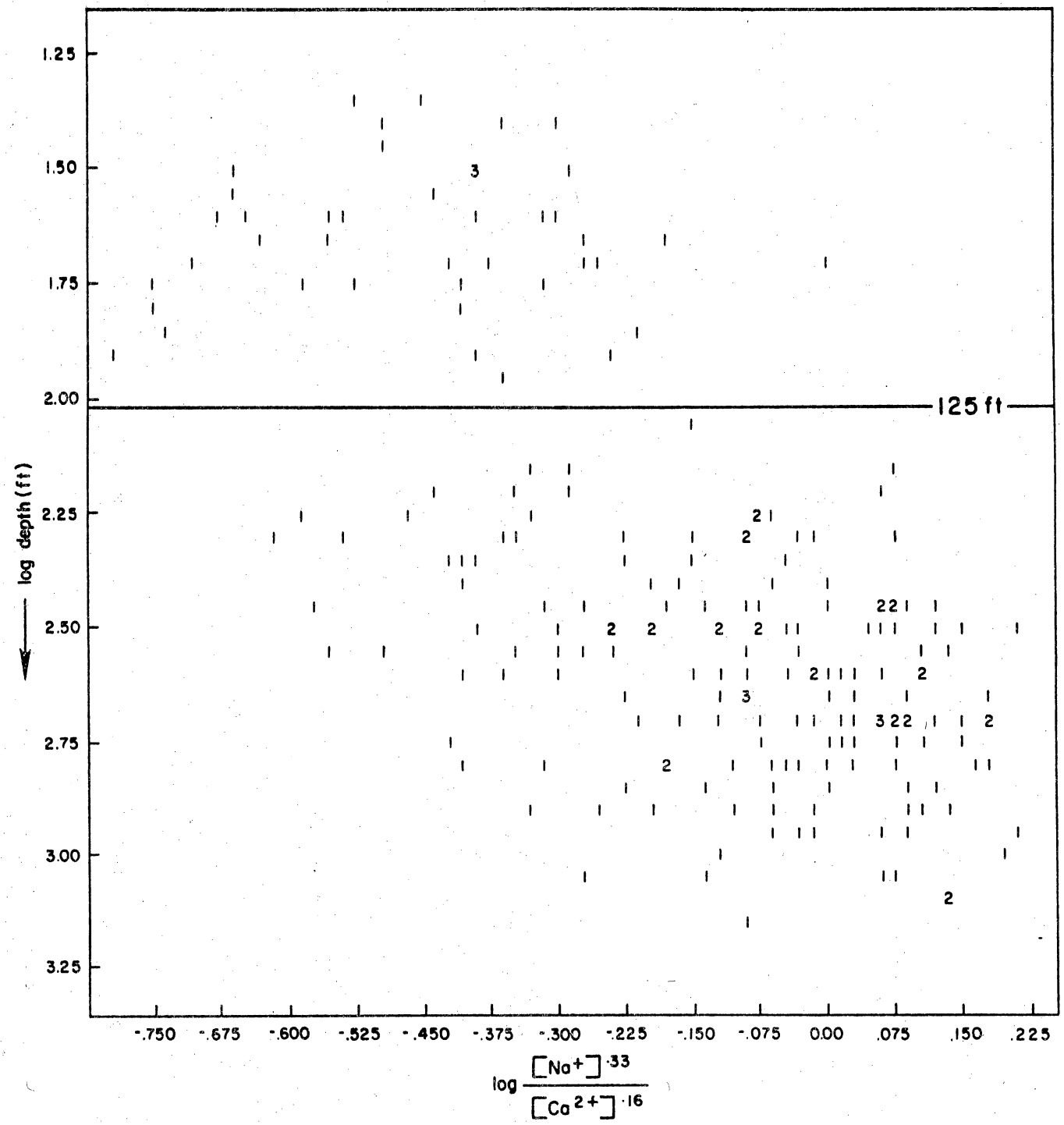

Figure 26. Scatter plot of Wilcox $\log [Na^+]^{.33}/[Ca^{2+}]^{.16}$ ratios versus depth. The log activity ratio increases with depth, reflecting longer travel time and greater distance from outcrop. Note data break at 125 ft. Numbers represent number of points that plot at that position up to 9, then letters are used starting with A equal 10, and so on.

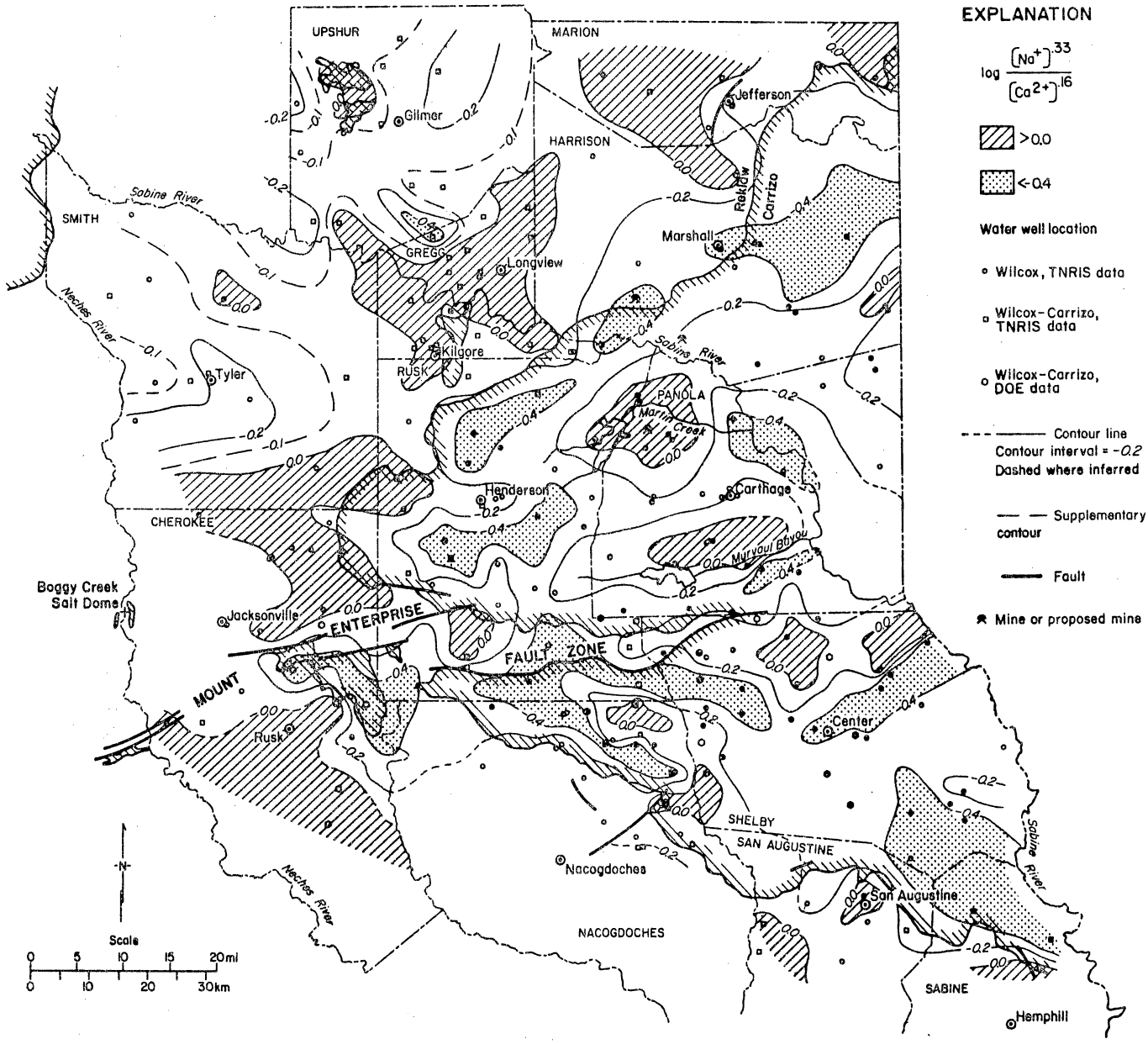

Figure 27. Map of Wilcox log $[Na^+]^{.33}/[Ca^{2+}]^{.16}$ ratios. Small log activity ratios, <-0.4, indicate areas of recharge and larger log values, > 0.0, lie in areas of discharge. Solid symbols are completions at depths of < 200 ft (61 m). Most of Wilcox completions are between depths of 144 and 1,000 ft (44 and 305 m).

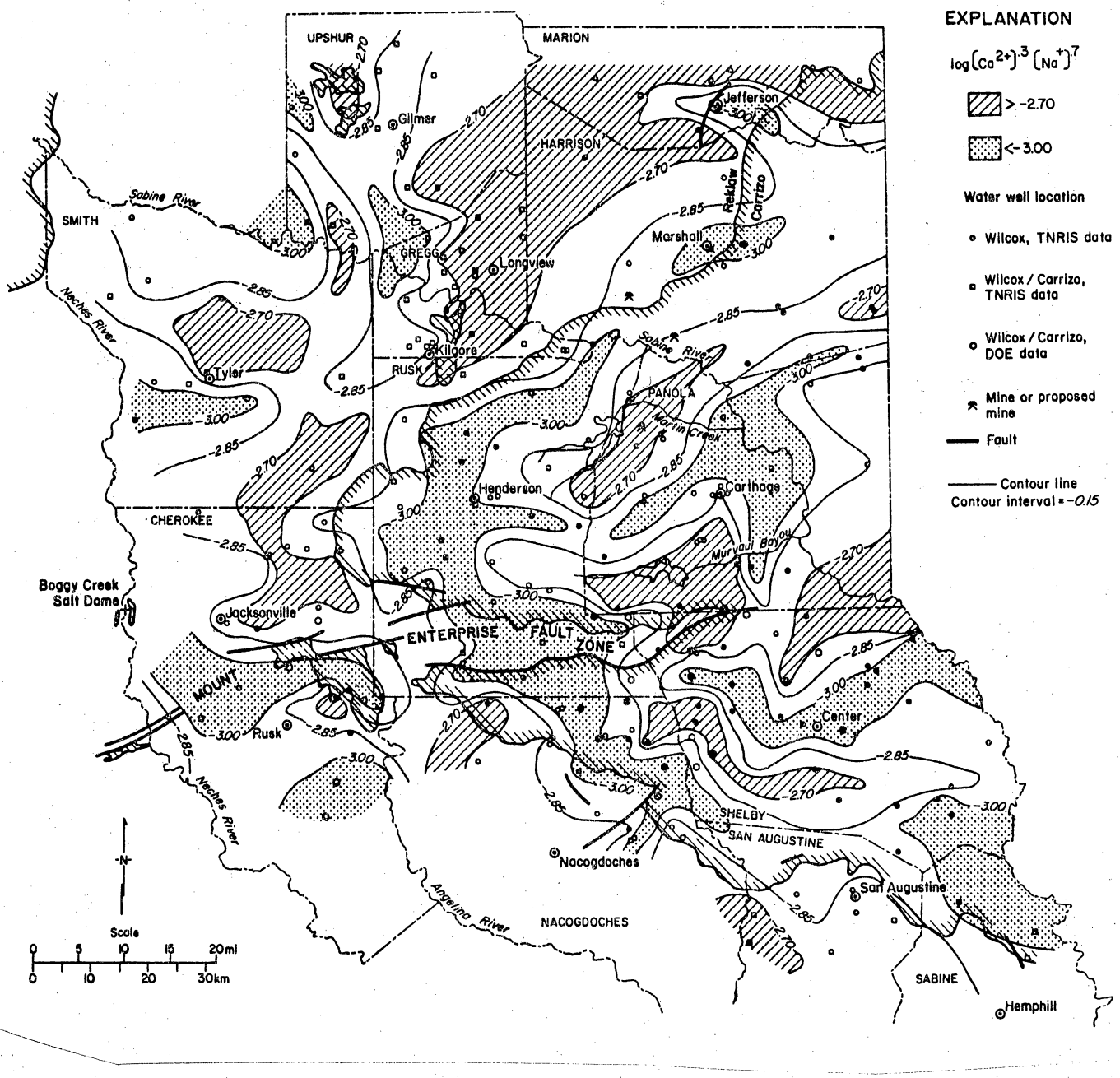

Figure 28. Map of Wilcox $\log[Ca^{2+}]^{.3}[Na^{+}]^{.7}$ products. Log activity products <-3.00 indicate areas of recharge, whereas log activity products >2.70 indicate areas of discharge.

Significantly, this map may reflect hydrologic communication between sands or interconnectedness. The most negative log values lie in areas of high percent sand in the Wilcox Group as mapped by Kaiser and others (1978). More positive log values lie in interchannel areas (north-central Cherokee County) as shown in figure 6.

Silicic acid activity ($[H_4SiO_4^o]$) decreases with depth, approaching a threshold value of -3.72 (fig. 29), the activity in equilibrium with chalcedony (eq. 3). The plot of $\log [Na^+]^{.33}/[Ca^{2+}]^{.16}$ versus $\log [H_4SiO_4^o]$, important species in montmorillonite stability (eq. 4), also converges on -3.72 (fig. 30). In figure 31, Ca-montmorillonite SI decreases to a threshold value of approximately 4.8. Average $\log [H_4SiO_4^o]$ at the SI threshold (range of 5.2 to 4.5) for Wilcox waters is -3.74. We conclude from these data that SiO_2 concentration is controlled by chalcedony equilibrium and not by montmorillonite (clay minerals).

The map of $\log [H_4SiO_4^o]$ (fig. 32) shows a basinward decrease in activity that reflects a similar decrease with depth (fig. 29). Areas with log values greater than -3.4 show positive correlation with previously identified areas of recharge in Rusk County (recharge mounds in Carrizo outcrop), Cherokee and adjoining counties (outcrop exposed by faulting), and Shelby County (along drainage divides). Areas of possible discharge (natural or induced) correlate with areas of small activities, less than -3.6 in Panola (Martin Creek), Rusk (the town of Henderson), and eastern Gregg Counties.

The map of Wilcox Ca-montmorillonite saturation indices (SI) (fig. 33) is difficult to interpret but is included as an example of an SI map. A band of SI greater than log 6.2 generally lies underneath the Carrizo outcrop (as in central Rusk County) and may indicate movement of water into the Wilcox aquifer through the Carrizo. Large values also occur along drainage divides in the Wilcox outcrop (central Shelby County). Areas containing an SI of less than log 5.2 fall in areas already identified as discharge. Examples are north-central Cherokee County on the downthrown side of the Mount

Enterprise Fault Zone, Martin Creek and Murvaul Bayou in Panola County, and in areas of induced discharge, as in Gregg County.

CONCLUSIONS

1. Activity indices generated from reactions keyed to ground-water evolution reflect its evolution and can be used to map areas of regional recharge and discharge. Activity indices are more sensitive to recharge and discharge than to concentrations. Hydrochemical mapping complements hydraulic head mapping, helping to define recharge and discharge where head data are sparse or ambiguous.
2. Small $\log [Na^+]^{.33}/[Ca^{2+}]^{.16}$ ratios and $\log [Ca^{2+}]^{.3}[Na^+]^{.7}$ products and large $\log [H_4SiO_4^o]$ values and montmorillonite saturation indices correlate with recharge areas defined by head mapping. Although each map reflects the same regional geochemical patterns, interpretation is best made from a suite of maps, where individual maps yield specific complementary data.
3. Active or proposed lignite mines are located in the following areas:
   (a) Martin Lake (ML) in a prominent discharge area,
   (b) Darco (D) in a transitional zone, and
   (c) South Hallsville (SH) (proposed) on the edge of a recharge zone.
4. Refinement and interpretation of hydrochemical data will dominate future work. Locations of data points have been digitized for computer mapping of activity indices. This will provide unbiased, computer-generated maps of our data for comparison with earlier, hand-drawn maps presented here. Major springs are being plotted to further test the predictive capability of the hydrochemical mapping.

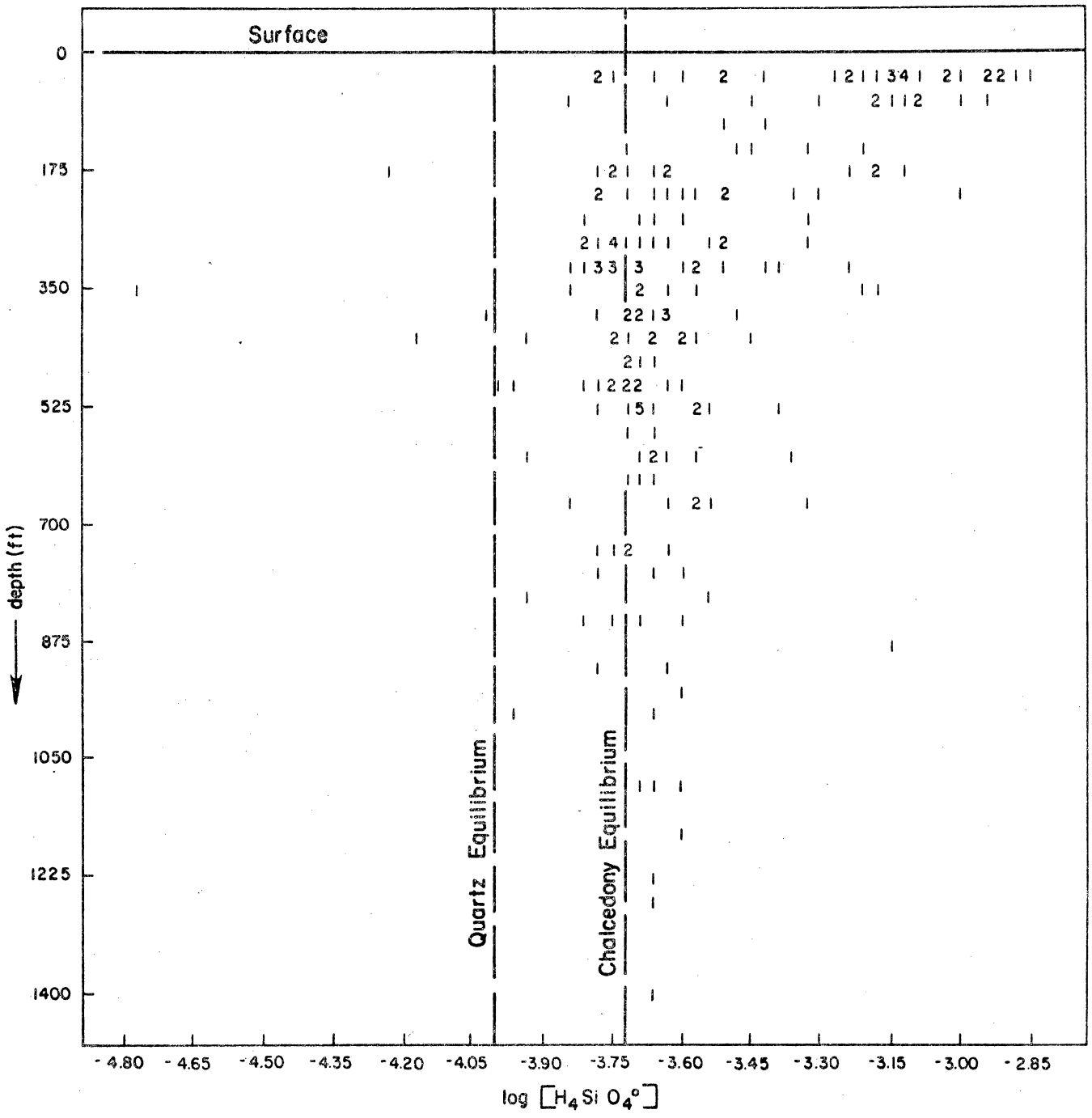

Figure 29. Scatter plot of Wilcox $\log[H_4SiO_4^o]$ values versus depth. $\text{Log}[H_4SiO_4^o]$ decreases with depth, converging on the chalcedony equilibrium value.

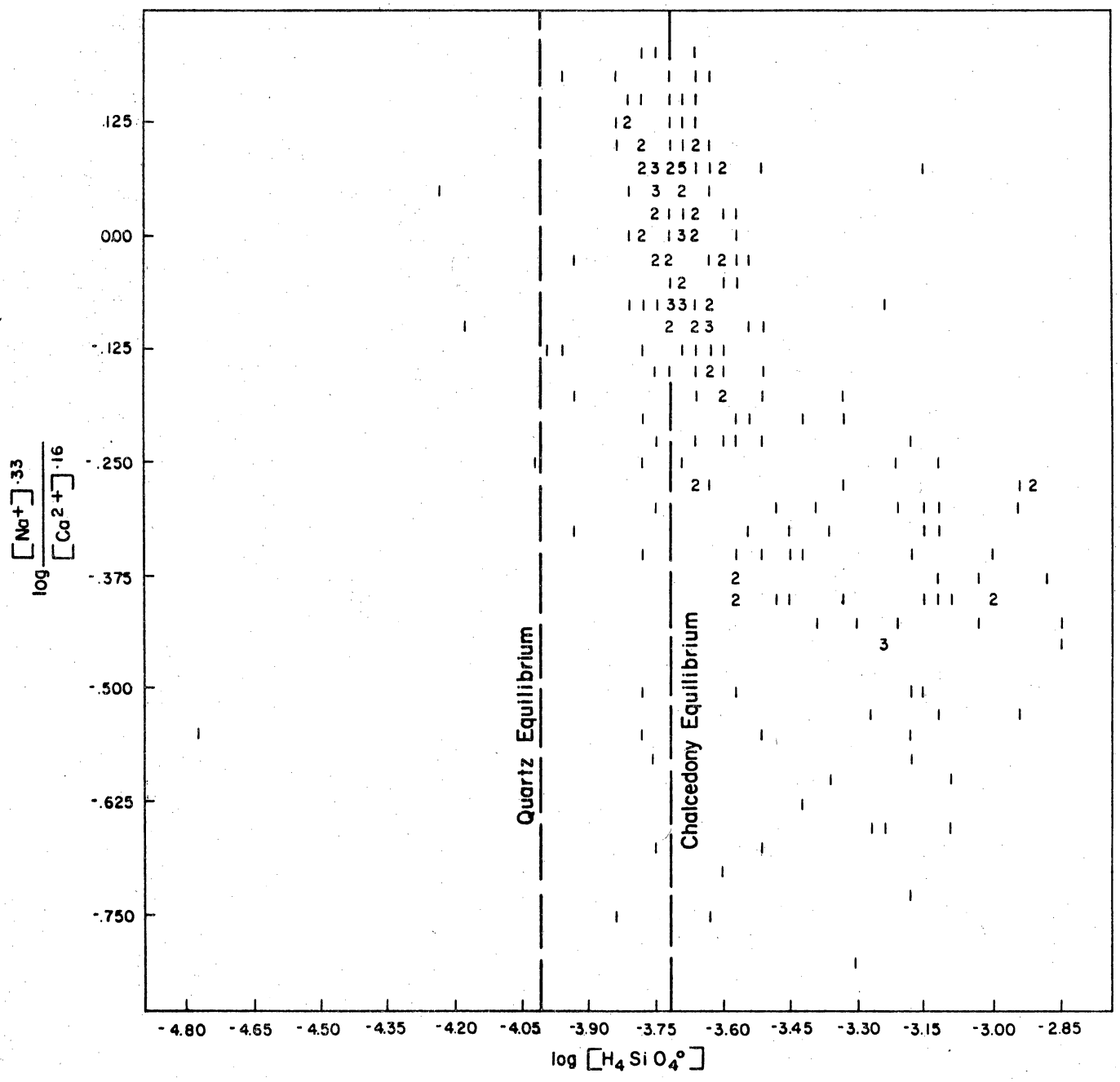

Figure 30. Scatter plot of Wilcox $\log[H_4SiO_4^\circ]$ values versus $\log[Na^+]^{.33}/[Ca^{2+}]^{.16}$ Note the convergence on the chalcedony equilibrium value as $\log[Na^+]^{.33}/[Ca^{2+}]^{.16}$ increases (depth increases, fig. 26).

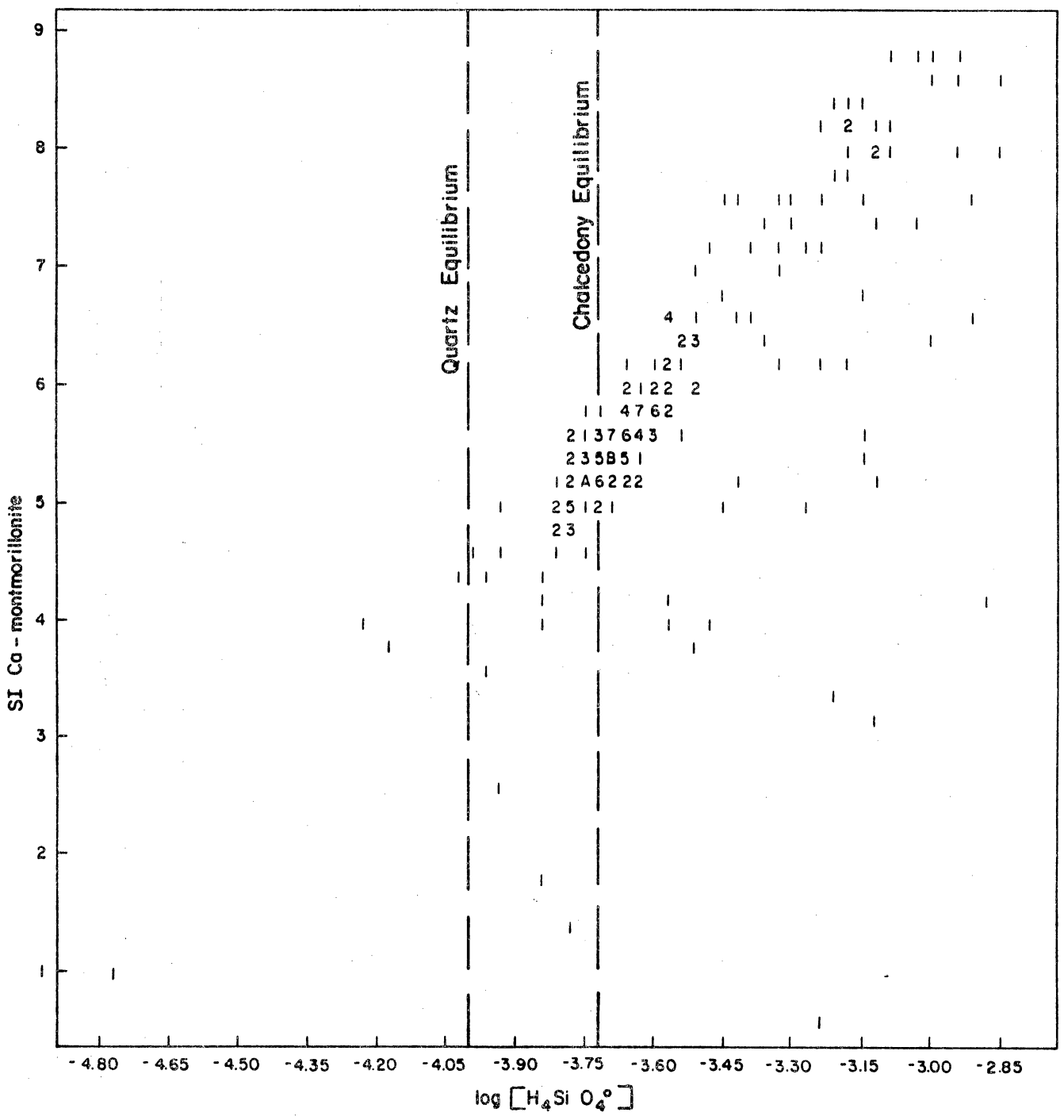

Figure 31. Scatter plot of Wilcox $\log[H_4SiO_4^\circ]$ values versus Ca-montmorillonite saturation indices. SI decreases to approximately 4.8 while $\log[H_4SiO_4^\circ]$ approaches a threshold near the chalcedony equilibrium value.

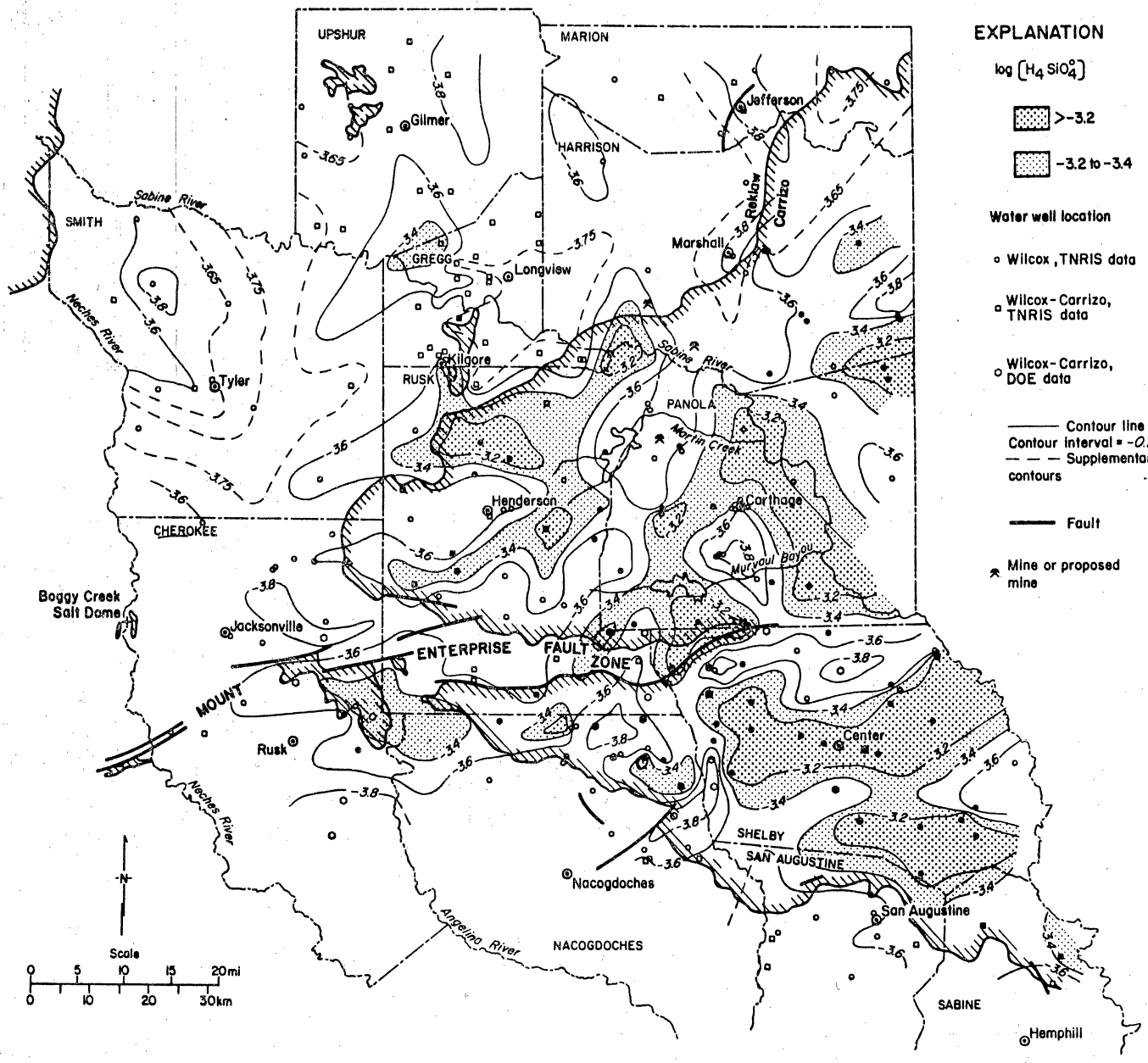

Figure 32. Map of Wilcox log $[H_4SiO_4^\circ]$ values. Recharge is indicated by log values > -3.4. Log values of < -3.6 correlate with areas previously identified as areas of discharge.

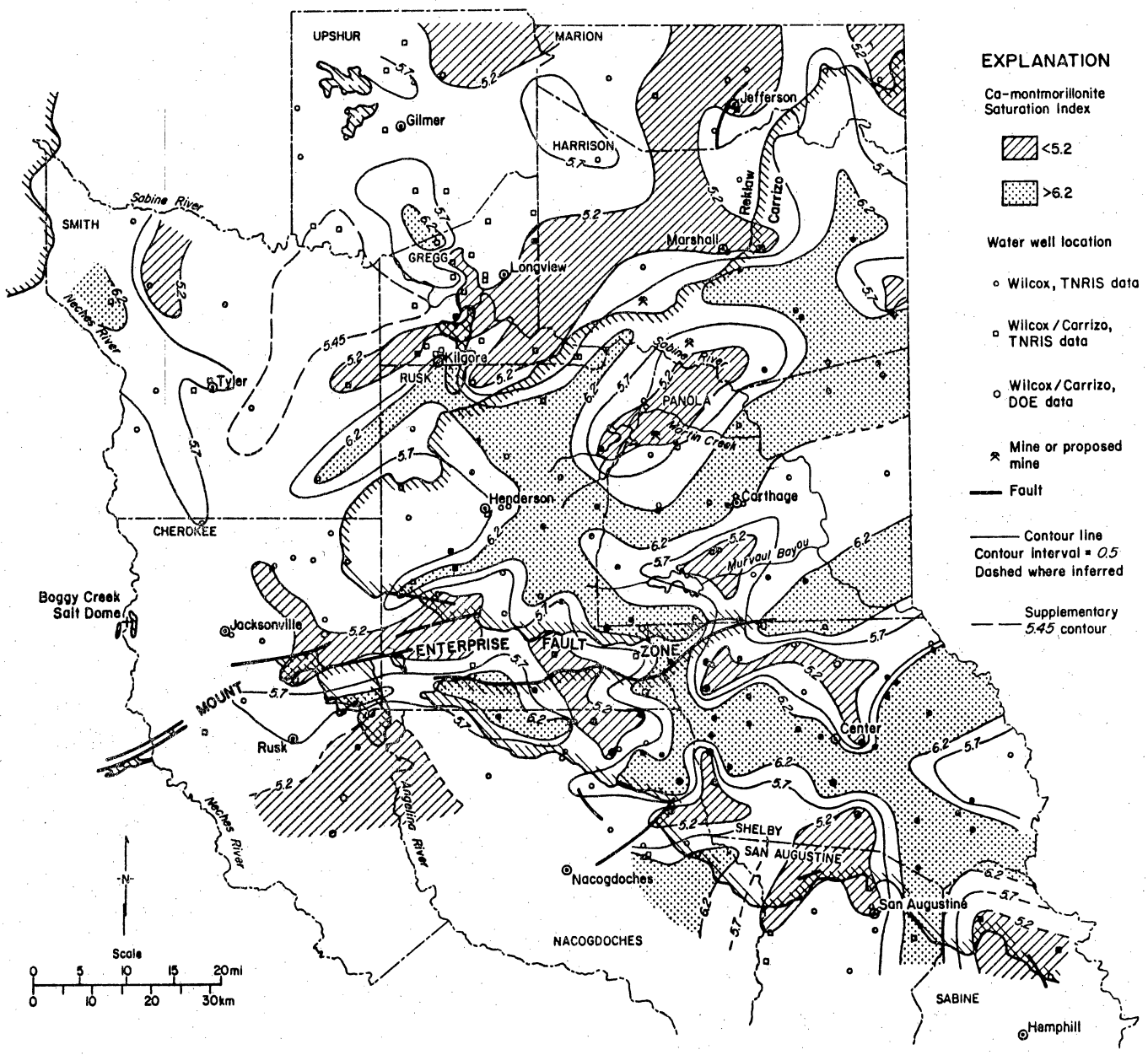

Figure 33. Map of Wilcox Ca-montmorillonite saturation indices. Areas of recharge are characterized by log values > 6.2, whereas areas of discharge have log values < 5.2.

HYDROCHEMISTRY OF THE CARRIZO SAND AND WILCOX GROUP IN EAST-CENTRAL TEXAS

G. L. Macpherson

ABSTRACT

In the Carrizo Sand and Wilcox Group in east-central Texas, the distributions of the $\log[Na^+]^{.33}/[Ca^{2+}]^{.16}$ ratio, the $\log[Ca^{2+}]^{.3}\ [Na^+]^{.7}$ product, and the $\log[H_4SiO_4^o]$ are closely related to the hydrology of the aquifers. Major recharge areas coincide with ground water that generally has a low activity ratio, a low activity product, and high silicic acid activity. Major discharge areas contain ground water that generally has a high activity ratio, a high activity product, and low silicic acid activity. These relations suggest that feldspar argillation, cation-exchange on clay minerals, and formation of authigenic clay minerals or precipitation of silica occur along flow paths from recharge to discharge areas. This analysis is limited by lack of a detailed lithologic and petrographic examination of the aquifers.

INTRODUCTION

Along and slightly downdip of the outcrop of the Carrizo Sand and the Wilcox Group between Limestone and Caldwell Counties, the water chemistry in the Wilcox and Carrizo aquifers undergoes mappable changes that help elucidate the hydrochemical evolution of these ground waters. Distributions of certain ion-activity ratios and ion activities reflect chemical reactions occurring in the aquifers. The link between hydrology and hydrochemistry in the aquifers can be inferred by comparing the hydrological and hydrochemical maps.

DATA BASE

All water-chemistry data used in this report were provided by the Water-Oriented Data Bank of the Texas Natural Resources Information System. The data used in the following discussion represent the most accurate analyses of those available; only those

analyses within ±2.5 percent of an ion balance are included. These data were processed through the solution-mineral equilibrium computer program SOLMNEQ (Kharaka and Barnes, 1973) using default values of 10 ppb for aluminum, 7.0 for pH, and 25°C for temperature. The activities of the dissolved species (calculated by SOLMNEQ) examined with respect to their spatial distribution in the aquifers are keys to hydrochemical changes. These, in turn, are related to ground-water movement through the aquifers.

CHEMICAL REACTIONS

Kaiser and Ambrose (this report) discuss the evolution of ground water and present key chemical reactions. Other chemical reactions also take place. Among these are dissolution of soluble salts, such as halite, gypsum, and anhydrite, alteration of potassium feldspar to a clay mineral, alteration of clay minerals to more stable clay minerals, formation of authigenic clay minerals, oxidation of pyrite and other reduced minerals or dissolved ions, reduction of oxidized minerals or dissolved ions, and formation of silica cements or carbonate cements. A suite of hydrochemical maps, some of which are shown here, help in evaluating the importance of these reactions to the water chemistry in the Wilcox and Carrizo aquifers.

HYDROCHEMICAL MAPS

The values mapped in figure 34 are the $\log [Na^+]^{.33}/[Ca^{2+}]^{.16}$ ratios. In general, the ratio is high in downdip areas (southeast of the Wilcox and Carrizo outcrops) and along rivers and major streams (fig. 20). In the Carrizo aquifer (fig. 34a), high sodium-calcium activity ratios are present in downdip areas and along some of the rivers and major streams. Low ratios coincide with most of the outcrop of the Carrizo Sand; in some areas low ratios extend into the downdip region (for example, eastern Caldwell County, east-central Bastrop County, and along the Lee County-Burleson county line). In the Wilcox

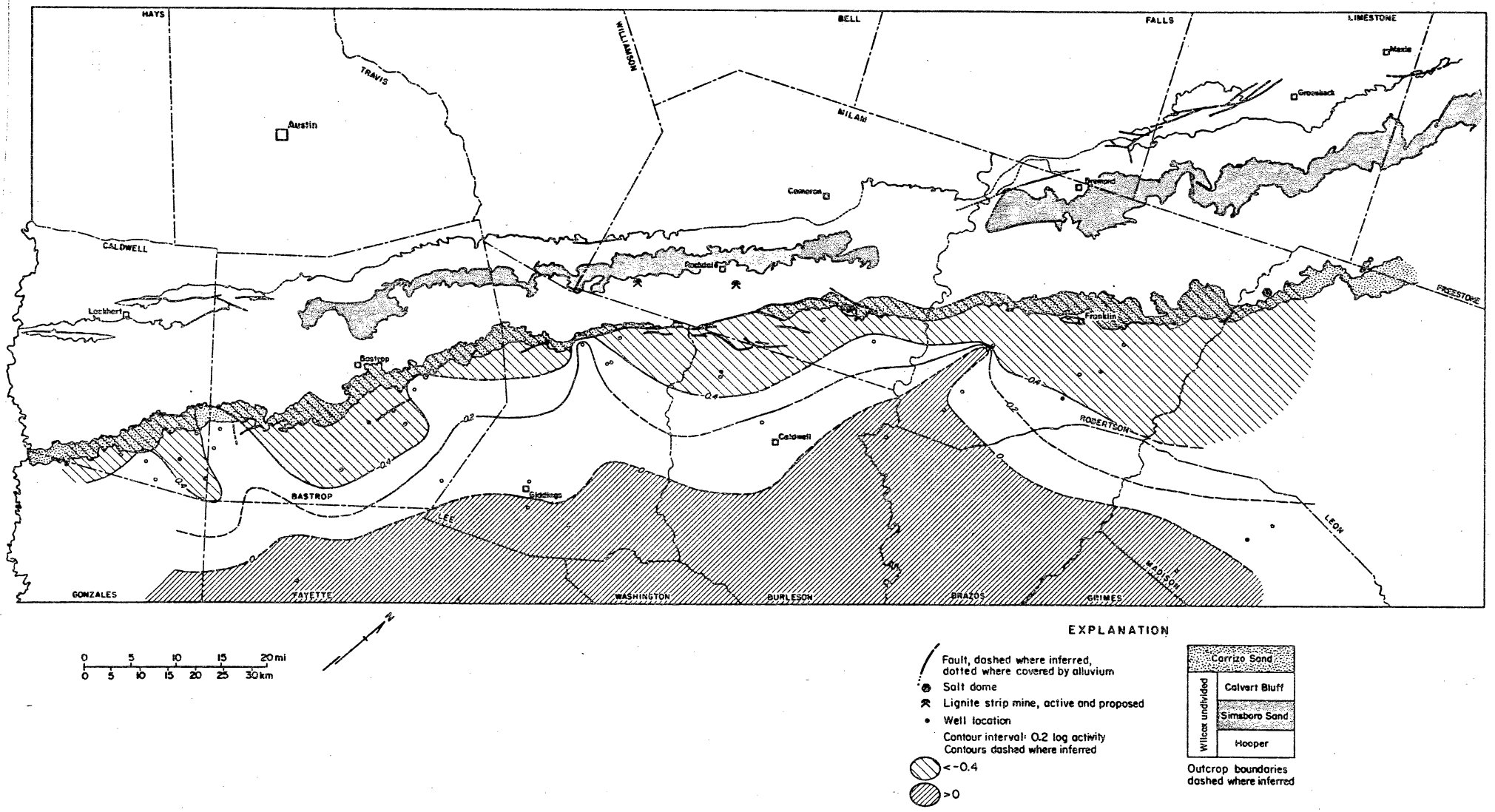

Figure 34A. Map of Carrizo $\log [Na^+]^{.33}/[Ca^{2+}]^{.16}$ ratios as derived from the montmorillonite-cation-exchange reaction. The areas with low activity ratios correspond to presumed recharge areas, and areas with high ratios correspond to presumed discharge areas.

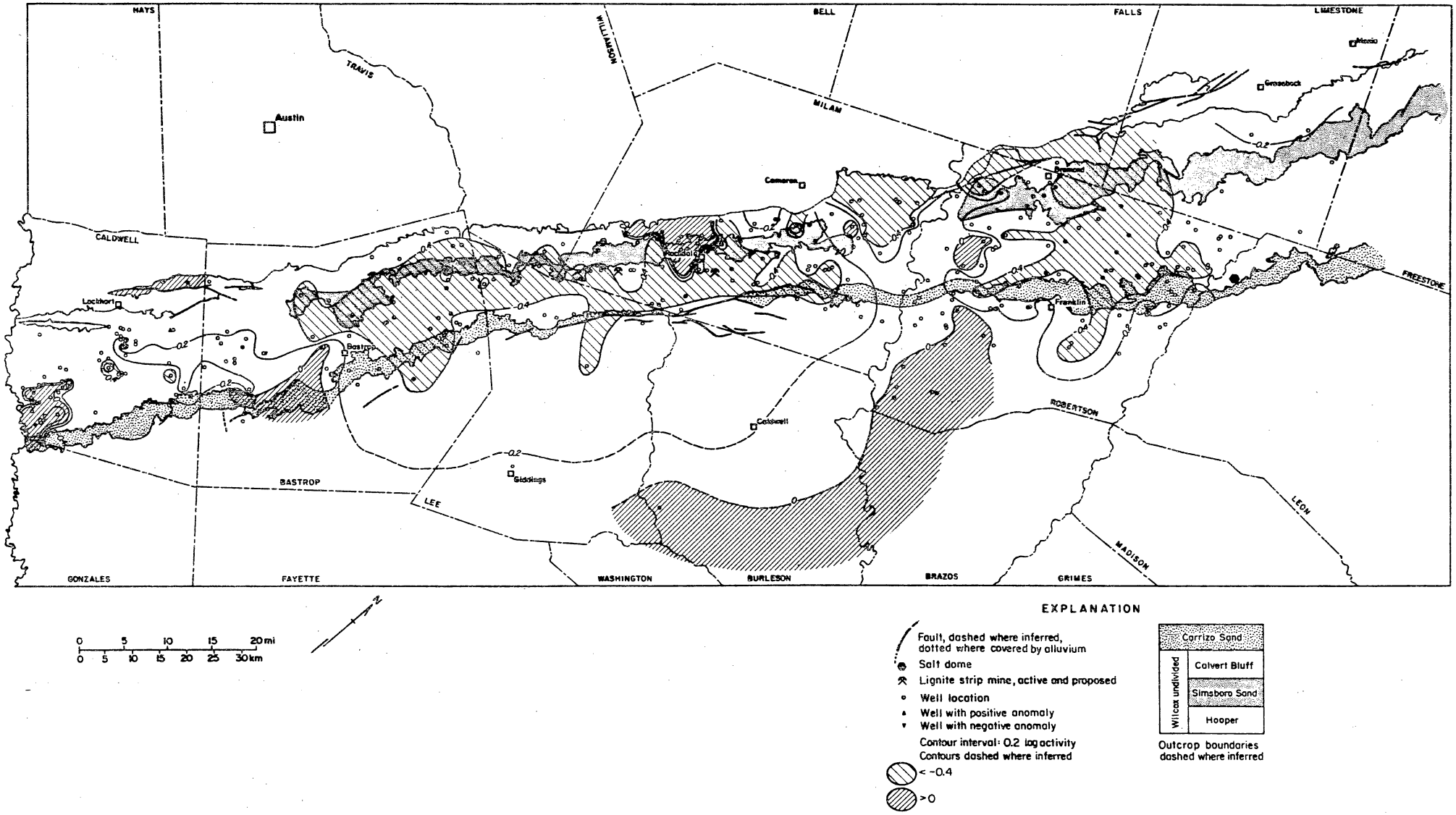

Figure 34B. Map of Wilcox $\log [Na^+]^{.33}/[Ca^{2+}]^{.16}$ ratios as derived from the montmorillonite-cation-exchange reaction. The areas with low activity ratios correspond to presumed recharge areas, and areas with high ratios correspond to presumed discharge areas.

aquifer (fig. 34b), the activity ratio is low near most of the outcrop of the Simsboro Formation of the Wilcox Group (except along rivers and major streams) and along surface-water drainage divides.

If low ratios are indicative of major recharge areas, as suggested by the coincidence with sand outcrops and drainage divides, then recharge waters are enriched in calcium relative to sodium. Conversely, discharge waters found in the vicinity of rivers and major streams and in the deeper basin are enriched in sodium relative to calcium. The implication here is that, since the relative abundance of the two cations reverses from presumed recharge areas to presumed discharge areas, a chemical reaction such as cation exchange on clay minerals causes the change. A further implication is that calcium-montmorillonite (or other clay with cation-exchange sites) is stable relative to sodium-montmorillonite, thus releasing sodium into the ground water. This assumes, of course, that the clays with cation-exchange sites contained sodium before the present ground-water flow system was established.

Figure 35 is a map of the $\log [Ca^{2+}]^{.3} [Na^{+}]^{.7}$ product. The geochemical patterns in these maps are similar to those in figure 34: higher values dominate along rivers and major stream, and in downdip areas, and lower values dominate along drainage divides and, to a certain extent, in sand outcrops. In the Carrizo Sand (fig. 35a), large areas of relatively low sodium-calcium activity product extend far downdip of the outcrop (Burleson County, Madison County, and parts of Robertson County). These extensions are markedly absent or less pronounced on the sodium-calcium activity ratio map (fig. 34a) and may suggest that argillation of plagioclase is not occurring in at least some parts of the Carrizo, whereas cation-anion exchange on clay minerals is occurring, or the extensions may reflect interconnected major Carrizo sand channel belts containing low-Ca^{2+} and -Na^{+} water. The activity product map of the Wilcox (fig. 35b) appears to be more sensitive than that of the activity ratio in that the areas of high and low activity

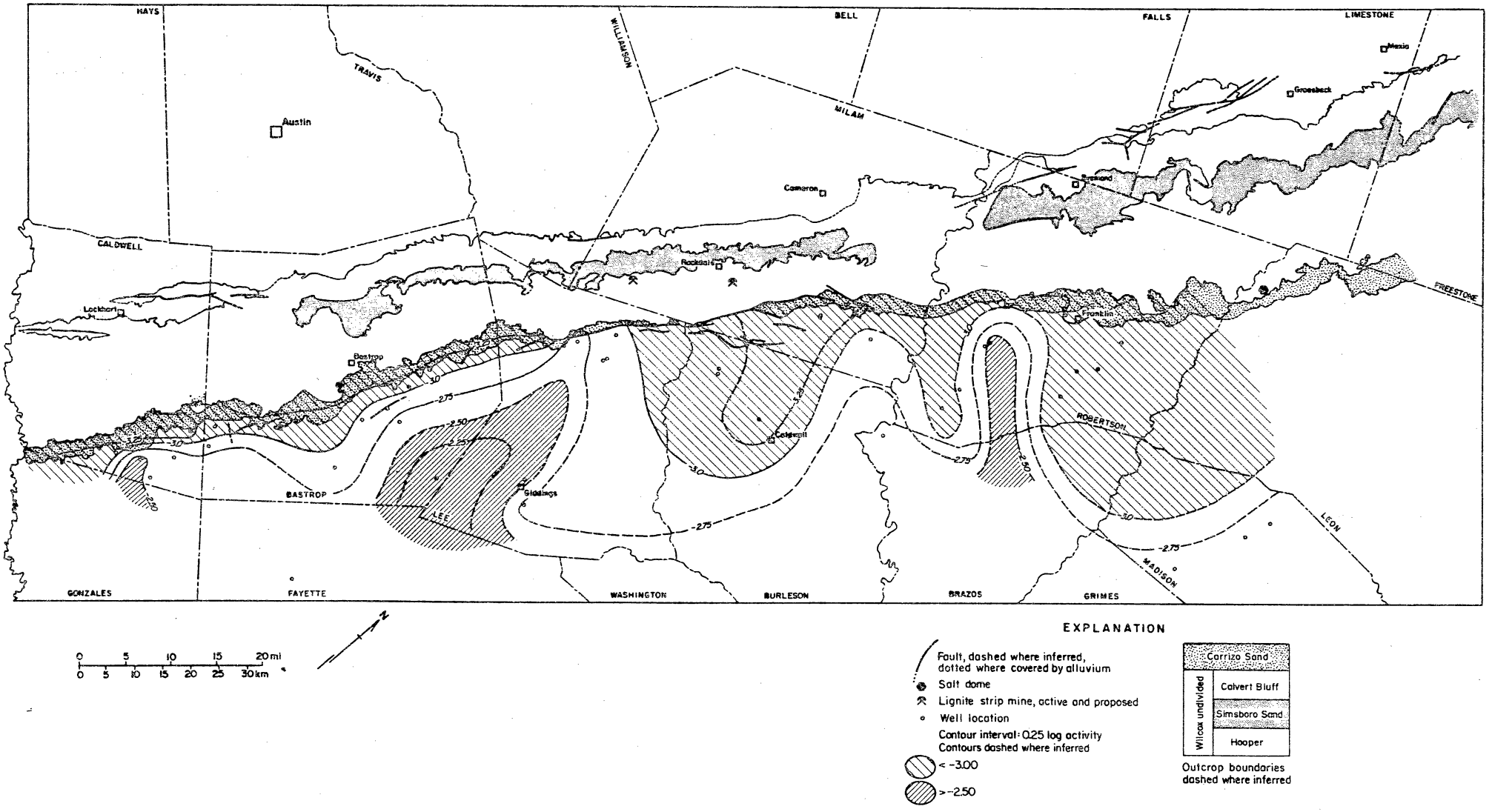

Figure 35A. Map of Carrizo $\log[Ca^{2+}]^{.3}[Na^{+}]^{.7}$ products as derived from the reaction describing feldspar argillation. The areas of low activity products correspond to presumed recharge areas or to areas where feldspar may be absent. The areas of high values of the sodium-calcium activity product correspond to presumed discharge areas.

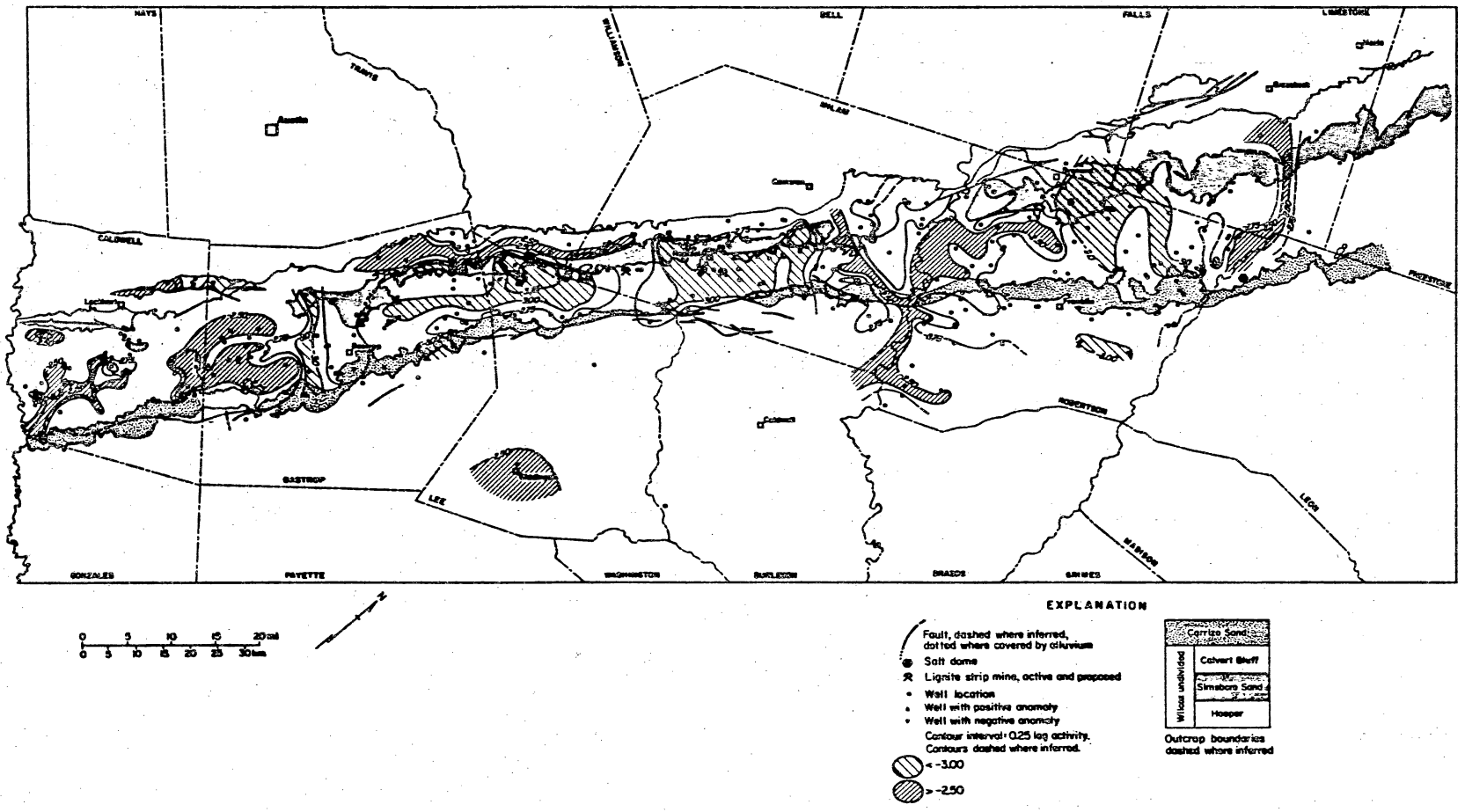

Figure 35B. Map of Wilcox $\log [Ca^{2+}]^{\cdot 3} [Na^{+}]^{\cdot 7}$ products as derived from the reaction describing feldspar argillation. The areas of low activity products correspond to presumed recharge areas or to areas where feldspar may be absent. The areas of high values of the sodium-calcium activity product correspond to presumed discharge areas.

products within the outcrop area are smaller and less continuous. However, the implications of the small areas of high sodium-calcium activity product relative to the activity ratio are not clear.

The dissolution of feldspar is complicated (Stumm and Morgan, 1981). First, feldspar dissolution causes release of aluminum, leading to oversaturation with respect to gibbsite. Kaolinite then begins to form from the gibbsite with increasing silicic acid concentration. With continuing dissolution of feldspar and consequent release of silicic acid, kaolinite may be converted into montmorillonite in high-pH waters. Because none of the chemical analyses in the study area include concentration of dissolved aluminum species, it is difficult to assess equilibrium with respect to any of the feldspars or clay minerals. However, because aluminum is rarely found in concentrations that are an order of magnitude greater than the default value used for this investigation (Hem, 1970), the following discussion of feldspar-clay equilibria is probably reasonable.

Silicic acid is released during the argillation of feldspar (Kaiser and Ambrose, this report, eq. 2). Figure 36 shows the distribution of silicic acid activity in the Carrizo and Wilcox aquifers. In both aquifers, areas of relatively high silicic acid activity coincide with drainage divides and, to a certain extent, with sand outcrops. Areas of relatively low silicic acid activity coincide with rivers and major streams and with downdip regions. These patterns are similar to those seen in figures 34 and 35, but suggest a decrease in silicic acid activity with an increase in the sodium-calcium activity ratio (fig. 34) and the sodium-calcium activity product (fig. 35). This implies that, if plagioclase argillation occurs, either (a) it occurs only in major recharge areas (along drainage divides and in sand outcrops), as evidenced by the relatively high silicic acid activity, or (b) it may be occurring throughout the aquifers but some other chemical reaction is controlling the silicic acid activity. Other possible controls on silicic acid activity appropriate to the study area include formation of authigenic clays and precipitation of silica, perhaps in the form of chalcedony (Kaiser and Ambrose, this report).

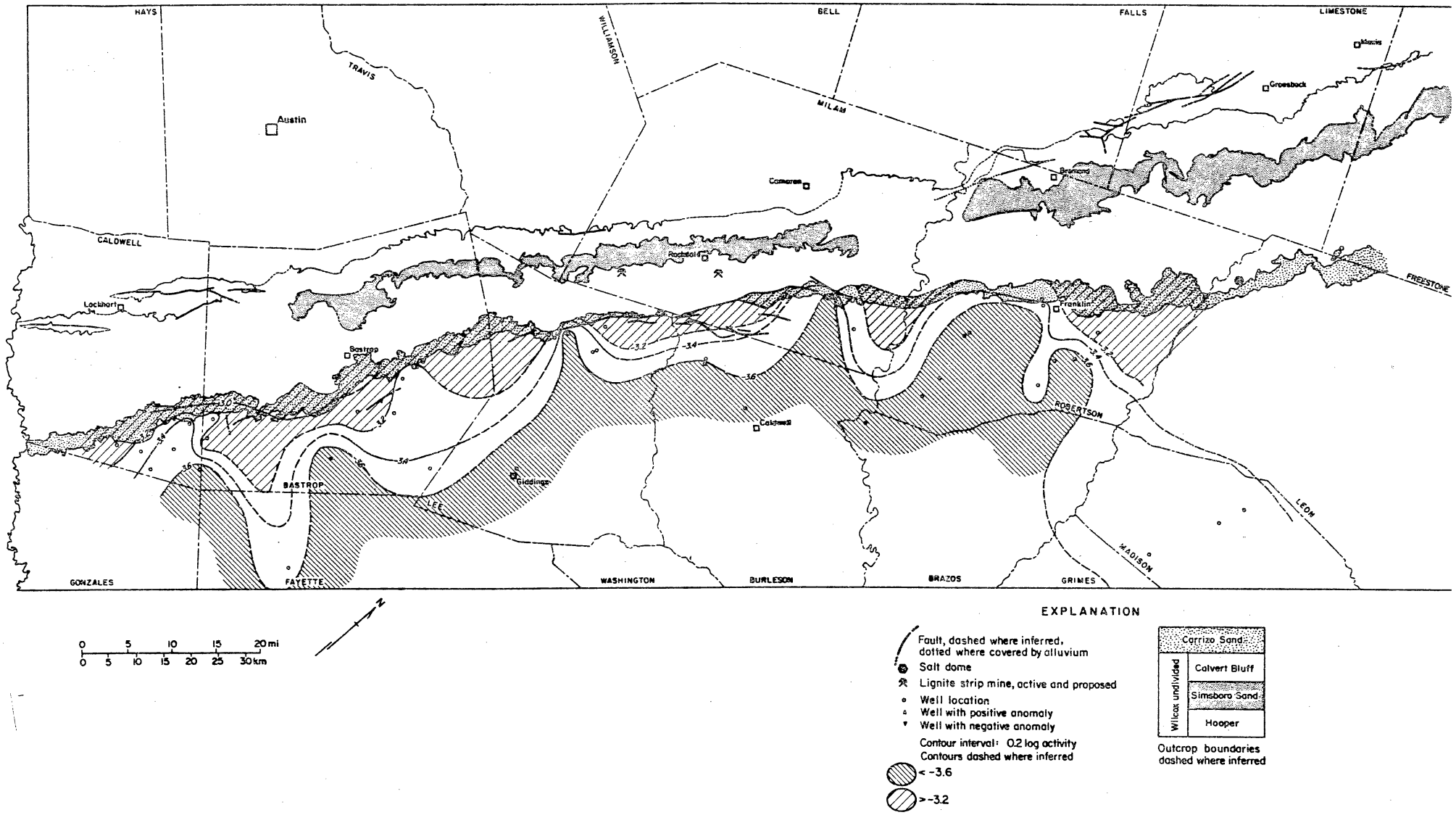

Figure 36A. Map of Carrizo $\log[H_4SiO_4^o]$ values. Areas of high activity correspond to presumed recharge areas and areas of low activity correspond to presumed discharge areas. The silicic acid activity approaches that of equilibrium with quartz ($\log a \simeq -4$) or chalcedony ($\log a \simeq -3.7$) in presumed discharge areas and that of silica glass ($\log a \simeq -2.95$) in presumed recharge areas.

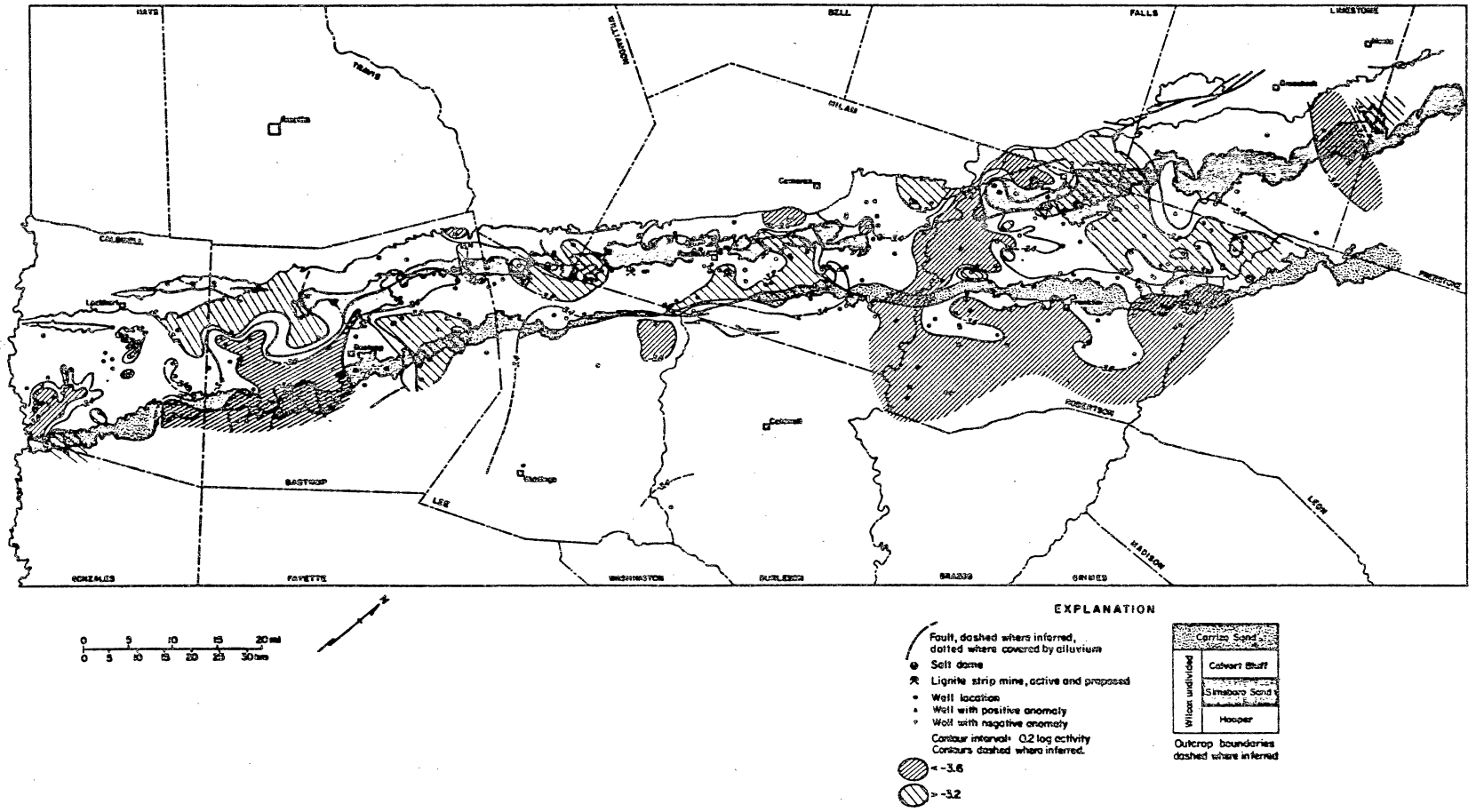

Figure 36B. Map of Wilcox log $[H_4SiO_4^o]$ values. Areas of high activity correspond to presumed recharge areas and areas of low activity correspond to presumed discharge areas. The silicic acid activity approaches that of equilibrium with quartz ($\log a \simeq -4$) or chalcedony ($\log a \simeq -3.7$) in presumed discharge areas and that of silica glass ($\log a \simeq -2.95$) in presumed recharge areas.

In the Wilcox outcrop in Limestone County and along the western edge of the Wilcox outcrop throughout much of the study area, the water chemistry does not reflect recharge conditions as would be expected (figs. 34-36), but it seems to show water chemistry typical of discharge areas. In Limestone County this may be the result of fewer sands in the Simsboro and Calvert Bluff Formations (Kaiser and others, 1980) and probable poor hydrologic communication among the sands. The water chemistry may reflect slower water movement through these areas (longer residence time), thus making the water similar to discharge-area water. Along the western part of the Wilcox outcrop the Hooper Formation of the Wilcox Group is the outcropping unit. The lower Hooper is less sand-rich than either the Simsboro Formation or the Calvert Bluff Formation of the Wilcox Group. As a result, the water chemistry may reflect longer residence time, as in Limestone County.

SUMMARY

The change in $\log[Na^+]^{.33}/[Ca^{2+}]^{.16}$, $\log[Ca^{2+}]^{.3}\ [Na^+]^{.7}$, $\log[H_4SiO_4^o]$ from major recharge areas to discharge areas or downdip suggests that cation exchange on clay minerals, argillation of feldspars, and formation of authigenic clay minerals or precipitation of silica may be occurring in all or parts of both the Wilcox and Carrizo aquifers. Petrographic evidence is necessary to verify these water-rock interactions, but their validity is supported by the close and fairly consistent relationship between presumed major recharge areas and small ratios and products and high $H_4SiO_4^o$ activity. A similar relationship exists for discharge areas and large ratios and products and low $H_4SiO_4^o$ activity. Exceptions occur in the Hooper Formation and in the undivided Wilcox Group of Limestone County.

This evaluation of the chemical composition of Wilcox and Carrizo ground water is limited by lack of detailed lithologic analysis of the aquifers. Dutton (1980) found that

Wilcox sandstones in the East Texas Basin range from quartzarenites to litharenites to arkoses. Of the feldspars, orthoclase is more abundant than plagioclase; most samples, however, contain far more quartz than feldspar or metamorphic and igneous rock fragments. Calcite cements, clay coats or cutans, and leached feldspars in the samples suggest that some diagenesis has occurred. If sediments in the study area are comparable to those described by Dutton (1980), then some of the reactions discussed earlier may well be occurring. The greater abundance of orthoclase relative to plagioclase is somewhat problematical; the presence of clay coats suggests that authigenic clays may be the sink for silicic acid.

RESISTIVITY MAPPING OF THE EAST-CENTRAL TEXAS WILCOX GROUP

Walter B. Ayers, Jr., and Amy H. Lewis

ABSTRACT

A resistivity-product map (RP map) was drawn to link sand-body geometry and hydrology. The product of thickness times resistivity of major sands was mapped in Anderson and Houston Counties. The sum of these products is a relative measure of aquifer transmissivity and is an additional tool for evaluating ground-water flow systems. Large products coincide with recharge areas and the axes of major channel sand belts. From the RP map, shallow ground-water flow is inferred to be downdip and toward the Neches and Trinity Rivers. The percent major-sands and RP maps show that major sands focus ground-water flow. The base of fresh-water map shows the depths to which aquifers should be protected and reflects stratigraphy and sedimentation.

INTRODUCTION

Earlier mapping of the Wilcox Group of Texas (Kaiser, 1974; Kaiser and others, 1978; Kaiser and others, 1980) has delineated the occurrence of lignite and its relationship to sand-body geometry in the exploitable deep basin (200 to 2,000 ft or 61 to 610 m) of east-central Texas (fig. 1). In order to clarify sand-body geometry, an expanded data base was required. The acquisition of 840 geophysical logs has increased the data base from 626 to 1,466 logs. Included are approximately 30 proprietary density logs that will prove useful in calibrating or refining our operational definition of lignites.

Thick lignites occur in the lower Calvert Bluff Formation immediately overlying the Simsboro Formation and in the upper Calvert Bluff Formation just beneath the Carrizo Sand. The Calvert Bluff and Simsboro Formations are regional aquifers that may affect and be affected by lignite recovery attempts. Therefore, this report presents the results of an experiment to construct maps that interrelate geology and hydrology of the Calvert Bluff and Simsboro Formations. In a search for links between geology and hydrology, we constructed a series of ten lithofacies and resistivity maps for a test area in Anderson and

Houston Counties. Those maps which appear to be most useful are the percent major sands, resistivity, and base of fresh water.

LITHOFACIES AND RESISTIVITY MAPS

Percent Major-Sands Map

The major sands, arbitrarily defined as those greater than 40 ft (12.2 m) thick, represent framework facies and are therefore useful in outlining Wilcox fluvial axes. The percent major-sands map (fig. 37) displays sand-body geometries similar to those mapped earlier by Fisher and McGowen (1967) and Kaiser and others (1978). Dip-oriented fluvial sand bodies in Anderson County terminate in lobate, deltaic sand bodies in Houston County. Low sand percentages over Concord, Keechi, Brushy Creek, and Palestine salt domes suggest that they were active during Wilcox sedimentation (Seni and Fogg, 1981). There are two advantages to mapping major sands rather than sands of all thicknesses. First, data can be evaluated more rapidly and second, the greater thickness and lateral extent of major sands imply that they exert maximum control on ground-water flow; sands in effect focus the flow.

Resistivity-Product Map

Major sands exert maximum control on equivalent hydraulic conductivity (K) as well as focus ground-water flow. Data from field pumping and laboratory tests indicate that in the 200 to 2,000 ft (61 to 610 m) depth range, sands with resistivities greater than 20 ohm-m have conductivities at least 10 to 100 times greater than sands with lower resistivities (Fogg and others, in press). Significantly, major sands of the same interval have higher resistivities than do thinner sands. It is clear that major sands and resistivity are indicators of framework facies or sand-body geometry and ground-water flow,

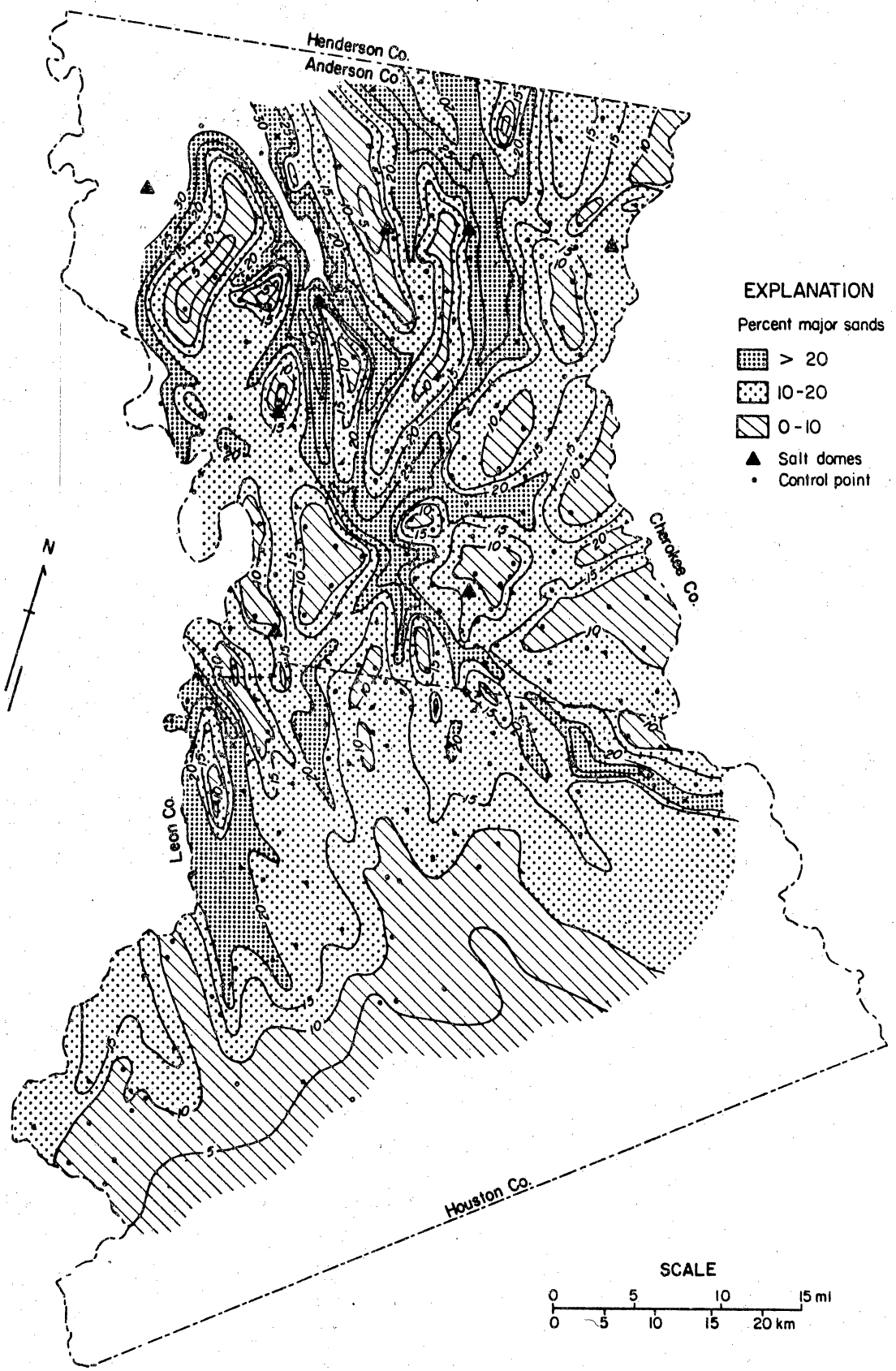

Figure 37. Percentage of major sands in the Wilcox Group.

respectively. Therefore, to link sand-body geometry and ground-water flow, the product of sand-body thickness and its resistivity was mapped to yield a resistivity-product map (fig. 38). Mapped is RP_{sum}, the sum of the thicknesses (b in meters) of major sands multiplied by their respective resistivities (R in ohm-m^2/m), in units of ohm-m^2. RP_{sum} is a relative measure of aquifer transmissivity (T) where true T is the product of equivalent K times aquifer thickness (T = Kb). Thus, because thick sands control ground-water flow and high resistivities tend to coincide with recharge areas, the mapped values of resistivity product (ohm-m^2) provide an additional tool for evaluating ground-water flow directions.

Ground-water flow, as inferred from the resistivity-product map, reflects the influence of the sand-body geometry of major sands (fig. 37). From the resistivity-product map of the Wilcox Group in Anderson and Houston Counties (fig. 38), we infer recharge (high ohm-m^2) around domes and at outcrop; flow (decrease in ohm-m^2) is inferred to be downdip and in the directions of the Trinity and Neches Rivers. Results of resistivity mapping compare favorably with Anderson County ground-water flow lines from potentiometric-surface mapping, the solid arrows on figure 38. Similarities between the resistivity-product map (fig. 38) and the percent major-sands map (fig. 37) suggest that the thick sands do indeed focus ground-water flow.

Base of Fresh Water Map

The base of fresh water (BFW) map, figure 39, shows the elevation below sea level of the deepest sand with a resistivity greater than 20 ohm-m (TDS ≈ 1000 mg/L; fig. 40). Updip, the BFW lies within the Wilcox Group, except in muddy interchannel areas overlying salt domes. There, it is stratigraphically higher and at the base of the overlying Carrizo sand (fig. 2). Downdip in northern Houston County, the Wilcox major sands have not been flushed by fresh water. In that region the BFW also occurs at the base of the Carrizo sand.

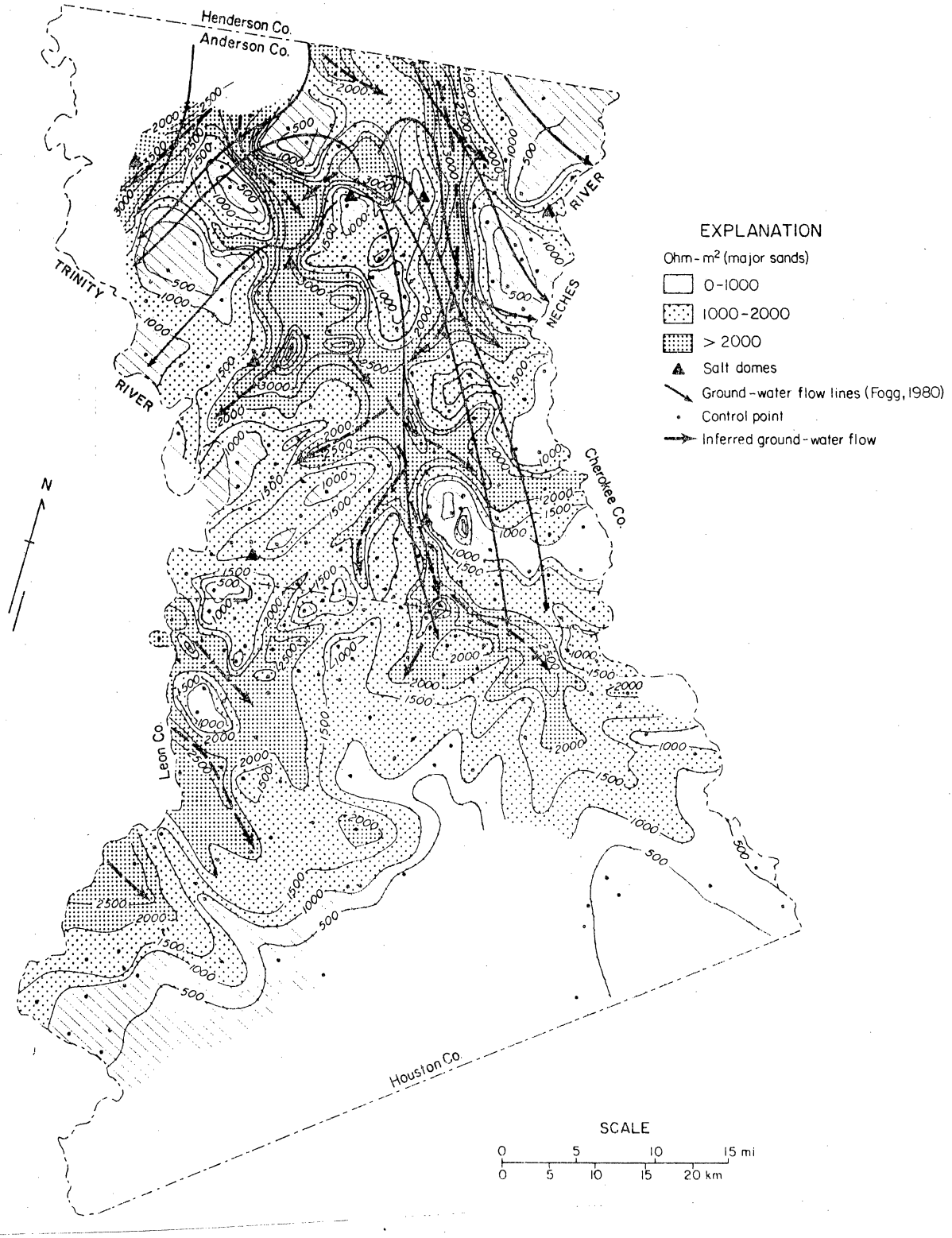

Figure 38. Map of resistivity product of major sands (RP_{sum}) in the Wilcox Group. Ground-water flow lines (solid) from Fogg (1980). Dashed arrows represent flow direction inferred from this map.

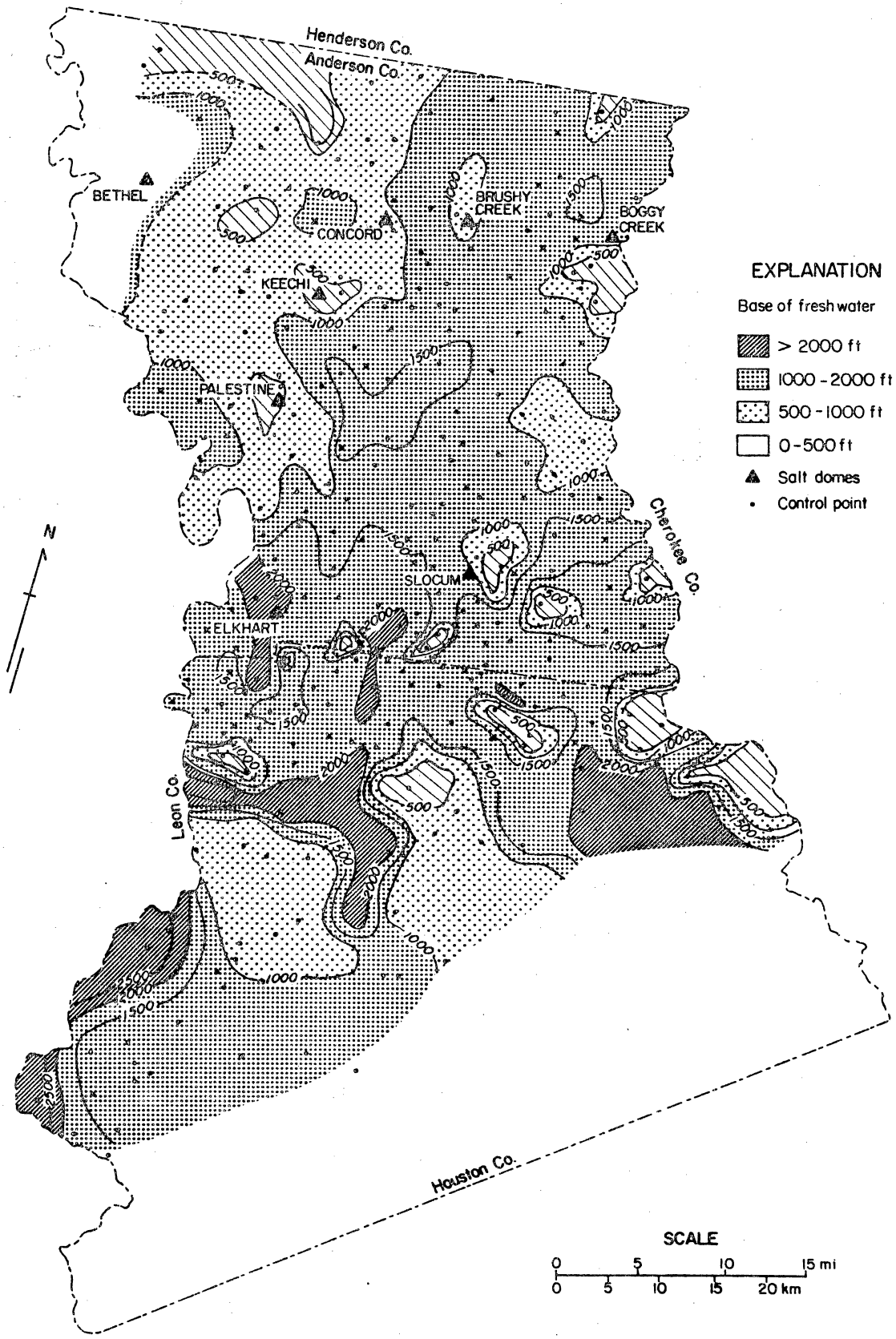

Figure 39. Base of fresh water below sea level.

CONCLUSIONS

The geometry and position of framework sand bodies are delineated by the percent major sands map, which reveals dip-oriented sands of Anderson County terminating as lobate sand bodies in Houston County. From the resistivity-product map we infer that recharge is around domes and at outcrop and that ground-water flow is downdip and in the direction of the Trinity and Neches Rivers. Major sands are dip-oriented conduits with flow restricted in areas of lower major sand percentages, especially over domes.

Currently, maps of resistivity and major sand percentages are being constructed for the east-central Texas Wilcox Group. Where the Wilcox Group can be subdivided, the Calvert Bluff and Simsboro Formations are being mapped separately in an effort to more accurately evaluate the hydraulic setting of the upper and lower Calvert Bluff lignites. The occurrences of lignites greater than 5 ft (1.5 m) thick will be mapped and their relationship to regional hydrology as determined from the resistivity mapping will be evaluated.

EMPIRICAL RELATIONS BETWEEN WILCOX GROUND-WATER QUALITY AND ELECTRIC-LOG RESISTIVITY, SABINE UPLIFT AREA

Graham E. Fogg and Paul E. Blanchard

ABSTRACT

Empirical relationships have been derived that relate Wilcox-Carrizo ground-water quality to electrical resistivities obtained from borehole geophysical logs. Data were obtained from water chemistry analyses and resistivity logs for water wells. The variations in TDS are caused primarily by variations in the major ionic constituents: sodium (Na^+) and bicarbonate (HCO_3^-). Consequently, TDS, Na^+, and HCO_3^- all correlate fairly well with electric log resistivity. The relations can be used to approximate quality and general composition of Wilcox ground-waters when actual chemical analyses are not available.

INTRODUCTION

Empirical relationships have been derived that relate electric log resistivity and concentrations of ground-water total dissolved solids (TDS), sodium (Na^+), bicarbonate (HCO_3^-), and chloride (Cl^-) for the Wilcox-Carrizo aquifer system (figs. 40 and 41a, b, and c). The data were obtained from water wells for which there are available both water chemistry analyses and induction or 64-inch normal resistivity logs. Electrical resistivity variations between units of similar lithology are primarily a function of water chemistry; hence, water quality can often be inferred from the resistivity log. The procedure used here entails simply plotting the chemical constituents versus electric log resistivity (R_o, resistivity of a formation 100 percent saturated with water) and observing any trends. Field tests have shown a prediction accuracy of $\pm$250 mg/L TDS for the method (Fogg and Kreitler, 1982).

STATISTICAL ANALYSIS

Least-squares regression lines and statistics computed using the SPSS statistical computer package (Nie and others, 1975) are plotted for each relationship (figs. 40 and

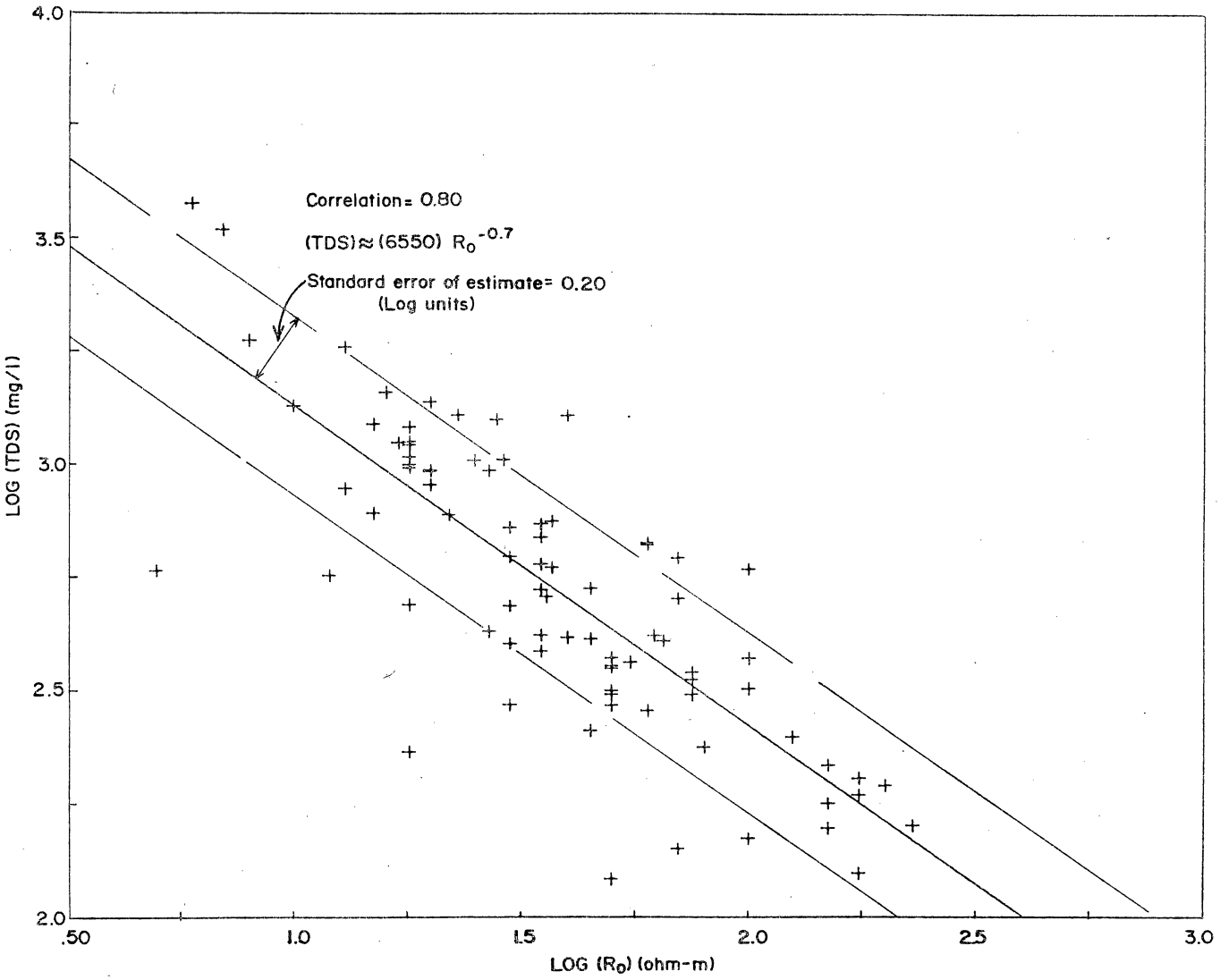

Figure 40. Graph of TDS versus electric log resistivity (R_O; 64-inch long normal or induction), Wilcox-Carrizo aquifer system, Sabine Uplift area. Data are from water wells that are screened primarily in channel-fill sands at depths of 200 to 1,200 ft (61 to 366 m).

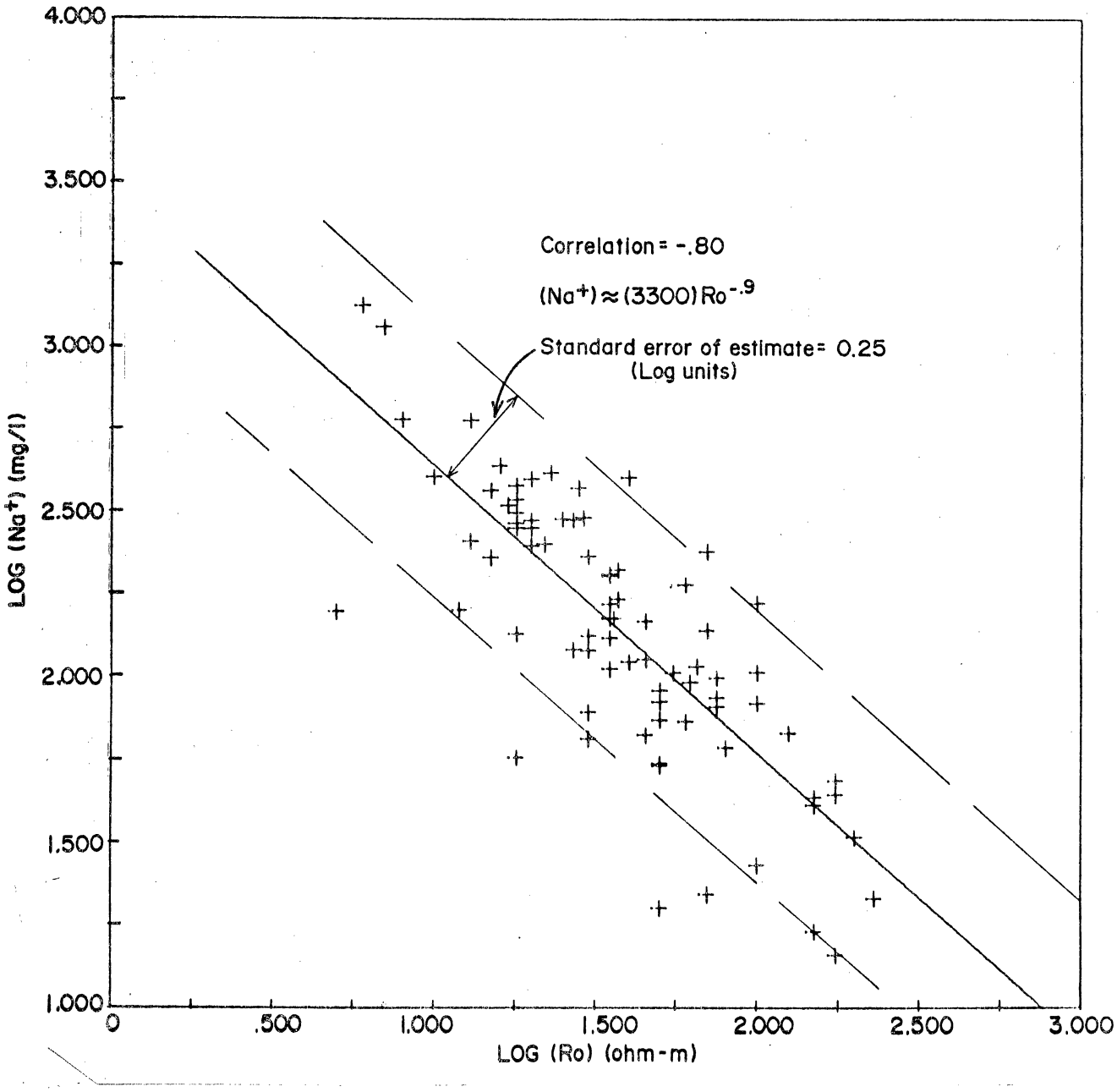

Figure 41A. Plot of sodium (Na^+), bicarbonate (HCO_3^-), chloride (Cl^-) concentrations versus R_o. Na^+ and HCO_3^- show better correlations than does Cl^-, because Na^+ and HCO_3^- are generally the dominant ions in Wilcox-Carrizo ground water.

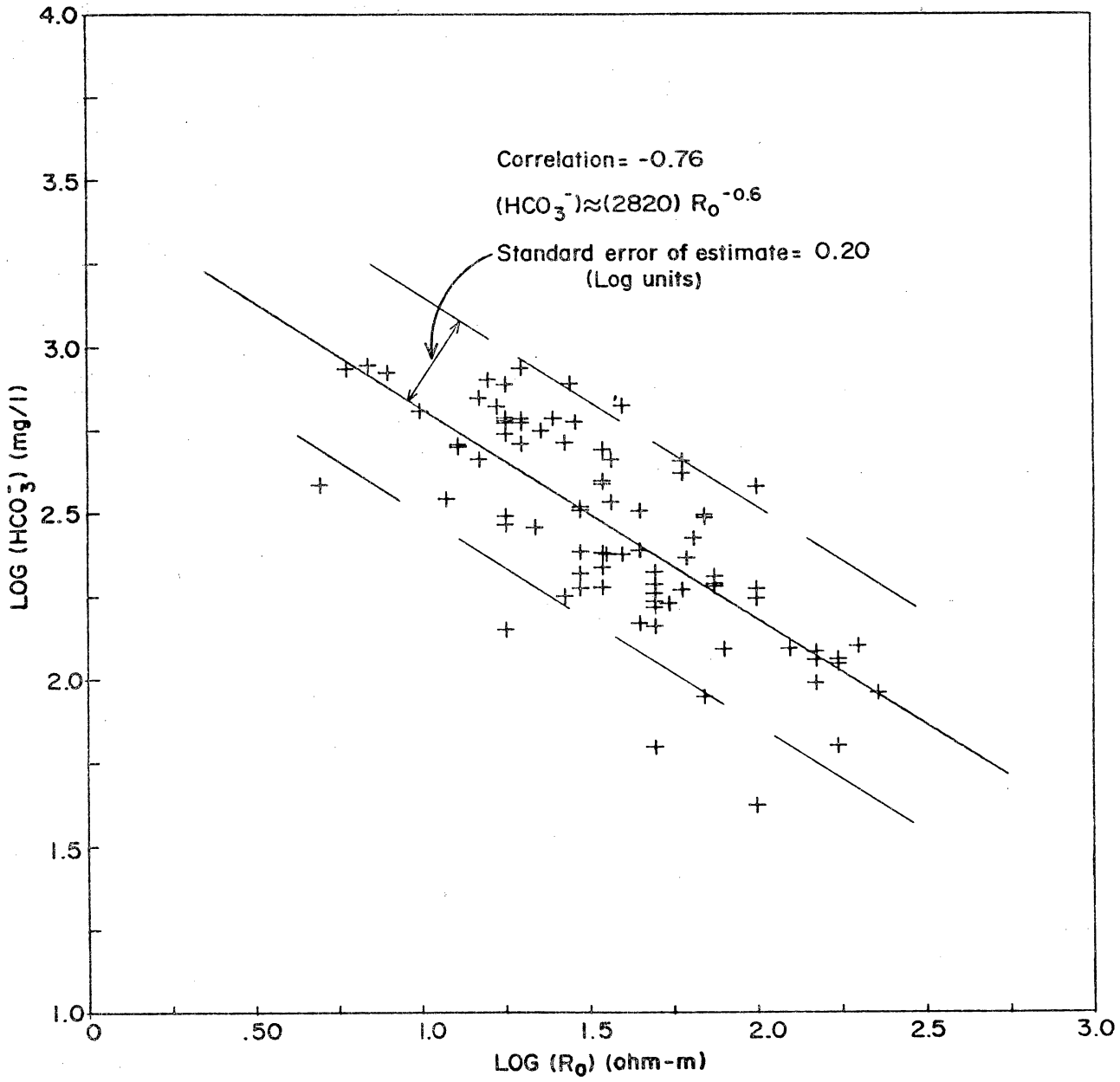

Figure 41B. Plot of bicarbonate (HCO_3^-) concentrations versus R_o. Na^+ and HCO_3^- show better correlations than does Cl^-, because Na^+ and HCO_3^- are generally the dominant ions in Wilcox-Carrizo ground water.

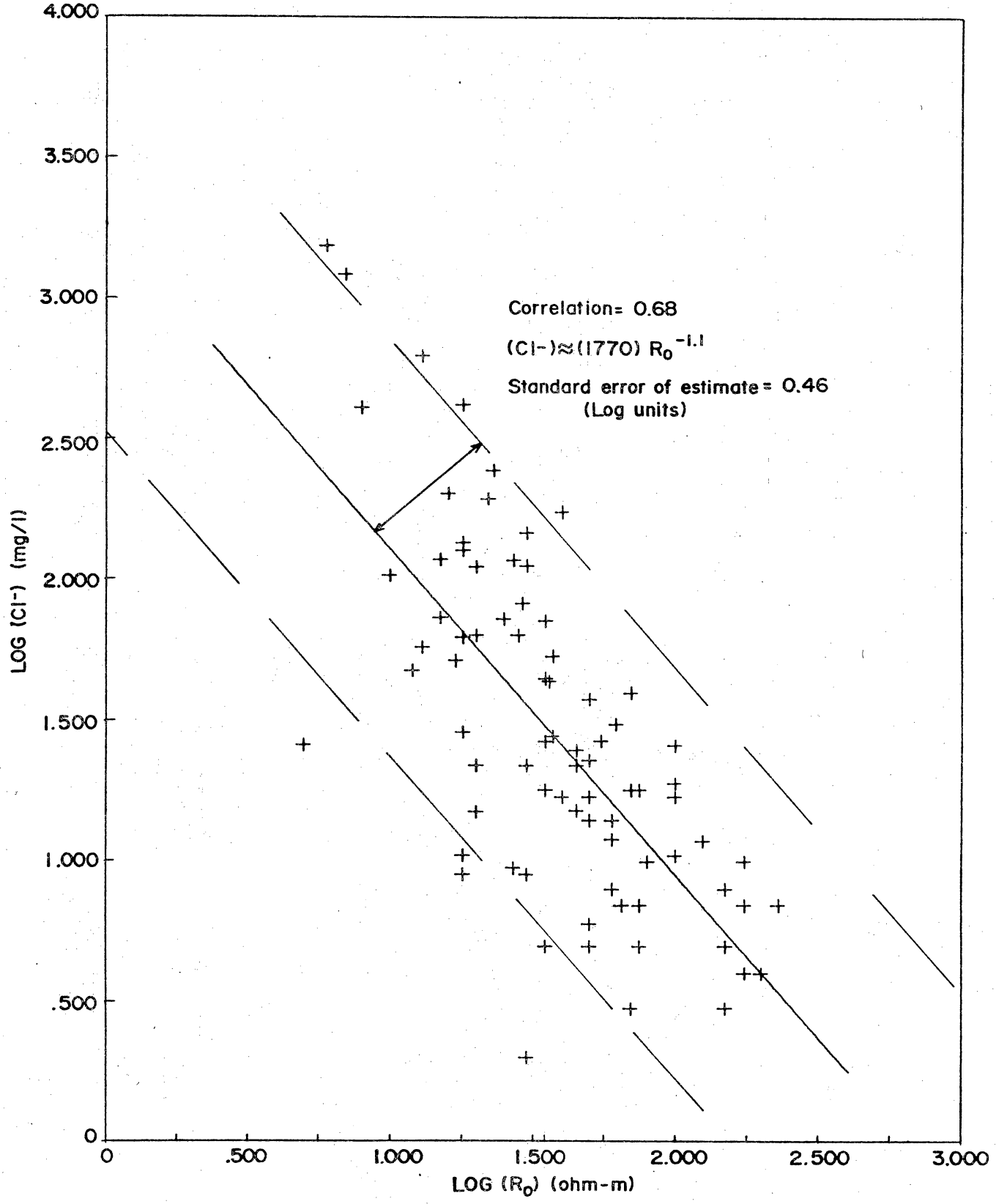

Figure 41C. Plot of chloride (Cl^-) concentrations versus R_o. Na^+ and HCO_3^- show better correlations than does Cl^-, because Na^+ and HCO_3^- are generally the dominant ions in Wilcox-Carrizo ground water.

41). Confidence limits can be calculated using the standard error of estimate values provided. For example, consider the equation and standard error of estimate for the TDS-R_o plot:

$$TDS = (6551.)\, R_o^{-0.69} \pm 0.20 \text{ log units}$$

For Ro = 30 ohm-m, the equation yields TDS = 627 mg/L; and because the standard error is in log units, the confidence interval must be calculated as follows:

$$\log (TDS) = \log (R_o) \pm 0.20$$
$$\log (TDS) = 2.80 \pm 0.20$$

or

TDS = 627. with standard error limits from 398. to 1,000. mg/L.

In other words, an R_o value of 30 indicates that TDS probably ranges from 398 to 1,000 mg/L.

The R_o-HCO_3^- and R_o-Na^+ plots show reasonable trends because Na^+ and HCO_3^- are the major ions in solution. As Wilcox-Carrizo ground water flows through the aquifer, it evolves progressively into a Na^+ - HCO_3^- water (Henry and Basciano, 1980, Fogg and Kreitler, 1982, and Kaiser and Ambrose, this report). The correlation between Cl^- and R_o is comparatively weak because the Cl^- concentrations are more erratic and generally lower than Na^+ and HCO_3^- concentrations. Anomalously high Cl^- concentrations in Gregg County (Fogg and Kreitler, 1982) might cause some of the scatter observed in the Cl^- -R_o plot. Also included is a regression plot of TDS versus specific conductance of the water samples (fig. 42). As is commonly found, the relationship is practically one-to-one.

CONCLUSIONS

The R_o chemistry relationships presented here can be used to approximate quality and general composition of Wilcox ground waters when actual chemical analyses are not

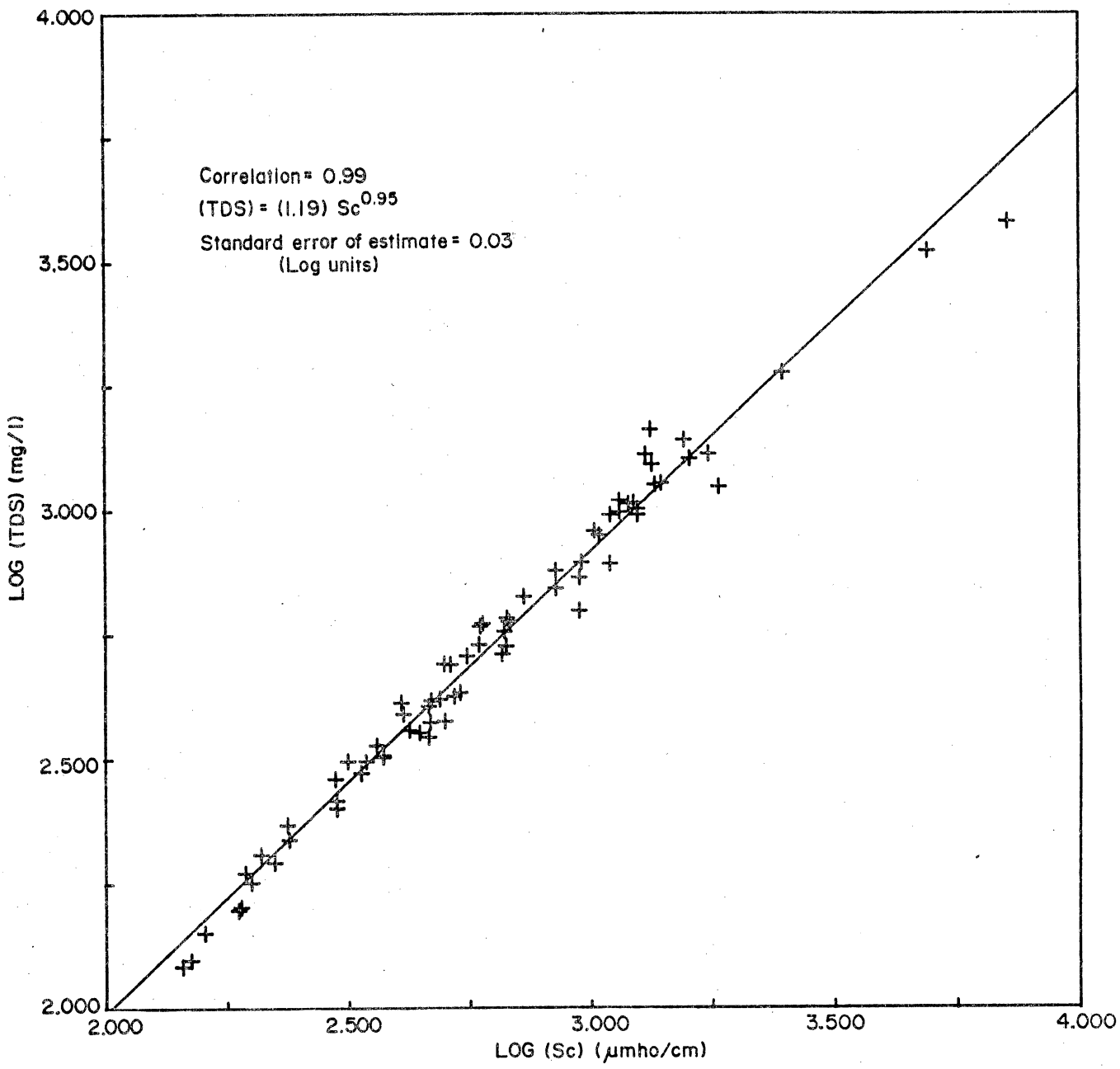

Figure 42. Graph of TDS versus specific conductance of the water samples.

available. The method is particularly useful for delineating water quality changes with depth in the Wilcox using oil and gas logs. Water chemistry analyses are not suitable for this, because they generally represent waters from discrete sand bodies or some mixture of waters from several different sands. A map of the elevation of the base of fresh water (TDS less than 1,000 mg/L) in the Sabine Uplift area made from available oil and gas logs will be included in a future report.

ANALYTICAL METHODS FOR LIGNITE CHARACTERIZATION

C. L. Ho, C. Mahan, S. Tweedy, and D. Gower

ABSTRACT

In coal characterization used, modern instrumental methods are preferred because of their sensitivity, reproducibility, and high efficiency; only a small amount of sample is needed for each type of analysis. The problem of "sample inhomogeneity" was overcome by proper sample splitting and pulverization of the split. Proximate analysis is performed using a thermogravimetric analyzer. Ultimate analysis (C, H, N) is accomplished with an automatic CHN-analyzer. A micro-Kjeldahl method is used to establish the reliability of the nitrogen value obtained by the CHN-analyzer. Total sulfur is measured with a semi-automatic sulfur analyzer. Oxygen content is obtained by subtraction. Total Btu is determined using an adiabatic bomb calorimeter. Sulfate and iron oxides are dissolved with hot 6N HCl; sulfate in solution is measured turbidimetrically. Pyritic mineral in the residue is oxidized with hot 2N HNO_3; ferric iron derived from oxidation of pyritic mineral is measured by atomic absorption spectrophotometer and pyritic-S is calculated stoichiometrically from the amount of iron measured. Organic sulfur is computed by subtracting SO_4-S plus pyritic-S from the total-S. Halides (Cl and F) in coal are released into solution by oxygen bomb combustion. Chloride is measured colorimetrically and fluoride by a specific ion electrode.

The mineralogical fraction in coal is isolated by low-temperature ashing and identified by X-ray diffraction. Non-silicate minerals are isolated by HF treatment following LTA ashing. Chemical composition of coal ash is determined by ICP-AES after the ash is fused with Li-metaborate plus Li-tetraborate flux and dissolved in dilute HNO_3. Inorganic composition in whole coal was determined by ICP-AES following total decomposition of the sample with HF, HNO_3 + H_2SO_4 + $HClO_4$ or HF, HNO_3 + $HClO_4$. Selected trace elements (B, Hg, Ag, As, Se, U_3O_8) are released into solution by oxygen bomb combustion; accurate measurement of each element is accomplished using various specific methods.

INTRODUCTION

This paper summarizes the methodology for coal characterization currently used at the Mineral Studies Laboratory (MSL) of the Bureau of Economic Geology at The University of Texas at Austin. The MSL has, for the most part, chosen to use modern instrumental techniques rather than the manual "classical methods" for the following reasons:

(1) Some instruments are automated;

(2) Some instruments are capable of analyzing multiple parameters simultaneously;

(3) Instrumentation provides precise regulation and control of desired experimental conditions;

(4) Instrumentation provides high sensitivity and precision;

(5) Instrumentation provides efficiency;

(6) The diverse area of investigation for coal and coal utilization make adaptation of modern instrumental techniques the only alternative.

A chief objection to instrumental methods is that the small amount of sample used for analysis is not representative of the whole coal. Our results, on available coal reference materials from various sources, have shown that this is not the case. We have had no difficulty reproducing the certified values for these materials. The problems of sample inhomogeneity can be overcome by proper sample splitting and subsequent pulverization of the split to less than 200 mesh (74 μm) particle size using a shatterbox (see also Tewalt, this report). However, it is imperative that optimal conditions for various instrumental analyses as well as appropriate sample-handling be experimentally established before sample analysis is performed. The following sections outline the MSL's methods for coal characterization, as summarized in table 3. Included, where necessary, are brief descriptions of mechanisms involved and comparisons with classical methods.

PROXIMATE AND ULTIMATE ANALYSES

Proximate Analysis

Proximate analysis includes the determination of moisture, volatile matter, fixed-carbon, and ash (Ho and others, 1982; Montgomery, 1978) and is done by thermogravimetric analyzer (TGA). Approximately 50 mg of sample is weighed in a platinum boat and inserted into the TGA's furnace chamber according to the program in table 4. Advantages of the TGA method are:

Table 3. Analytical methods for lignite characterization.

Parameters to be Analyzed	Condition for Sample Preparation/Analysis	Technique Used for Analysis	Reference
Sample Preparation	Dried at 40°C	Shatterbox to <200 mesh (<74 μm)	Ho and others, 1982
Proximate and Ultimate Analysis			
Proximate Analysis			
Moisture	120°C	Thermogravimetric analyzer	Ho and others, 1982 Montgomery, 1978
Volatile Matter	850°C, N_2		
Fixed-C	900°C		
Ash	900°C, O_2		
Moisture	110°C	Muffle furnace; gravimetric	ASTM, 1982
Ash	450°C, 750°C, Air		
Ultimate Analysis			
CHN	Combustion in O_2 at 970°C; reduction by Cu/He at 675°C	Simultaneous automatic CHN analyzer	Ho and others, 1982
N	Micro-Kjeldahl digestion-steam distillation	Titration or spectrophotometry	Ho, in press
Total-S	Combustion in O_2 at 1350°C with release of SO_2	Sulfur analyzer (amperometric titration)	ASTM, 1982
Ash	(See text)		
Oxygen	———	Calculation	Given and Yarzab, 1978

Table 3 (continued)

Parameters to be Analyzed	Condition for Sample Preparation/Analysis	Technique Used for Analysis	Reference
Total Btu	Pellet/O_2 (300 psi)	Adiabatic Parr bomb calorimeter	Montgomery, 1978
Forms of Sulfur			
SO_4-S	Hot HCl extraction	Turbidimetric	Bradsley and Lancaster, 1965
Pyritic-S	Indirectly measured by oxidation of FeS_2 to Fe^{3+} after removal of Fe_2O_3 with hot HCl	Fe^{3+} measured by atomic absorption	Burns, 1970
Organic-S	———	Calculation	
Halides	Sample dissolution	Parr oxygen bomb combustion	Montgomery, 1978
Total Halides	Mercuric thiocyanide $Hg_2(SCN)_2$ + $FeCl_3$ reaction	Spectrophotometric	Crowe and Breidenbach, 1974
Fluoride	Standard addition	Selective ion electrode	Ho and others, 1982
Characterization of Mineral Matter and Ash			
Mineral Matter			
Isolation of Mineral Matter	50W RF power; 100 cm^3/min O_2; chamber pressure of 2 torr	Low temperature asher	Miller, 1977
Mineralogic Composition	Ground to <200 mesh	X-ray diffraction	Ho and others, 1982
Clay Mineralogy	Isolation of clay minerals/ preferential orientation/air dry/ glycolated/550°C	X-ray diffraction	Ho and others, 1982

Table 3 (continued)

Parameters to be Analyzed	Condition for Sample Preparation/Analysis	Technique Used for Analysis	Reference
Chemical Composition of Mineral Grains	None	SEM	
Fusion Characterization of Mineral Matter	Various temperatures up to 1500°C	DTA or other high temperature device (not available at MSL)	not available at the MSL
Ash:			
Major Oxides (SiO_2, Na_2O, K_2O, MnO, CaO, MgO, Al_2O_3, Fe_2O_3, P_2O_5, TiO_2, BaO)	Fusion with flux at 1040°C/ dilute acid dissolution	Simultaneous determination by ICP-AES	Ho and others, 1982
Selected Trace Elements (U_3O_8, As, Se, Mo, etc.)	High temperature fusion or multiple acid digestion	Graphite furnace A.A., fluorometric, spectrophotometric	Ho and others, 1982
Chemical Composition of Ash Grains	———	SEM	
Inorganic Composition of Whole Coal			
Major, Minor, Trace Elements (Na, K, Mg, V, Al, Fe, Ti, Co, Cr, Cu, Mn, Ni, Mo, Zn, As, Cd, Ca, Pb, Sb, Se, Sn, Li, Be, Sr, Zr, Th, P, La, Ce)	Perchloric acid, HNO_3, HCl, HF digestion	Simultaneous determination by ICP-AES	Ho and others, 1982
Accurate Determination of Selected Trace Elements (Hg, B, Ag, As, Se, etc.)	Oxygen bomb combustion	Hg: Cold vapor AA, Ag: GF AA, As: GF AA, Se: Fluorometric, B: ICP-AES/calorimeter	Ho and others, 1982
Thermal Characteristics of Lignite as an Indication of Rank	Programmed to 1000°C at high O_2 pressure	Differential scanning calorimetry	Benson and Schobert, 1982

(1) Both moisture and volatile matter are determined in an inert N_2 atmosphere in less than 15 minutes, thus oxidation of unstable organic matter and sulfide minerals is minimized. By classical methods, on the contrary, these analyses are performed in a furnace in air, and a much longer time is required for heating and cooling before weighing can be done. Such conditions of measurement may lead to the risk of sample alteration, and thus to eroneous results.

(2) Fixed-C is directly measured in the same sample used for moisture and volatile matter and is determined by rapid combustion in an O_2 atmosphere. In the classical method, fixed-C is obtained indirectly by subtracting the weights for moisture, volatile matter, and ash from total sample weight. Thus, the reliability of fixed-C value will depend on that of other values.

(3) Organic and pyritic sulfur are converted to SO_2 and swept away. In the classical method, sulfur retention, as sulfate, in the ash occurs. Thus, by definition, the true ash value must be obtained by subtracting the weight of sulfate which, in turn, must be determined by a reliable method.

(4) The precise temperature ($\pm$5°C) and controlled atmosphere of the TGA account for the reproducibility and reliability of proximate analysis results regardless of the sample types. In the classical method, it is difficult to control the atmosphere and temperature. This may have accounted, in part, for the poor reproducibility encountered in ash determination, especially for low-rank coals.

Determination of Moisture and Ash, TGA Method

If volatile and fixed-C of a sample are not required, the TGA is then programmed from the condition for hygroscopic moisture directly to the condition for ash determination, as discussed previously (Ho and others, 1982). Our experience showed that reproducible ash results, especially for low-rank coals, were difficult to obtain. This

Table 4. Thermogravimetric analysis (TGA) procedure.

Temperature	Time	Gas	Comments
ambient	--	N_2	To purge the system.
120°C	10-15 min	N_2	Weight loss[a] at this temperature was designated as hygroscopic moisture.
850°C (lignite)[b] 900°C (hard coal)[b]	7 min	N_2	Weight loss[a] at this temperature was designated as volatile matter.
900°C	5-10 min	O_2	Weight loss[a] at this temperature was designated as fixed-C.
900°C	3-5 min	O_2	Residue is designated as ash.

[a]All weight losses were plotted on a recorder as precent of the intial sample weight.

[b]The temperatures and time used for volatile matter determinations were adapted from specifications of ASTM procedures (Montgomery, 1978).

difficulty may be attributed to (1) varied degree of sulfur retention as sulfate in ash, (2) incomplete decomposition of mineral constituents at 750°C (e.g., carbonates, hydrated silicates, etc.).

Determination of Moisture and Ash, Classical Method

The coal sample is heated at 110°C for 1 to 1.5 hours preferably in an air-free atmosphere or dry N_2 to prevent oxidation (Montgomery, 1978). Weight loss is measured as moisture on a balance. The moisture-free sample is then heated at 500°C for one hour and at 750°C for two hours in a well-ventilated furnace to oxidize carbon. The residue is weighed as ash. It is assumed that carbonate decomposes to CO_2, pyritic and organic sulfur are removed as SO_2, and hydrated silicates are dehydrated to H_2O under the specified condition for ash determination.

Ultimate Analysis

Ultimate analysis includes the determinations of carbon, hydrogen, nitrogen, sulfur, and oxygen on a moisture and ash-free basis (Montgomery, 1978). C, H, and N are determined by automated analyzer. Each sample is transported into the combustion chamber where a constant temperature of 970°C and flow of oxygen are maintained. During combustion, the tin capsule melts and acts as a catalyst to quantitatively convert carbon (organic and fixed forms) to CO_2, organic-H to H_2O, and organic-N to nitrogen oxides. Other gases released from samples (halides, SO_2) are removed by a trap containing $AgVO_3$ and Ag_2WO_4. The purified gas mixture of CO_2, H_2O, and nitrogen oxides is then carried by a He gas stream through a reduction tube of copper wire, where a temperature of 675°C is maintained, nitrogen oxides are reduced to N_2, and oxygen is removed. The homogeneous gas mixture (He as carrier, H_2O, CO_2, and N_2) is sequentially carried through three pairs of thermal conductivity cells (or catharometer). Between the first pair of cells, an absorption trap containing $Mg(ClO_4)_2$ removes H_2O from the gas mixture. The differential signal of the cells shown before and after the H_2O removal

measures the water content, which is then related to the hydrogen concentration. Between the second pair of thermal conductivity cells, a trap containing ascarite removes CO_2 from the gas mixture of He, CO_2, and N_2. The differential signal of the cells shown before and after the CO_2 removal measures the CO_2 concentration, which is then related to the carbon concentration. The remaining gas mixture, which consists of He and N_2, is carried to the last set of cells. The mixture flows through one of the third pair of cells, while at the same time, pure He flows through the other cell. The differential signal of the cells is related to the nitrogen concentration.

Carbon, hydrogen, and nitrogen (C, H, N) are determined simultaneously by automated CHN-analyzer. About 1.5 mg of oven-dry (105°C) sample is weighed on a micro-balance in a tin capsule. The capsule is crimped, placed into a nickel sleeve, and loaded into one of the 64 positions of the sample holder. Normally, a full run on the CHN-analyzer consists of about 48 samples with blanks, acetanilide ($CH_3CONC_6H_5$) standards, and reference materials occupying the remaining slots in the sample holder. Complete processing of all 64 units (samples, standards, controls, and blanks) takes about 18 hours without operator attention (Ho and others, 1982).

Determination of Nitrogen by Micro-Kjeldahl Method

This method was used to check nitrogen values obtained with the CHN-analyzer. A sample (0.5 to 250 mg) is weighed and digested with hot, concentrated sulfuric acid in the presence of a salt mixture as a catalyst. This enables organic forms of nitrogen to be converted to ammonium sulfate. Ammonium sulfate in the digest is decomposed in a hot alkaline medium to release ammonia gas. The gas is steam distilled and absorbed in 2 percent boric acid. The boric acid solution is titrated with a standard acid in the presence of a mixed indicator. Nitrogen concentration is calculated from the amount of acid used (Ho, in press). Values determined using the micro-Kjeldahl method and CHN-analyzer were the same.

Total-S by Automated Sulfur Analyzer

A sample (approximately 100 mg) is weighed into a ceramic boat and mixed with V_2O_5 as a catalyst. The boat is introduced into the combustion tube, where a temperature of 1350°C and an oxygen atmosphere are maintained. Sulfur is converted to SO_2 and quantitatively absorbed by a mixture of pyridine, methanol, and water. A titrant containing iodine dissolved in the same mixture is used to titrate the SO_2. The micro-current change at the endpoint is detected by a platinum and a reference electrode. The entire analysis requires only 3 min, and it is free from interferences (Ho and others, 1982; ASTM, 1982).

Oxygen (ASTM D3176-74)

There is no satisfactory method of directly determining oxygen. Therefore, oxygen content is approximated by subtracting from 100 the sum of the other components of the ultimate analysis. By definition, oxygen calculated as a weight percentage of the sample according to this procedure does not include oxygen in the mineral matter or in the ash. However, the results so obtained were affected by errors incurred largely by the changes in mineral constituents on ignition (Montgomery, 1978; Given and Yarzab, 1978).

TOTAL BTU (ASTM D2015)

The calorific value was determined by combusting a known amount of sample (approximately 1 g) in an adiabatic oxygen-filled bomb calorimeter. The calorific value is then calculated from the temperature rise of the calorimeter with proper correction for heat of formation of HNO_3, H_2SO_4, and heat of combustion of fuse wire (Montgomery, 1978).

FORMS OF SULFUR

Sulfate Sulfur

A sample (approximately 1 g) is weighed and treated with 6N HCl at 120°C. The digest is filtered through a glass filter and the residue thoroughly washed with 6N HCl and deionized water. Sulfate in filtrate is measured by a turbidimetric method using a light-scatter path on a spectrophotometer (Ho and others, 1982; Bradsley and Lancaster, 1965).

Pyritic Sulfur

The residue from above together with the filter is treated with 2N HNO_3 at 120°C. Pyrite (FeS_2) is oxidized to Fe^{3+} and SO_4^{2-}. The solution is filtered through a glass filter. The concentration of iron in the filtrate is determined by atomic absorption spectrophotometry (AAS). Pyritic-S is calculated stoichiometrically from the amount of FeS_2-Fe (Burns, 1970).

Organic Sulfur

Organic sulfur was obtained by subtracting sulfate-sulfur and pyritic-sulfur from total sulfur. An alternative method of measuring organic-S would be to determine total-S in the residue after 2N HNO_3 extraction. However, our tests showed that a serious drawback of this method was that some of the organic-S was lost as a result of oxidation to SO_4^{2-} and solubilization of organic matter during HNO_3 treatment. Organic-S measured by the alternative method was much lower than that determined by subtraction.

HALIDES

Sample dissolution is by oxygen bomb combustion (Montgomery, 1978). A sample (approximately 1 g) is weighed and combusted in a Parr oxygen bomb fitted with a quartz

liner to prevent corrosion of the bomb's interior. Volatiles, resulting from ignition, are absorbed with a 5 percent Na_2CO_3 solution in the liner. The latter is acidified with HNO_3. The clear solution is used for determination of halides, As, Se, B, and U_3O_8.

Total Halides

Total halides are determined colorimetrically. Solutions of mercuric thiocyanate and ferric ammonium sulfate are added to an aliquot of the solution from bomb combustion. Chloride in solution combines with mercury to form an insoluble Hg_2Cl_2. The liberated SCN^- ion then reacts with ferric ion, forming a red-colored ferric thiocyanate. The resulting color is measured with a spectrophotometer at 460 nm (Ho and others, 1982; Crowe and Breidenbach, 1974).

Fluoride

Fluoride is measured using a specific ion electrode. The standard additions is used.

CHARACTERIZATION OF MINERAL MATTER AND ASH

Mineral Matter

Isolation of Mineral Matter

Mineral matter is isolated using oxygen plasma low-temperature ashing (LTA). A sample (about 1 g per chamber, 4 chambers) is spread in a quartz dish to about 1 mm thickness. The dish is placed in the center of the asher under a controlled condition such that alteration of minerals is minimal (Miller, 1977). Complete removal of carbon is indicated by a whitish appearance of the residue. The entire process takes from 24 to 36 hours and yields a total of 400 mg of ash if the lignite contains 10 percent ash. See Tewalt (this report) for additional details on LTA procedure.

Mineralogical Composition

Mineral matter isolated from LTA is packed into a sample holder and scanned on an X-ray diffractometer. A diffractogram is usually obtained for the 2θ angle range of 2° to 60°. Identification of mineral species is made from the diffractogram.

Clay Mineralogy

Clay minerals are separated from the mineral matter isolated by LTA according to Stoke's law. Clay platelets in suspension are allowed to settle in a glass disc for preferential orientation and enhancement of basal reflections. The clay films are scanned from 2° to 16° (2θ). Identification of clay mineral species is made from basal spacings obtained from three diffractograms on each sample treated by air-drying, glycol solvation, and heating at 550°C.

Chemical Composition of Coal Ash

Determination of major oxides (SiO_2, Na_2O, K_2O, MnO, CaO, MgO, Al_2O_3, Fe_2O, P_2O_5, TiO_2, and BaO) is done by inductively coupled plasma-atomic emission spectrometer (ICP-AES). A sample (approximately 50 mg) of ash is weighed and fused with Li-borate flux (1 part Li-metaborate and 2 parts Li-tetraborate) at 1040°C. The melt is dissolved in 1 percent HNO_3. All elements in solution are determined simultaneously by ICP-AES (Ho and others, 1982).

Determination of major, minor, and trace elements retained in ash (Li, Na, K, Rb, Be, Mg, Ca, Sr, Ba, La, Ti, Zr, V, Cr, Mo, Mn, Fe, Co, Ni, Cu, Zn, Cd, Al, Sn, Pb, P, As, Sb, Se, Ce, Th, and U) is done by ICP-AES. A sample of ash (approximately 200 mg) is weighed and treated with concentrated HNO_3 and HF to decompose the silicates. Excess HF is removed by evaporation at 120°C. The residue is further treated with a mixture of HNO_3 and $HClO_4$ at 150° to 160°C. The solution is heated at this temperature to near dryness. The salts are dissolved in $HClO_4$ and dilute HNO_3. All 32 elements are determined simultaneously by ICP-AES.

Inorganic Composition of Whole Coal

Determination of 32 Elements by ICP-AES

A sample (approximately 1 g) of whole coal is weighed and treated with concentrated HNO_3 and HF. The excess HF is evaporated at 120°C. The resulting powder is treated with concentrated HNO_3 at 80°C until all foaming subsided. The temperature is then raised to 120°C to further destroy organic material. The solution is cooled and treated with concentrated $HClO_4$ at 150° to 160°C to near dryness. Residual salts are dissolved in $HClO_4$ and dilute HNO_3. All 32 elements in solution are determined simultaneously by ICP-AES.

Single Element Determination

The solution for determining As, Ag, B, Se, and U_3O_8 is obtained by Parr oxygen bomb combustion (see Halides above). For Hg determination, the absorption solution of Na_2CO_3 is replaced with a solution of HNO_3 and $KMnO_4$ in the quartz liner in the oxygen bomb. The determinations are as follows:

(1) Arsenic and silver are determined by heated graphite analyzer-atomic absorption spectrophotometry (HGA-AAS). Silver is determined directly by atomic absorption utilizing a heated graphite furnace atomizer. Arsenic is determined directly by HGA-AAS after addition of $Ni(NO_3)$ as matrix modification (Ho and others, 1982).

(2) Boron is determined spectrophotometrically as the rosocyanin complex after interfering ions are removed by a boron-specific ion exchange resin and a solvent extraction procedure.

(3) Selenium is complexed with 2,3-naphthalene diamine and the complex is extracted into cyclohexane. Selenium in the form of selenite reacts with orthodiamine to form piazselenols that fluoresce in an organic solvent. The fluorescence of the piazselenols is measured by a spectrofluorometer.

(4) Uranium is complexed with trioctylphosphine oxide (TOPO) and the uranium-TOPO complex is extracted into cyclohexane. An aliquot of the extract is fused with a mixture of LiF and NaF. The resulting fluorescence is measured by a spectrofluorometer.

(5) Mercury in solution is released as mercury vapor (Hg^{o}) after treatment with hydroxylamine and stannous chloride. The mercury vapor is measured by a Coleman Hg-analyzer.

LIGNITE SAMPLE COLLECTION AND PREPARATION

S. J. Tewalt

The recovered core is placed in plastic sleeves and stored in sealed PVC pipe until opened for megascopic description and sampling. The coals are sampled in 1-ft intervals or where natural breaks or changes occur. Two-thirds of the coal core will be sampled for quantitative analysis, the remaining one-third will be archived. Grab samples are collected from overburden and interburden when present. The coal samples are collected with plastic spatulas and stored in plastic jars. Both storage jars and the archived core are stored in a cold room (4°C) until prepared for analysis (table 5).

Current sample preparation consists of washing the sample with distilled water, weighing the sample, and air-drying at approximately 40°C for approximately 15 hours in a convection oven. The samples are milled to approximately 12 - 5 mm (1/2 - 1/5 in) for long-term storage or ground to less than 200 mesh (74 µm) for quantitative analysis. The gross sample is split for analysis by the BEG Mineral Studies Lab (MSL) staff and other researchers. The procedure for preparing low-temperature ash (LTA) is presented in table 6.

Every time a coal sample is handled, there is potential for contamination. Materials added during drilling in order to improve mud viscosity (bentonite, synthetic liquid polymers, etc.) are removed with the mud during sample washing. Further sample handling (sampling, storing, milling, and splitting) can contaminate the sample with plastic, metal, and possibly flecks of paint. Plastic contamination should not readily affect quantitative analysis. The metal components of the equipment used are largely aluminum, which occurs in coal in moderate concentrations; therefore, the cumulative effects of sample contamination should not be serious.

Table 5. Core sample collection and preparation.

1. Describe core, either by foot intervals or according to natural breaks; include brightness, hardness, physical structures, and fracture.

2. Sample two-thirds of core, by foot or same intervals as described, and store in sealed plastic jars.

3. Archive remaining core.

4. Store both samples and archived core in cold storage room at 4°C.

5. Rinse samples with distilled water to remove any remaining drilling mud; allow sample to air-dry briefly.

6. Crush larger blocks of lignite in rock crusher, if necessary, or break into smaller fragments by hand.

7. Weigh approximately 250-300 gm of sample into aluminum pans, place six pans in convection oven.

8. Dry samples at approximately 40°C for 15 hours, stirring samples twice (after 2 and 6 hours, respectively).

9. Weigh sample to determine gross moisture loss.

10. Separate sample fragments less than No. 4 sieve (-4) in size (~5 mm), place remaining +4 sample in mill. Create splits from entire sample interval.

11. Return samples for storage to plastic jars and place in cold storage.

12. Place MSL sample in shatterbox for pulverization to less than 200 mesh (74 μm).

Table 6. Preparing low-temperature ash (LTA).

Leaching procedure for exchangeable cations.

1. Weigh 1 gram of minus 200 mesh coal sample into 50 ml tube.
2. Add 25 ml 1N ammonium acetate, shake hard several times over a 2-hour period.
3. Filter mixture through a no. 42 no-ash, cellulose filter on funnel using vacuum pump, rinsing with distilled water three times to remove excess ammonium acetate.
4. Dry filter on watch glass in 40°C convection oven for several hours or until dry.
5. Scrape coal into LTA boat and ash.

Ashing procedure.

1. Spread 1 gram of sample per boat evenly, four boats total.
2. Radio frequency (RF) = 50, oxygen pressure <1.5 mm Hg.
3. Stir samples every few hours or when top layer appears whitish in color. Ashing is considered complete when weight loss is approximately 2 mg per 2-hour period.

   Weighing procedure.

   Low-temp. asher is turned off, samples remaining in cells several minutes until vacuum ceases. Remove boat and weigh immediately. Return to cell if necessary for further ashing.
4. LTA is dried in convection oven for 9 - 10 hours and then weighed to determine percent LTA of whole coal.
5. The LTA sample is then divided into representative subsamples.

REFERENCES

American Society for Testing and Materials (ASTM), 1982, Proposed standard method for total-S in the analysis sample of coal and coke using idiometric titration procedure: ASTM working document for addition or revision of D-3177-75, p. 1-5.

Anders, R. B., 1967, Ground-water resources of Sabine and San Augustine Counties, Texas: Texas Water Development Board Report 37, 115 p.

Benson, S. A., and Schobert, H. H., 1982, Structural characteristics and relationships in low-rank coals, in Kube, W. R., Sondreal, E. A., and White, D. M., compilers, Technology and use of lignite: U.S. Department of Energy, Grand Forks Energy Technology Center, GFETC/IC-82/1(DE82015926), p. 442-470.

Bradsley, C. E., and Lancaster, J. D., 1965, Sulfur, in Black, C. A., ed., Methods of soil analysis: Madison, WI, American Society of Agronomy, Inc., Part 2, p. 1108-1116.

Broom, M. E., 1969, Ground-water resources of Gregg and Upshur Counties, Texas: Texas Water Development Board Report 101, 76 p.

_____ 1971, Ground-water resources of Cass and Marion Counties, Texas: Texas Water Development Board Report 135, 66 p.

Broom, M. E., and Myers, B. N., 1966, Ground-water resources of Harrison County, Texas: Texas Water Development Board Report 27, 73 p.

Burns, M. S., 1970, Determination of FeS_2-S in Australian coal: Fuel, v. 49, p. 126-133.

Chasen, Steve, 1979, Bivariate (scatter) plots 6D, in Dixon, W. J., and Brown, M. B., eds., BMDP-79 biomedical computer programs P-series: Berkeley, University of California Press, 880 p.

Chebotarev, I. I., 1955, Metamorphism of natural waters in the crust of weathering, pts. 1, 2, and 3: Geochimica et Cosmochimica Acta, v. 8, p. 22-48, 137-170, and 198-212.

Committee on Ground-Water Resources in Relation to Coal Mining, Board on Mineral and Energy Resources, Commission on Natural Resources, and National Research

Council, 1981, Coal mining and ground-water resources in the United States: Washington, D.C., National Academy Press, 197 p.

Crowe, R. E., and Breidenbach, A. W., 1974, Chloride, automated, in Methods for chemical analysis of water and wastes: Cincinnati, OH, National Environmental Research Center, Methods Development and Quality Assurance Research Laboratory, p. 31-34.

Dillard, J. W., 1963, Availability and quality of ground water in Smith County, Texas: Texas Water Commission Bulletin 6302, 35 p.

Dixon, W. J., ed., 1981, BMDP Statistical Software 1981: Berkeley, University of California Press, 726 p.

Dutton, S., 1980, Petrography and diagenesis of Wilcox sandstones, in Kreitler, C. W., and others, Geology and geohydrology of the East Texas Basin--a report on the progress of nuclear waste isolation feasibility studies (1979): The University of Texas at Austin, Bureau of Economic Geology Geological Circular 80-12, p. 83-87.

Edmunds, W. M., 1981, Hydrogeochemical investigations, in Lloyd, J. W., ed., Case-studies in groundwater resource evaluation: New York, Oxford University Press, p. 87-112.

Fisher, W. L., Brown, L. F., Jr., Scott, A. J., and McGowen, J. H., 1969, Delta systems in the exploration for oil and gas: syllabus for research colloquium: The University of Texas at Austin, Bureau of Economic Geology, 212 p.

Fisher, W. L., and McGowen, J. H., 1967, Depositional systems in the Wilcox Group of Texas and their relationship to occurrence of oil and gas: Gulf Coast Association of Geological Societies Transactions, v. 17, p. 105-125.

Fogg, G. E., 1980, Regional aquifer hydraulics, East Texas Basin, in Kreitler, C. W., and others, Geology and geohydrology of the East Texas Basin--a report on the progress of nuclear waste isolation feasibility studies (1979): The University of Texas at Austin, Bureau of Economic Geology Geological Circular 80-12, p. 55-67.

_____ 1981, Fluid-pressure versus depth relationships in the Wilcox-Carrizo aquifer system, East Texas, in Kreitler, C. W., and others, Geology and geohydrology of the East Texas Basin--a report on the progress of nuclear waste isolation feasibility studies (1980): The University of Texas at Austin, Bureau of Economic Geology Geological Circular 81-7, p. 115-122.

Fogg, G. E., and Kreitler, C. W., 1981, Ground-water hydrology around salt domes in the East Texas Basin: a practical approach to the contaminant transport problem: Bulletin of the Association of Engineering Geologists, v. 18, no. 4, p. 387-411.

_____ 1982, Ground-water hydraulics and hydrochemical facies of Eocene aquifers in the East Texas Basin: The University of Texas at Austin, Bureau of Economic Geology Report of Investigations No. 127, 71 p.

Fogg, G. E., Seni, S. J., and Kreitler, C. W., in press, Three-dimensional modeling of ground-water flow through depositional systems, Oakwood salt dome vicinity, East Texas: The University of Texas at Austin, Bureau of Economic Geology Report of Investigations.

Foster, M. D., 1950, The origin of high sodium bicarbonate waters in the Atlantic and Gulf Coastal Plains: Geochimica et Cosmochimica Acta, v. 1, p. 33-48.

Freeze, R. A., 1975, A stochastic-conceptual analysis of one-dimensional groundwater flow in nonuniform homogeneous media: Water Resources Research, v. 11, no. 5, p. 725-741.

Freeze, R. A., and Cherry, J. A., 1979, Groundwater: Englewood Cliffs, NJ, Prentice-Hall, 604 p.

Galloway, W. E., and Kaiser, W. R., 1980, Catahoula Formation of the Texas Coastal Plain: origin, geochemical evolution, and characteristics of uranium deposits: The University of Texas at Austin, Bureau of Economic Geology Report of Investigations No. 100, 81 p.

Given, P. H., and Yarzab, R. F., 1978, Analysis of the organic substance of coals: problems posed by the presence of mineral matter, in Karr, C., Jr., ed., Analytical methods for coal and coal products: New York, Academic Press, v. II, p. 3-41.

Guyton, W. F., and Associates, 1970, Ground-water conditions in Angelina and Nacogdoches Counties, Texas: Texas Water Development Board Report 110, 125 p.

_____ 1972, Ground-water conditions in Anderson, Cherokee, Freestone, and Henderson Counties, Texas: Texas Water Development Board Report 150, 250 p.

Hem, J. D., 1970, Study and interpretation of the chemical characteristics of natural water: U.S. Geological Survey Water-Supply Paper 1473, 363 p.

Henry, C. D., and Basciano, J. M., 1979, Environmental geology of the Wilcox Group lignite belt, East Texas: The University of Texas at Austin, Bureau of Economic Geology Report of Investigations No. 98, 28 p.

Henry, C. D., Basciano, J. M., and Duex, T. W., 1979, Hydrology and water quality of the Eocene Wilcox Group: significance for lignite development in East Texas: Gulf Coast Association of Geological Societies Transactions, v. 29, p. 127-135.

Ho, C. L., in press, Determination of nitrogen in coal, coke and lignite by micro-Kjeldahl method: ASTM standard test method for coal and coke.

Ho, C. L., Tweedy, S., Mahan, C., and Gower, D., 1982, Analytical methods of rocks, coals and waters: The University of Texas at Austin, Bureau of Economic Geology Mineral Studies Laboratory, unpublished methods.

Hoel, P. G., 1971, Introduction to mathematical statistics, 4th ed.: New York, John Wiley, 409 p.

Kaiser, W. R., 1974, Texas lignite: near-surface and deep-basin resources: The University of Texas at Austin, Bureau of Economic Geology Report of Investigations No. 79, 70 p.

_____ 1978, Depositional systems in the Wilcox Group (Eocene) of east-central Texas and the occurrence of lignite, in Kaiser, W. R., ed., Proceedings, Gulf Coast lignite conference: geology, utilization, and environmental aspects: The University of Texas at Austin, Bureau of Economic Geology Report of Investigations No. 90, p. 33-53.

Kaiser, W. R., Ayers, W. B., Jr., and LaBrie, L. W., 1980, Lignite resources in Texas: The University of Texas at Austin, Bureau of Economic Geology Report of Investigations No. 104, 52 p.

Kaiser, W. R., Johnston, J. E., and Bach, W. N., 1978, Sand-body geometry and the occurrence of lignite in the Eocene of Texas: The University of Texas at Austin, Bureau of Economic Geology Geological Circular 78-4, 19 p.

Kharaka, Y. K., and Barnes, I., 1973, SOLMNEQ: solution-mineral equilibrium computations: Springfield, VA, National Technical Information Service, Technical Report PB-215899, 81 p.

Kreitler, C. W., Agagu, O. K., Basciano, J. M., Collins, E. W., Dix, O., Dutton, S. P., Fogg, G. E., Giles, A. B., Guevara, E. H., Harris, D. W., Hobday, D. K., McGowen, M. K., Pass, D., and Wood, D. H., 1980, Geology and geohydrology of the East Texas Basin--a report on the progress of nuclear waste isolation feasibility studies (1979): The University of Texas at Austin, Bureau of Economic Geology Geological Circular 80-12, 112 p.

Kreitler, C. W., Collins, E. W., Davidson, E. D., Jr., Dix, O. R., Donaldson, G. A., Dutton, S. P., Fogg, G. E., Giles, A. B., Harris, D. W., Jackson, M. P. A., Lopez, C. M., McGowen, M. K., Muehlberger, W. R., Pennington, W. D., Seni, S. J., Wood, D. H., and Wuerch, H. V., 1981, Geology and geohydrology of the East Texas Basin--a report on the progress of nuclear waste isolation feasibility studies (1980): The University of Texas at Austin, Bureau of Economic Geology Geological Circular 81-7, 207 p.

Kreitler, C. W., and Fogg, G. E., 1979, Geochemistry of ground water in the Wilcox aquifer, in Kreitler, C. W., and others, Geology and geohydrology of the East Texas Basin--a report on the progress of nuclear waste isolation feasibility studies (1979): The University of Texas at Austin, Bureau of Economic Geology Geological Circular 80-12, p. 73-79.

Miller, R. N., 1977, Geochemical study of the inorganic constituents in some low-rank coals: University Park, PA, Pennsylvania State University, Ph.D. dissertation, 319 p.

Montgomery, W. J., 1978, Standard laboratory testing methods for coal and coke: ASTM 2361 chlorine in coal, bomb combustion method, in Karr, C., Jr., ed., Analytical methods for coal and coal products: New York, Academic Press, v. I, p. 191-246.

Myers, B. N., 1969, Compilation of results of aquifer tests in Texas: Texas Water Development Board Report 98, 532 p.

Nie, N. H., Hull, C. H., Jenkins, J. G., Steinbrennar, K., and Bent, D. H., 1975, SPSS: Statistical Package for the Social Sciences, 2nd ed.: New York, McGraw-Hill, 675 p.

Oak Ridge Gaseous Diffusion Plant, 1979, Hydrogeochemical and stream sediment reconnaissance basic data for Palestine NTMS Quadrangle, Texas: Grand Junction, CO, U.S. Department of Energy, GJBX-92(79) (ORGDP No. K/UR-123), Open-File Report, 39 p.

Seni, S. J., and Fogg, G. E., 1981, Wilcox Group facies and syndepositional salt dome growth, southern East Texas Basin: The University of Texas at Austin, Bureau of Economic Geology, Milestone Report No. DE-AC97-80ET46617 for U.S. Department of Energy.

Stumm, W., and Morgan, J. J., 1981, Aquatic chemistry: an introduction emphasizing chemical equilibria in natural waters, 2nd ed.: New York, John Wiley, 780 p.

Tóth, J., 1963, A theoretical analysis of groundwater flow in small drainage basins: Journal of Geophysical Research, v. 68, p. 4795-4812.

FIGURE CAPTIONS

Figure 1. Distribution of deep-basin lignite in Texas (Kaiser and others, 1980).

Figure 2. Eocene stratigraphy in east-central Texas and the Sabine Uplift area.

Figure 3. Wilcox stratigraphy in the Sabine Uplift area and the occurrence of lignite. NS-1-82 is in Trawick gas field; see figure 5 for location.

Figure 4. East-west cross section showing lignite occurrence in the Wilcox Group. See figure 6 for location of section.

Figure 5. Map of lignite occurrence in the Wilcox Group.

Figure 6. Maximum-sand map of the Wilcox Group.

Figure 7. Identification of lignite on a TENRAC/BEG log and oil and gas log from nearby. See figure 5 for location of logs.

Figure 8. Net sand map of the stratigraphically highest sandstone in the Newby Sandstone Member in Bastrop, Lee, and Fayette Counties.

Figure 9. Isopach map of the Carrizo Formation and Newby Sandstone Member in Bastrop, Lee, and Fayette Counties showing the location of paleovalleys at the base of the Carrizo.

Figure 10. Poentiometric-surface map, Wilcox-Carrizo aquifer system. Data are from wells tapping Wilcox and Wilcox (undivided) strata. Measurements are circa 1960's and early 1970's. The map is considered reliable for regional interpretation, but local hydraulic gradients can be much more complex.

Figure 11. Ground-water flow lines inferred from the Wilcox-Carrizo potentiometric surface map. Major discharge areas are the Sabine River, Big and Little Cypress Bayous, Attoyac Bayou, and several of their tributaries. Major recharge areas are in the Wilcox-Carrizo outcrop areas in Rusk, Nacogdoches, and Shelby Counties.

Figure 12. Potentiometric-surface map, Carrizo aquifer.

Figure 13. Graph of fluid pressure versus depth (P-D) for Wilcox-Carrizo system. Data are from wells tapping Wilcox-Carrizo (undivided). Measurements are circa 1960's and early 1970's. Pressure data indicating water levels deeper than 300 ft (91.4 m) were not included in order to minimize errors caused by drawdowns from heavy pumpage; virgin water levels are presumed to have been less than 300 ft (91.4 m) deep. Slope ($\underline{m}$) of the P-D regression line indicates direction of the vertical flow component: flow is upward when $m > 1$ and downward when $m < 1$. The depth intercept represents the depth at which the regression line intersects zero pressure. The vertical component of flow is generally downward in the Sabine Uplift region, except below 500 ft (152 m), where there is apparently little potential for vertical flow.

Figure 15. Map showing vertical component of the hydraulic gradient ($\partial h/\partial z$) determined by least-squares linear regression for data in each 7.5-minute quadrangle. Postive and negative values indicate potential for upward and downward movement, respectively. Presence of a measurable $\partial h/\partial z$ value indicates potential for vertical flow and poor vertical interconnection of sand bodies. The standard error values shown can be used to calculate confidence limits for the vertical hydraulic gradient.

Figure 16. Generalized version of figure 6 indicating only the signs of $\partial h/\partial z$: positive indicates upward flow and negative, downward flow. Darker patterns represent relatively reliable trends for which the standard error is less than the absolute value of $\partial h/\partial z$; lighter patterns indicate less reliable trends for which the standard error is greater than or equal to the absolute value of $\partial h/\partial z$.

Figure 17. Histograms showing frequencies of (a) log [hydraulic conductivity] (ft/day) and (b) log [transmissivity] (ft^2/day). Data are from pumping test results published in W. F. Guyton and Associates (1972, 1970), Myers (1969), and Broom (1971). Hydraulic conductivity is distributed approximately log-normally.

Figure 18. Cumulative exceedance probability for (a) log [hydraulic conductivity] (ft/day) and (b) log [transmissivity] (ft^2/day) showing probability that a given value of K or T would be exceeded in a random sampling. For example, there is a 27 percent chance that a log (K) value of 1.25 ($K = 10^{1.25} = 17.8$ ft/day) would be exceeded. Most of these data are from depths of less than 1,000 ft (305 m).

Figure 21. Piper diagrams of Carrizo and Wilcox waters show them to be Na^+-HCO_3^- dominated. Wilcox samples are divided by depth into two groups based on a data break at approximately 125 ft on scatter plots (fig. 26). Shallow waters are Ca^{2+}-HCO_3^- dominated, becoming Na^+-HCO_3^- dominated in the deeper, confined portion of the Wilcox.

Figure 22. Schematic diagram illustrating ground-water evolution from Ca^{2+}-HCO_3^- to Na^+-HCO_3^- domination. Ca^{2+}-HCO_3^- waters typify recharge, whereas Na^+-HCO_3^- waters characterize discharge.

Figure 23. Map of Carrizo $\log[Na^+]^{.33}/[Ca^{2+}]^{.16}$ ratios. Log activity ratios <-0.4 indicate recharge. Flow is basinward, toward areas of log ratio values > 0.0. Martin Lake (ML), Darco (D), and South Hallsville (SH) lignite mines are shown for reference. Nearly all Carrizo completions are between depths of 200 and 760 ft (61 and 232 m).

Figure 24. Map of Carrizo $\log[Ca^{2+}]^{.3}[Na^+]^{.7}$ products. Log activity products <-3.15 indicate recharge. More positive values occur basinward.

Figure 25. Electric logs illustrating the Carrizo-Wilcox boundary. The 200-ft interval directly below the Carrizo is sandier in Q23. See figures 23 and 24 for location of logs.

Figure 26. Scatter plot of Wilcox $\log[Na^+]^{.33}/[Ca^{2+}]^{.16}$ ratios versus depth. The log activity ratio increases with depth, reflecting longer travel time and greater distance from outcrop. Note data break at 125 ft. Numbers represent number of points that plot at that position up to 9, then letters are used starting with A equal 10, etc.

Figure 27. Map of Wilcox $\log[Na^+]^{.33}/[Ca^{2+}]^{.16}$ ratios. Small log activity ratios, <-0.4, indicate areas of recharge and larger log values, > 0.0, lie in areas of discharge. Solid symbols are completions at depths of < 200 ft (61 m). Most of Wilcox completions are between depths of 144 and 1,000 ft (44 and 305 m).

Figure 28. Map of Wilcox $\log[Ca^{2+}]^{.3}[Na^+]^{.7}$ products. Log activity products <-3.00 indicate areas of recharge, whereas log activity products >2.70 indicate areas of discharge.

Figure 29. Scatter plot of Wilcox $\log[H_4SiO_4^o]$ values versus depth. $\log[H_4SiO_4^o]$ decreases with depth, converging on the chalcedony equilibrium value.

Figure 30. Scatter plot of Wilcox $\log[H_4SiO_4^o]$ values versus $\log[Na^+]^{.33}/[Ca^{2+}]^{.16}$ Note the convergence on the chalcedony equilibrium value as $\log[Na^+]^{.33}/[Ca^{2+}]^{.16}$ increases (depth increases, fig. 26).

Figure 31. Scatter plot of Wilcox $\log[H_4SiO_4^o]$ values versus Ca-montmorillonite saturation indices. SI decreases to approximately 4.8 while $\log[H_4SiO_4^o]$ approaches a threshold near the chalcedony equilibrium value.

Figure 32. Map of Wilcox $\log[H_4SiO_4^o]$ values. Recharge is indicated by log values > -3.4. Log values of < -3.6 correlate with areas previously identified as areas of discharge.

Figure 33. Map of Wilcox Ca-montmorillonite saturation indices. Areas of recharge are characterized by log values > 6.2, whereas areas of discharge have log values < 5.2.

Figure 37. Percentage of major sands in the Wilcox Group.

Figure 38. Map of resistivity product of major sands (RP_{sum}) in the Wilcox Group. Ground-water flow lines (solid) from Fogg (1980). Dashed arrows represent flow direction inferred from this map.

Figure 39. Base of fresh water below sea level.

Figure 40. Graph of TDS versus electric log resistivity (R_o; 64-inch long normal or induction), Wilcox-Carrizo aquifer system, Sabine Uplift area. Data are from water wells that are screened primarily in channel-fill sands at depths of 200 to 1,200 ft (61 to 366 m).

Figure 41A. Plot of sodium (Na^+), bicarbonate (HCO_3^-), chloride (Cl^-) concentrations versus R_o. Na^+ and HCO_3^- show better correlations than does Cl^-, because Na^+ and HCO_3^- are generally the dominant ions in Wilcox-Carrizo ground water.

Figure 41B. Plot of bicarbonate (HCO_3^-) concentrations versus R_o. Na^+ and HCO_3^- show better correlations than does Cl^-, because Na^+ and HCO_3^- are generally the dominant ions in Wilcox-Carrizo ground water.

Figure 41C. Plot of chloride (Cl^-) concentrations versus R_o. Na^+ and HCO_3^- show better correlations than does Cl^-, because Na^+ and HCO_3^- are generally the dominant ions in Wilcox-Carrizo ground water.

Figure 42. Graph of TDS versus specific conductance of the water samples.

Figure 14. Graph of mean slope ($\underline{m}$) of P-D regression lines (table 1) for 50-ft (15.2 m) intervals of land surface elevation. The outcrop data show a general trend of decreasing $\underline{m}$ with increasing elevations, reflecting greater recharge (and hence greater downward movement) at higher elevations. In comparison, the subcrop $\underline{m}$ values are everywhere closer to a value of 1.00 and generally increase with elevation. This increase in partly caused by high $\underline{m}$ values in Smith county above 500 ft (152.4 m) (table 1).

Figure 19. Potentiometric-surface map of the Wilcox Group. Within each county, a time period was selected to include the most data within a reasonably short time. For this reason, contours are not continuous over county lines. The map is considered reliable for regional interpretation, but local hydraulic gradients can be much more complex.

Figure 20. Ground-water flowlines in the Wilcox Group. Ground water appears to move away from surface-water drainage divides toward rivers or streams; only a very small proportion of ground water recharging the Wilcox moves downdip to become part of the deep Wilcox system.

Figure 34A. Map of Carrizo $\log [Na^+]^{.33}/[Ca^{2+}]^{.16}$ ratios as derived from the montmorillonite-cation-exchange reaction. The areas with low activity ratios correspond to presumed recharge areas, and areas with high ratios correspond to presumed discharge areas.

Figure 34B. Map of Wilcox $\log [Na^+]^{.33}/[Ca^{2+}]^{.16}$ ratios as derived from the montmorillonite-cation-exchange reaction. The areas with low activity ratios correspond to presumed recharge areas, and areas with high ratios correspond to presumed discharge areas.

Figure 35A. Map of Carrizo $\log [Ca^{2+}]^{.3}[Na^+]^{.7}$ products as derived from the reaction describing feldspar argillation. The areas of low activity products correspond to presumed recharge areas or to areas where feldspar may be absent. The areas of high values of the sodium-calcium activity product correspond to presumed discharge areas.

Figure 35B. Map of Wilcox $\log [Ca^{2+}]^{.3}[Na^+]^{.7}$ products as derived from the reaction describing feldspar argillation. The areas of low activity products correspond to presumed recharge areas or to areas where feldspar may be absent. The areas of high values of the sodium-calcium activity product correspond to presumed discharge areas.

Figure 36A. Map of Carrizo $\log [H_4SiO_4^o]$ values. Areas of high activity correspond to presumed recharge areas and areas of low activity correspond to presumed discharge areas. The silicic acid activity approaches that of equilibrium with quartz ($\log a \simeq -4$) or chalcedony ($\log a \simeq -3.7$) in presumed discharge areas and that of silica glass ($\log a \simeq -2.95$) in presumed recharge areas.

Figure 36B. Map of Wilcox $\log [H_4SiO_4^o]$ values. Areas of high activity correspond to presumed recharge areas and areas of low activity correspond to presumed discharge areas. The silicic acid activity approaches that of equilibrium with quartz ($\log a \simeq -4$) or chalcedony ($\log a \simeq -3.7$) in presumed discharge areas and that of silica glass ($\log a \simeq -2.95$) in presumed recharge areas.